PISTON SLAP NOISE IN DIESEL ENGINES

by

JAMES W. SLACK

S.B., Massachusetts Institute of Technology
(1973)

SUBMITTED IN PARTIAL FULFILLMENT
OF THE REQUIREMENTS FOR THE
DEGREE OF

DOCTOR OF PHILOSOPHY

at the

MASSACHUSETTS INSTITUTE OF TECHNOLOGY

February, 1982

Signature of Author ________________________
Department of Ocean Engineering
February 5, 1982

Certified by ________________________
Richard H. Lyon
Thesis Supervisor

Accepted by ________________________
A. Douglas Carmichael
Chairman, Department Committee

PISTON SLAP NOISE IN DIESEL ENGINES

by

JAMES W. SLACK

Submitted to the Department of Ocean Engineering
on February 5, 1982 in partial fulfillment of the
requirements for the Degree of
Doctor of Philosophy in Ocean Engineering

ABSTRACT

Piston slap is typically the major source of noise and vibration in a turbocharged diesel engine. An investigation of piston slap in a motored diesel engine has been carried out. Vibration measurements were made on the connecting rod, cylinder wall, and block surface while motoring. Drive point and transfer mobility measurements were made on the non-running engine. The measured mobilities are used to construct a model of piston-cylinder wall interaction which predicts the excitation due to piston slap. The measured transfer mobilities are used to predict vibration transfer to the block surface. Bending of the connecting rod is shown to play an important role in both the excitation of vibration and the transmission of vibrational energy to the block surface.

Thesis Supervisor: Richard H. Lyon

Title: Professor of Mechanical Engineering

ACKNOWLEDGEMENTS

I wish to thank Professor Richard H. Lyon for his guidance and supervision of this research and for all that I have learned from him about acoustics and vibration. I would also like to thank Professor John B. Heywood and Professor J. Kim Vandiver for serving on my thesis committee.

I am grateful to Dr. Richard G. DeJong of Cambridge Collaborative, Inc. for his help and for the use of his company's computer facility.

I am grateful to all of the members of the Acoustics and Vibration Laboratory for their friendship and for challenging me to always think about what I was doing; especially Charles Thompson, who was always ready to discuss any problem or offer an honest opinion.

I also wish to thank William Finley whose insight as a mechanic was most helpful; and Mary Toscano for her friendship, for typing this thesis, and for all she has done for me.

Finally, I thank my wife and 14 month old son for keeping my life in perspective and not letting me think that this thesis was the most important thing in the world.

TABLE OF CONTENTS

TABLE OF CONTENTS (CONTINUED)

LIST OF FIGURES

LIST OF FIGURES (CONTINUED)

LIST OF FIGURES (CONTINUED)

NOMENCLATURE

A	cross-sectional area
$a(t)$	acceleration
$A(\omega)$	Fourier transform of acceleration
b, B	width
c	wave speed
E	modulus of elasticity
f	circular frequency
$f(t)$	force
$F(\omega)$	Fourier transform of force
G	amplifier gain
h, H	thickness
$h(t)$	impulse response
$H(\omega)$	transfer function (frequency response)
i	$\sqrt{-1}$
I	moment of inertia
K	spring constant
ℓ, L	length
M	mass
$n(t)$	noise
$N(\omega)$	Fourier transform of noise
p	pole of transfer function
P	cylinder pressure
P_n	Legendre Polynomial

NOMENCLATURE (CONTINUED)

r, R	radius
s	Laplace transform variable
S	transducer sensitivity
t, T	time
u	displacement
$v(t)$	velocity
$V(\omega)$	Fourier transform of velocity
$\underline{Y}(\omega)$	mobility matrix
$Y_{ij}(\omega)$	element of mobility matrix
z	zero of transfer function
δ	clearance
η	loss factor
ρ	density
ω	angular frequency (radians)

CHAPTER ONE: INTRODUCTION

1.1 Piston Slap

Piston slap is the impact of the piston against the cylinder wall in a reciprocating engine or compressor. It arises when the resultant transverse force exerted by the connecting rod changes direction, causing the piston to leave the side of the cylinder it was previously held against and impact the opposite side. Piston slap at top dead center before the power stroke is shown in detail in Fig. 1.1 It is seen that the axial gas pressure loads and inertial loads are balanced by the axial component of the thrust applied by the connecting rod. The resultant transverse component is balanced by a reaction force exerted by the cylinder wall. If the operating clearance (δ in Fig. 1.1) is small, the kinetic energy gained by the piston while crossing the cylinder is also small, and the impact is not significant. Audible piston slap in a modern gasoline engine is not normal and indicates a need for service.

In a diesel engine, however, peak cylinder temperatures and pressures are higher than in a gasoline engine; and the piston must be more robust. In addition, aluminum alloy pistons have a coefficient of thermal expansion which is about twice that of the cast iron cylinder block. These con-

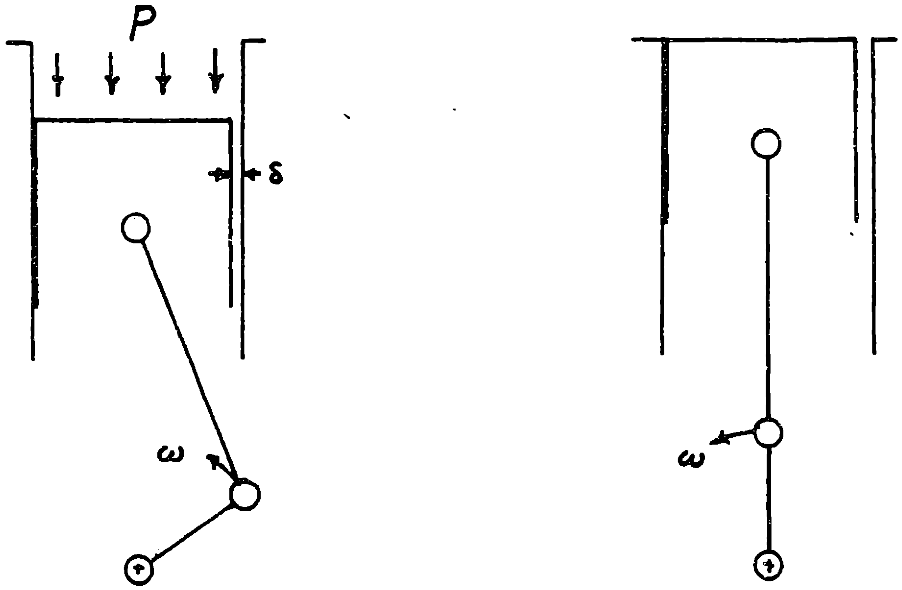

a) piston slides on cylinder wall

b) piston at top dead center

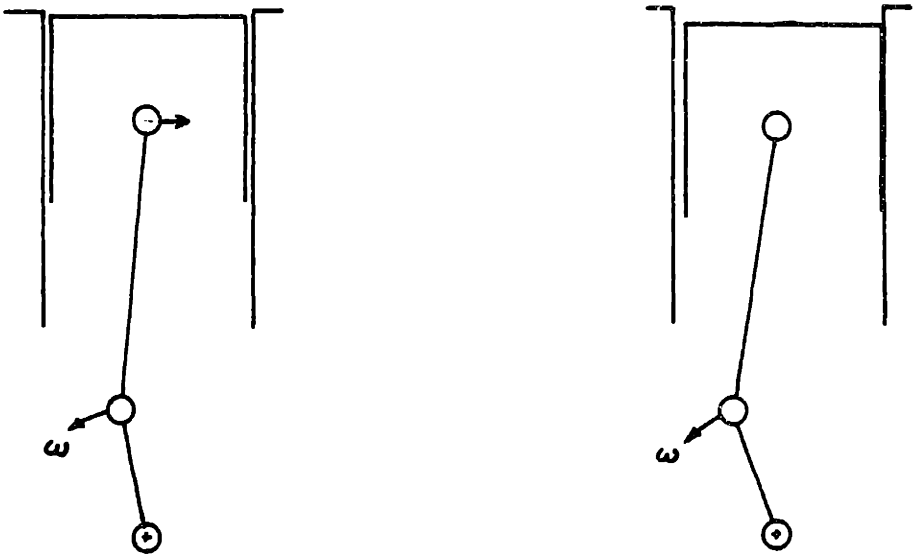

c) piston accelerates through operating clearance

d) piston impacts major thrust side

Figure 1.1: Piston Slap

siderations lead to greater operating clearances which alon with greater peak cylinder pressures result in the piston having significant kinetic energy at the time of impact. I a diesel engine, the vibration excited by the piston slap impact can radiate a significant amount of noise.

1.2 Engine Noise

The noise generated by marine diesel engines has received serious attention for many years. Data presented Zinchenko [1] in 1957 shows why. Noise levels measured nea the main engine are given for 34 diesel powered ships and three steamships. For the diesels, the levels range from 96 dB to 118 dB with a median of 109 dB. For the steamship the measured levels are 78, 92, and 96 dB. The difference between the median steamship and the median motorship is 17 dB, so that even relatively speaking, diesel powered shi are very noisy. Zinchenko determines that the dominant source of noise at low frequencies is piston slap.

For automotive engines, one might suppose that the first complaints about noise were expressed shortly afte the first successful test of an Otto engine. In 1876 Gas Motoren Fabrik Deutz brought out the "Otto" Silent gas engine based on the four-stroke cycle suggested by Beau de Rochas in 1862 [2]. By this time, piston slap was recogniz as a source of noise and vibration, although the principle instrument was a modified stethoscope which was used to discover sources rather than to measure levels.

Recognition of piston slap as an important source of noise in automotive diesel engines seems to have come rather late. While authors in the United States, the United Kingdom and Germany [3*,4,5] recognize piston slap, Austen and Priede [6] make no mention of it in their 1958 paper: "Origin of Diesel Engine Noise." This apparent oversight is probably due to the fact that Austen and Priede were considering naturally aspirated high speed automotive diesels while the other authors were considering the larger marine diesels. It has since been shown that in the former, combustion is usually the dominant source of noise; while in the latter, piston slap is usually the dominant source [7]. Turbocharging however, leads to quieter combustion and higher peak cylinder pressures. With the application of turbocharging to automotive diesels, the balance is shifted and piston slap

---

[*] Mercy, Ref. [3] does not specifically mention piston slap. In a series of experiments motoring an eight cylinder in-line two stroke marine diesel, he rates the importance of sources by selectively operating various components. The pistons and connecting rods are rated second after the scavenging blower, but Mercy attributes the noise to unbalance of reciprocating parts. He does mention large clearances as having an influence on noise, so one may suppose he is also aware of impacts.

commonly becomes the dominant source [8].

1.3 Reduction of Piston Slap Noise

Although piston slap has received serious attention for over thirty years, it continues to be a serious problem for manufacturers who are being forced by government regulations to produce even quieter vehicles. To make matters worse, demand for greater fuel economy and reduced emissions, within the scope of current technology, lead to conflicting design requirements [9]. Thus performance in all three areas must be compromised to achieve an acceptable design. Therefore, a review of the current understanding of the phenomenon was undertaken to determine which aspects of piston slap are well understood and which aspects are not. This review will separately consider the piston slap as a source of vibration and the path which the vibration follows from the source to external surfaces of the engine block.

1.3.1 The Source

The phenomenon of piston slap is described in Section 1.1. There may be either two, four, or six impacts per crankshaft revolution, depending on speed and cylinder pressure [10,11,12]. This motion has been analyzed by many authors using models ranging from very simple to very detaile

[5, 10, 12, 13, 14, 15, 16, 17]. The intensity of the impact is then measured by the kinetic energy of the piston at the time of impact. By changing various parameters such as running clearance, piston pin offset, cylinder pressure, or engine speed, the various researchers have examined the influence of these parameters on piston slap intensity. With the application of high speed digital computers, it is possible to identify design parameters which give minimum piston slap intensity [18].

Unfortunately, mechanical design considerations place a finite lower limit on operating clearance; while manufacturing costs limit the piece to piece tolerances. Pflaum and Hempel in 1965 predicted "the use of pistons with controlled heat expansion and piston eccentricity (i.e., piston pin offset) will in most of the cases make it possible to eliminate the noise from the lateral piston movement entirely." [19] Such pistons have been implemented and shown to be quieter [20], but they have not eliminated piston slap noise.

Piston pin offset can reduce the impact intensity, but not enough to achieve desired noise levels. Offset towards the major thrust side (see Fig. 1.1) advances the timing of the piston lateral motion (for the impact at T.D.C. before the power stroke) so that the cylinder pressure is lower. Offseting this direction leads to a higher maximum resultant side force exerted by the connecting rod onto the piston, which led Alvarez to erroneously conclude that the piston kinetic energy upon impact would also be greater [11]. Ross and Ungar [7], following Alvarez, recommend piston pin offset away from the major thrust side. Other authors, however, recommend offset towards the major thrust side, and actual measurements have shown this recommendation to be correct [12,5].

Investigation of the piston-cylinder wall interaction during and immediately following the impact has been much less thorough. This interaction must be well understood in order to accurately predict the spectrum of the interaction force. Typically, the piston has been modeled as a lumped mass which drives the cylinder wall with an impulsive force of finite time duration [10]. The spectrum of such an impulse would be broad band and smooth in frequency. One may use a force gauge mounted on a hammer to produce this type of excitation, and a typical force time history and spectrum are shown in Fig. 1.2. Experimental evidence in support of this model of piston slap excitation is lacking.

Haddad and Fortescue [13] model piston-cylinder wall interaction using a mass for the piston and two masses,

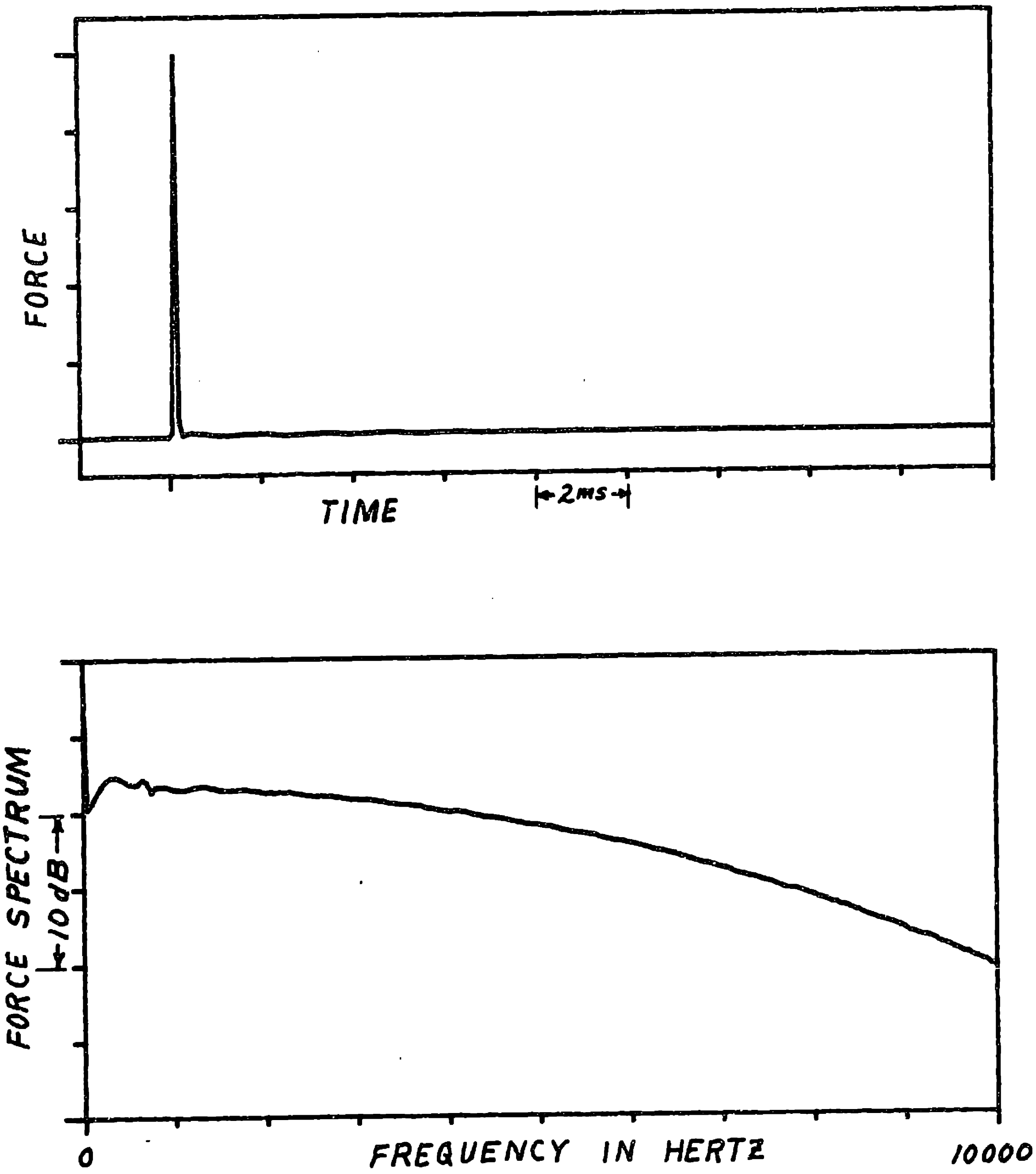

Figure 1.2: Time History and Spectrum of Impulse Force

three springs, and three dashpots for the cylinder liner. Fig. 1.3 shows schematically their model. The parameters for this model were chosen to match observed resonant frequencies of the liner which are 1250 Hz and 2950 Hz. This model implies poles and zeroes in the spectrum of the interaction force. Oil film thickness between the piston and the cylinder wall was measured on the running engine, but this data does not indicate how well the model predicts cylinder wall vibration.

1.3.2. The Path

Obvisouly, piston slap noise is structureborne from the cylinder wall to the exterior surfaces of the block and airborne from these surfaces to the receiver's ear. Actually the path may be more complex. Enclosures may be used to reduce the noise level at the receiver; or conversely, there may be mechanical connections to the engine which provide additional structural paths. In this work, attention will be limited to the problem of transmission to the block surface, since further transmission is common to all engine noise problems and has received much attention [21].

The transmission path of piston slap noise has always been assumed to be from the cylinder wall to the external surfaces of the engine directly through the block

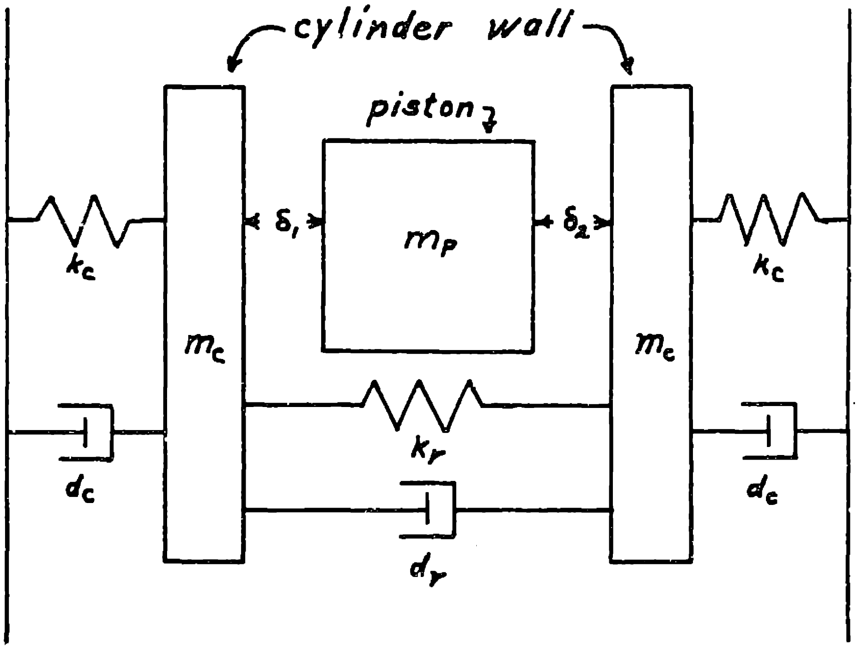

Figure 1.3: Model of Piston and Cylinder Wall by Haddad and Fortescue [13]

structure. Oguchi [22], using mechanical mobility measurements, studied the transmission of piston slap induced vibration from different cylinders to various points on the block surface as well as the effects of cooling water and the presence of the cylinder head. He determined that the major path was through the upper deck (top surface) of the block. He does not consider the connecting rod as a possible path, nor has anyone else to this author's knowledge. This seems curious since the connecting rod has been shown to play an important role in the transmission of combustion noise [23, 24].

1.4 Scope of this Work

For both the source and the path, areas have been identified where more research is needed. A model which accurately predicts the spectrum of the force applied to the cylinder wall would greatly improve our understanding of how the vibration is generated. If the connecting rod is shown to play an important role in vibration transmission, then different transmission path treatments will be required. Finally, transfer mobilities using point driving forces must be shown to be significant in structural vibration problems where point contact is not obviously the case. All of these issues will be addressed, with the goal of formulating a model for piston-cylinder wall interaction and how the resulting vibration is transmitted to the block surface. Piston slap data taken from a motored engine will be used to evaluate the model.

1.5 Mechanical Mobility Work at MIT

In recent years, three investigators at MIT have made substantial use of mechanical mobility for investigating various aspects of diesel engine vibration and noise. DeJong [23] studied the transmission of combustion noise through the piston, connecting rod, and crankshaft to the engine block. This work demonstrates how measured mechanical mobility may be used to generate a model for a vibration path which may in turn be studied to determine ways of reducing the amount of vibration transmitted.

Oguchi [22] made a number of transfer mobility measurements on a four cylinder diesel engine to study the effect of various parameters on the transmission of piston slap induced vibration from the cylinder wall to various points on the engine surface. These first two investigators illustrate the use of mobility to study transmission paths.

Ordubadi [25] used mechanical mobility in order to infer a remote source of excitation (cylinder pressure) from a vibration response measured on the engine surface. This work illustrates the use of mobility to indirectly measure a source which may not be conveniently measured directly.

This investigator will make use of these techniques and others to investigate the interaction between the piston and cylinder wall during piston slap. The principle additional technique to be used is the inference of source location by taking the ratio of velocity responses at two locations to a known force applied to the cylinder wall and comparing with the corresponding ratio of velocity responses to piston slap excitation. A detailed discussion of this comparison may be found in Appendix C.

CHAPTER TWO: MECHANICAL MOBILITY MEASUREMENTS

Mobility is a useful concept when dealing with linear time invariant mechanical systems. It is the inverse of the fourier transform of the differential operator which relates the velocity response of a system to a set of forces applied to the system. As a result of the linear time invariant assumption, these differential equations transform to linear algebraic equations in the frequency domain. Specifically, for a system described by the motion of N discrete velocities V_i, i=1,N, with $f_i(t)$ the force applied to the point at which V_i is measured; then if

$$F_j(\omega) = \int_{-\infty}^{\infty} e^{i\omega t} f_j(t)\, dt \qquad (2.1)$$

and

$$V_i(\omega) = \int_{-\infty}^{\infty} e^{i\omega t} V_i(t)\, dt \qquad (2.2)$$

then $\vec{F}(\omega)$ and $\vec{V}(\omega)$ are related by the mobility matrix $\underline{Y}(\omega)$ by the equation:

$$\vec{V} = \underline{Y}\cdot\vec{F} \qquad (2.3)$$

This equation, although not used here to define mobility, does indicate the method commonly used to measure mobility. A known force $f_j(t)$ is applied to point

j while all other $f_k (k \neq j)$ remain zero. The velocity response $V_i(t)$ is measured and each matrix element Y_{ij} is computed by taking the ratio of the fourier transforms:

$$Y_{ij} = \frac{V_i(\omega)}{F_j(\omega)} \tag{2.4}$$

The diagonal elements of the mobility matrix (Y_{ij}, $i=j$) are commonly called drive point mobilities while the off-diagonal elements are called transfer mobilities.

Another important result for linear systems is reciprocity. When a linear system is bilateral and passive as well as time invariant, it can be shown that $Y_{ij} = Y_{ji}$ for all i and j. This property will be used quite often to make transfer mobility measurements on the engine where it is not possible to position the shaker at the desired driving point. In such cases the engine will be driven at the desired response point and the response will be measured at the desired driving point. The principle of reciprocity will be invoked to argue that the desired result was obtained from the actual measurement.

Reciprocity will also be used as a confidence check on the data. Reciprocal measurements will be made and compared as a check on the validity of the various assumptions made about the engine structure.

For a more detailed discussion of the use of mechanical mobility in modeling vibration transmission, see reference [23].

2.1 Instrumentation and Engine Block Assembly.

The measurement of mechanical mobility of a given structure requires that a known driving force be applied to a structure and that the velocity response be measured. A convenient way of making this measurement on an engine block is by driving with an electrodynamic shaker through a piezoelectric force gauge and measuring acceleration response with a piezoelectric accelerometer. These mobility measurements were made using a Ling Model 203 Shaker rated at 3 lbf. r.m.s. without forced air cooling, a Wilcoxon type Z-602 impedance head using the force gauge only, and a Bruel & Kjaer Type 4344 accelerometer. Both the impedance head and the accelerometer were mounted on threaded stud bases which were in turn cemented to the engine with quick setting epoxy cement.

The excitation for the shaker was white noise from a B&K Type 1402 random noise generator band limited by a Krohn-Hite Model 3550 filter and amplified by a McIntosh 40 watt power amplifier. The output of the power amplifier was fused to 2 1/2 amps to avoid damaging the shaker. The output impedance of the electrodynamic shaker is extremely small compared to the engine block, so that the driving force applied to the engine was nearly constant with frequency in the range of interest. The flat force spectrum helped to minimize noise in the form signal in order to be consistent with the assumptions made later when estimating the transfer function between the force and acceleration signals (see Appendix B).

The outputs of the force gauge and accelerometer were amplified by two Ithaco Model 452 instrumentation amplifiers, band pass filtered from 200 to 5000 Hz by two Ithaco Model 4112 filters, and recorded on magnetic tape with a Nagra SJ-IV direct tape recorder. See Fig. 2.1 for instrumentation block diagram.

Each data taking session was begun by first recording the same random white noise signal on each channel of the tape and then recording mobility data for a known calibration mass. Then mobility data was taken for the various mobilities to be measured. The white noise signal was not normally used to reduce data, but was helpful if problems arose with the data reduction program or the tape recorder.

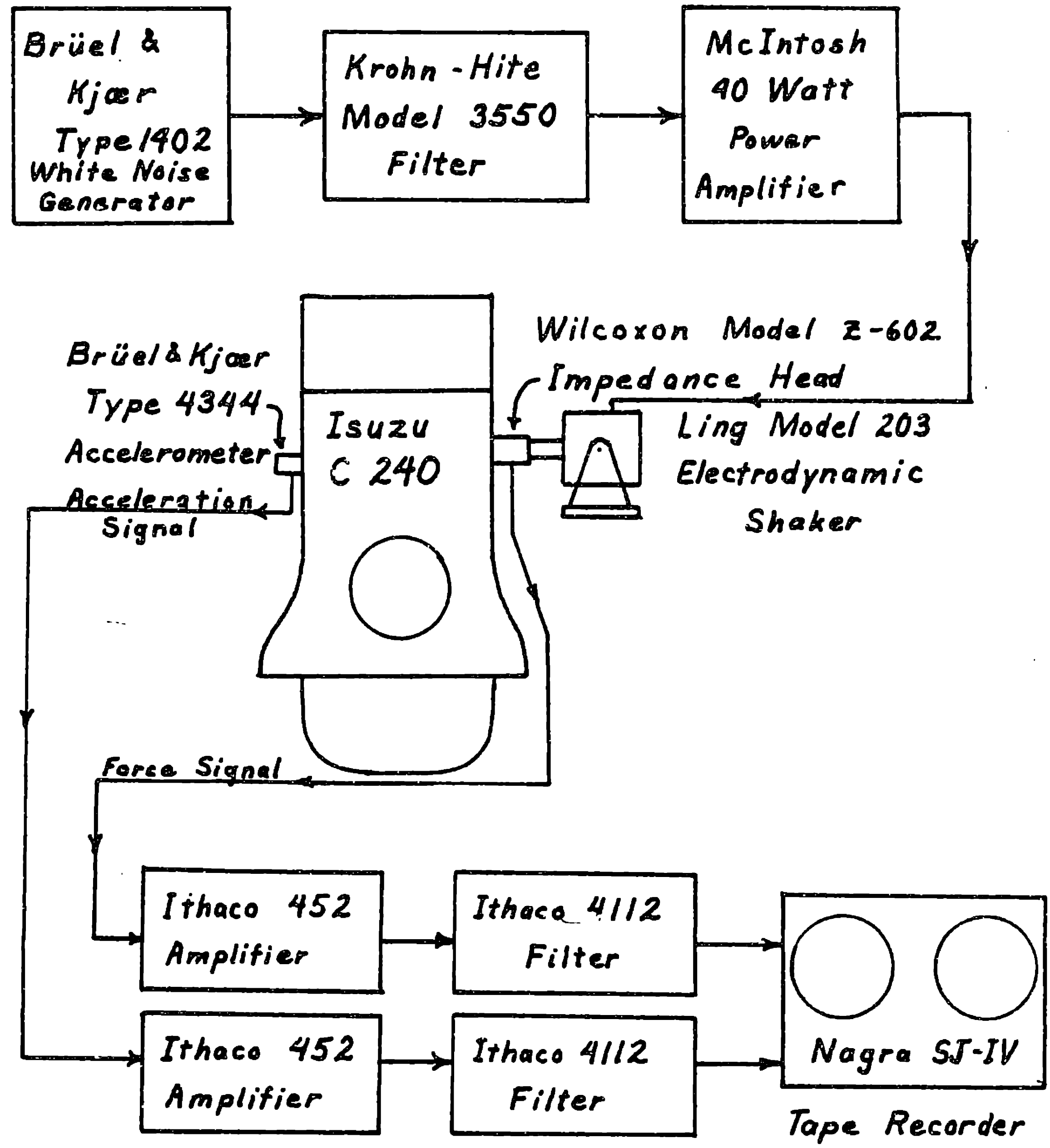

Figure 2.1: Instrumentation Block Diagram for Mobility Measurements

Since the calibration mass mobility data and the engine mobility data were taken using the same transducers and recorded by the same tape recorder, the transducer sensitivities were not used directly in the data reduction. If the recorded force and acceleration signals are V_F and V_A respectively, then for the measurement

$$V_F = F \cdot S_F \cdot G_F \tag{2.5a}$$

$$V_A = A \cdot S_A \cdot S_B \tag{2.5b}$$

where

F is force
A is acceleration
S_F is force sensitivity
G_F is force channel gain
S_A is acceleration sensitivity
G_A is acceleration channel gain

similarly for the calibration data:

$$V_{F,CAL} = F_{CAL} \cdot S_F \quad \cdot G_{F,CAL} \tag{2.6a}$$

$$V_{A,CAL} = A_{CAL} \cdot S_A \quad \cdot G_{A,CAL} \tag{2.6b}$$

$$F_{CAL} = M_{CAL} \cdot A_{CAL} \tag{2.7}$$

Therefore:

$$\frac{F}{A} = \frac{V_F}{V_A} \cdot \frac{S_A G_A}{S_F G_F} \qquad (2.8)$$

also:

$$\frac{S_F}{S_A} = \frac{V_{F,CAL}}{V_{A,CAL}} \; \frac{A_{CAL}}{M_{CAL} A_{CAL}} \; \frac{G_{A,CAL}}{G_{F,CAL}} \qquad (2.9)$$

combining:

$$\frac{F}{A} = M_{CAL} \; \frac{V_F / V_A}{V_{F,CAL} / V_{A,CAL}} \; \frac{G_A / G_F}{G_{A,CAL} / G_{F,CAL}} \; . \qquad (2.10)$$

As is shown here, the only additional information needed to reduce the mobility data is calibration mass in consistent units and the overall force channel and acceleration channel gains used while recording the data. The data was reduced on a digital computer using an algorithm described in detail in Appendix B. The source code is not included because it is specific to the system on which it was implemented.

The mobility measurements were made on the engine in the same partly assembled condition used when the engine was motored. In order to save time and improve access to the basic engine structure, the manifolds, valve cover, pushrod cover, injection pump, filters, and auxilaries were removed. Since the engine was not run, these parts were considered extraneous. Vibration transmission from the block to covers has been studied using statistical energy analysis methods [21] and it is considered sufficient for this research to understand how piston slap excites the block.

2.2 Drive Point Mobility Measurements on the Piston and Cylinder Wall

Drive point mobilities were measured on the cylinder wall and on the piston opposite the wrist pin. The results of these measurements are shown in Figs. 2.2 and 2.3, respectively. These results provide the basis for the models formulated in Chapter 4. The vertical location opposite the piston pin was chosen because the resultant force which holds the piston against the cylinder wall is applied through the center of the pin. The piston and connecting rod assembly was removed from the cylinder and reconnected to the crank with the connecting rod upside down as shown in Fig. 2.3. Since the structure is assumed to be linear and bending of the connecting rod will be shown to be the only important mode at the big end, the mobility as measured should be the same as when the piston is in the cylinder. At any rate, it is the best compromise between providing the correct constraint at the big end and

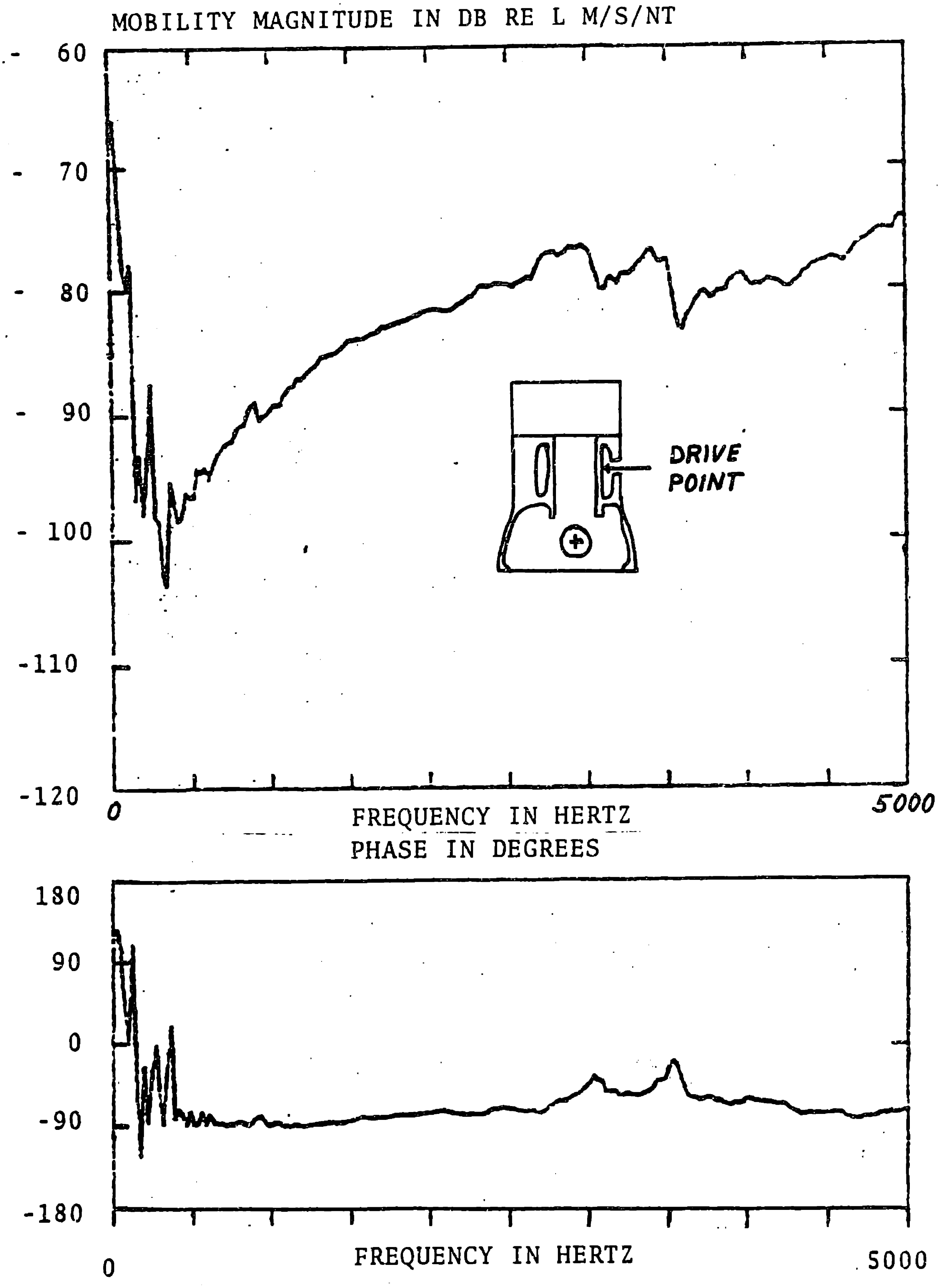

Figure 2.2: Drive Point Mobility of Cylinder Wall

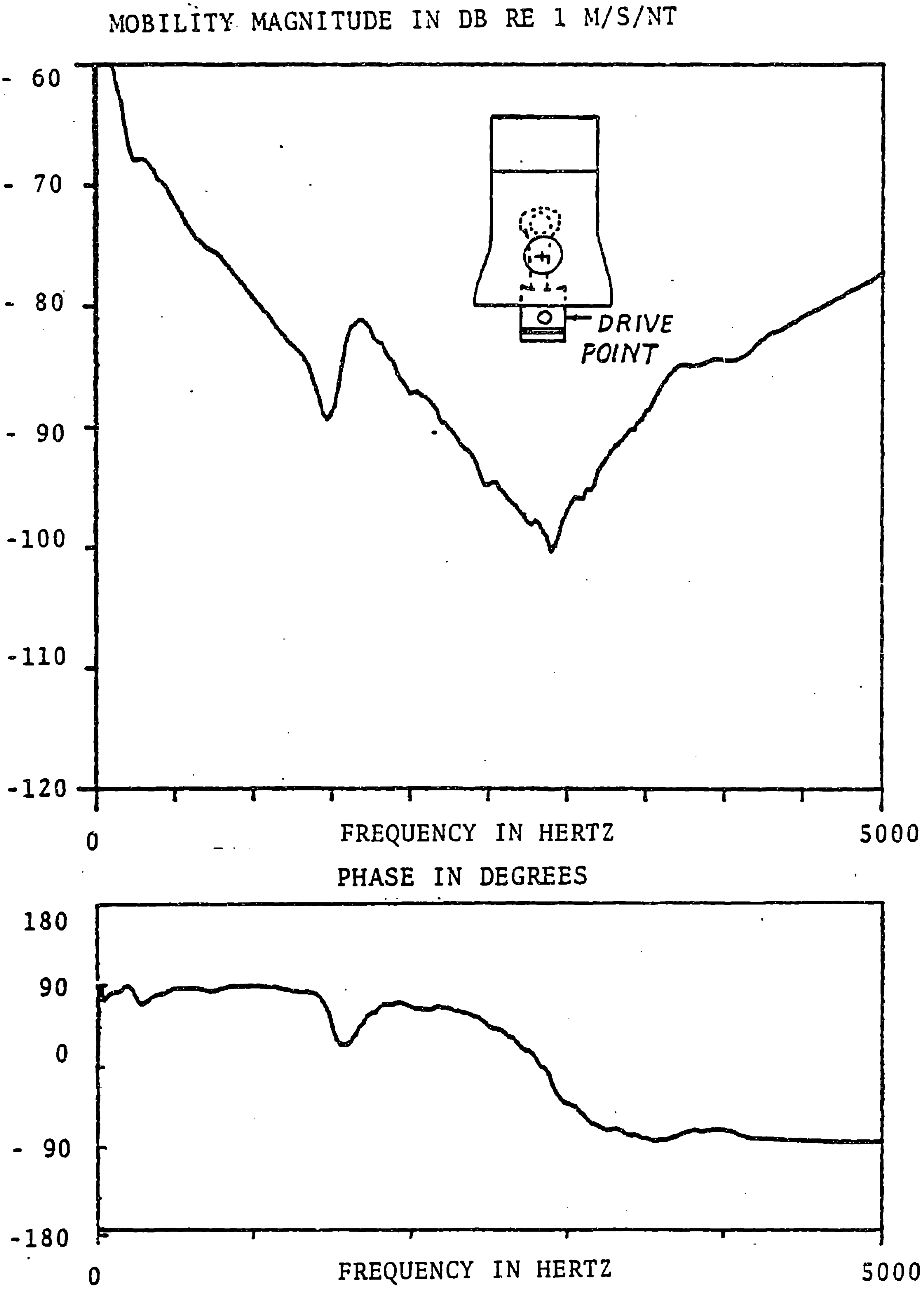

Figure 2.3: Measured Drive Point Mobility of Piston

providing access to the piston.

The drive point mobility of the cylinder wall was measured at a position approximately 2.5 cm below the piston pin at top dead center where contact was assumed. Removal of a freeze plug allowed access at this point without radical modification of the block. Since drive point mobilities measured at various points on the block were similar and insensitive to location (when not directly over ribs or stiffeners) it was assumed that the measurement as made accurately represented the desired mobility. For this measurement the accelerometer was located inside the cylinder opposite the impedance head.

2.3. Transfer Mobility Measurements on the Block

Transfer mobilities from the cylinder wall to selected points on the block surface were measured in order to determine how vibrational energy reached the block surface. These transfer mobilities were determined to be sensitive to transducer location, so the selected points were permanently marked with a center punch.

Since the shaker and impedance head could not be mounted on the desired point on the cylinder wall, reciprocal measurements were used. The impedance head was mounted on the block surface and the response accelerometer was mounted on the cylinder wall at the assumed piston slap drive point. To verify that reciprocal measurements can be accurately made as well as to support the assumption of linear time invariance, reciprocal pairs of transfer mobility measurements were made using the freeze plug hole location on the cylinder wall and points on the block surface. A pair of reciprocal measurements is shown in Fig. 2.4. The agreement is very good. It was during this test that the sensitivity to transducer location was discovered. Since it was required for the transfer mobility data reduction algorithm, drive point mobility data was taken for each drive point used.

2.4 Connecting Rod Transfer Path Measurements

In order to evaluate another possible path of vibrational energy transfer, the transfer mobility from the piston (as shown in Fig. 2.2) to the block surface was measured. The resonance in the piston drive point mobility was determined to be due to bending of the connecting rod. Therefore, at this frequency, one expects a peak in the transfer mobility along this path, and the transfer mobility of the block path is seen to be low. The comparison is shown in Figs. 2.5 and 2.6 and the rod path is indeed dominant between 1 kHz and 2 kHz.

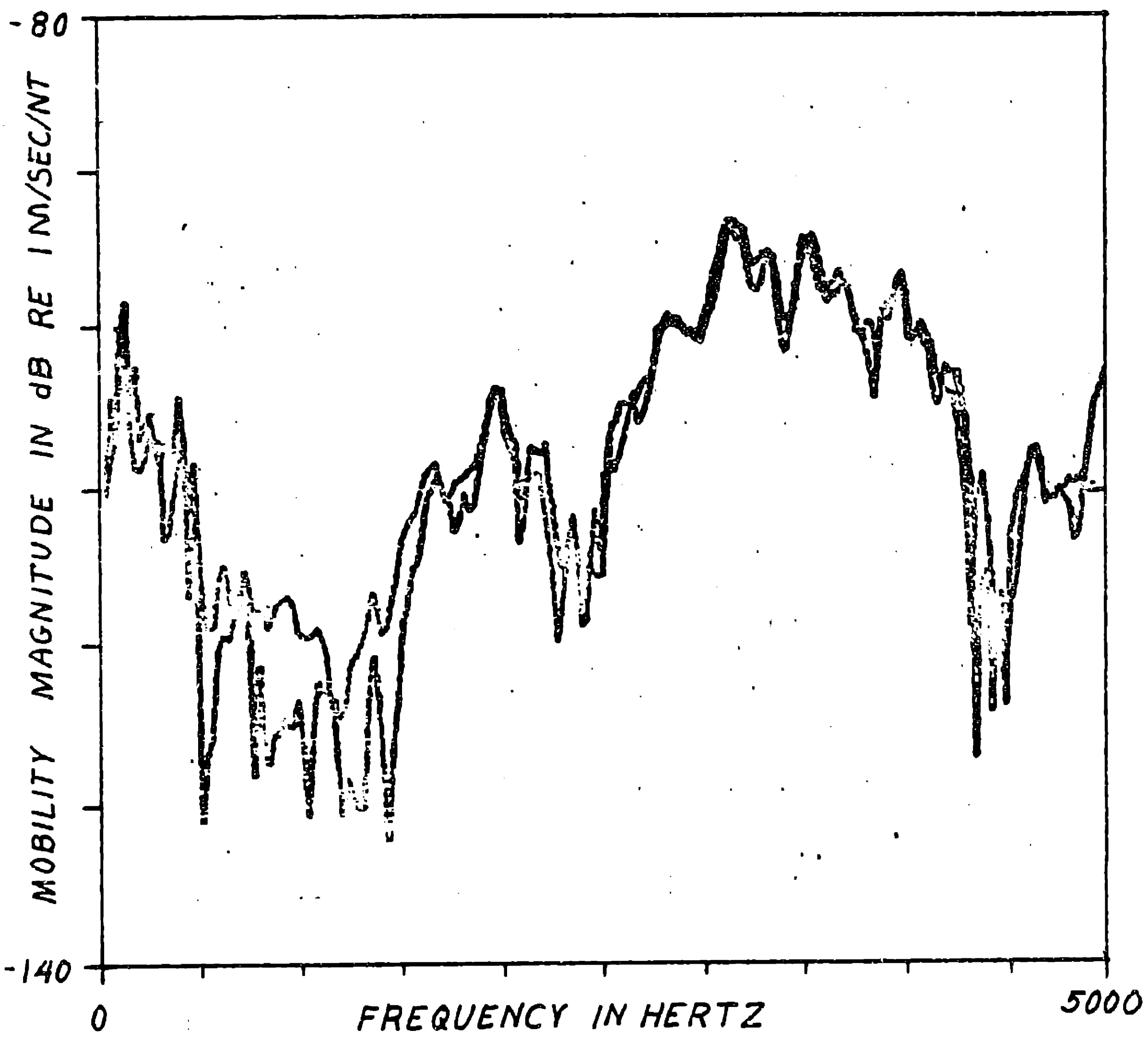

Figure 2.4: Reciprocal Pair of Transfer Mobility Measurements on Engine Block

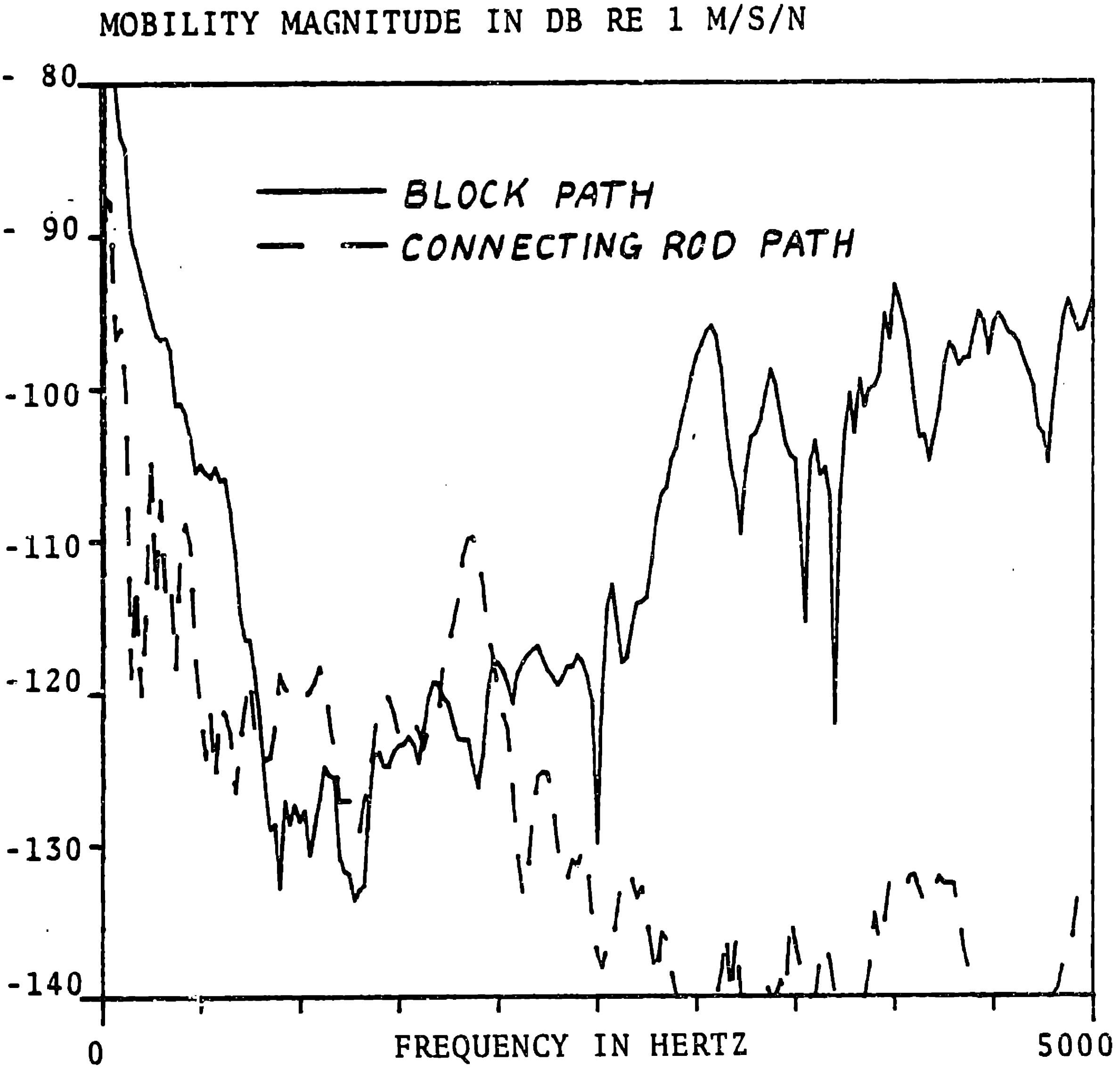

Figure 2.5: Transfer Mobility to Block Surface, Right Side

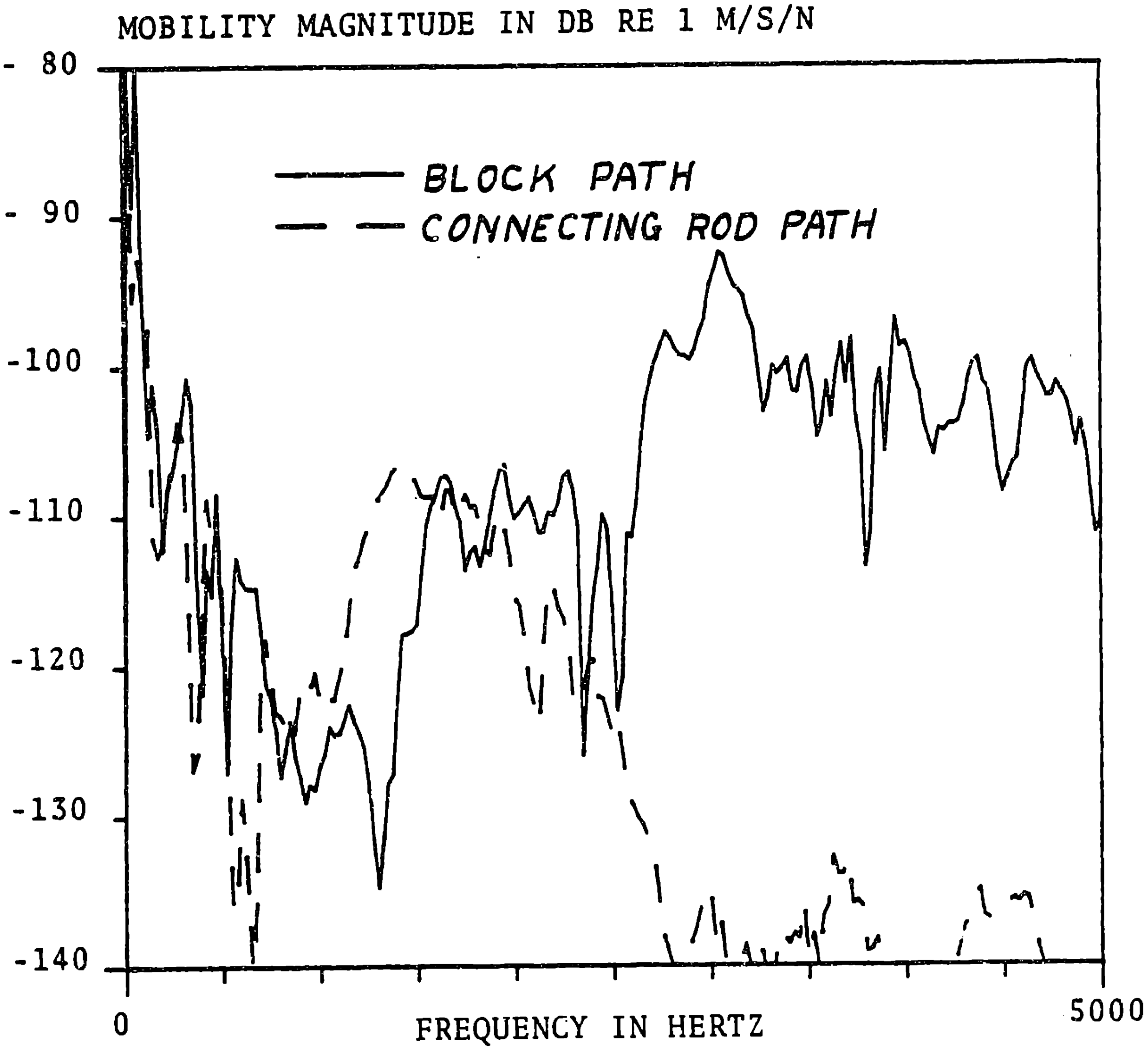

Figure 2.6: Transfer Mobility to Block Surface, Left Side

Longitudinal vibration of the connecting rod has already been shown to be an important path for combustion noise [23]. It was felt that the contribution of longitudinal vibration to the transmission of piston slap noise should be evaluated. A transmission loss type measurement was designed for this purpose, since it would avoid the problem of resolving forces at the small end of the rod. This description of this experiment refers to the block diagram in Fig. 2.7.

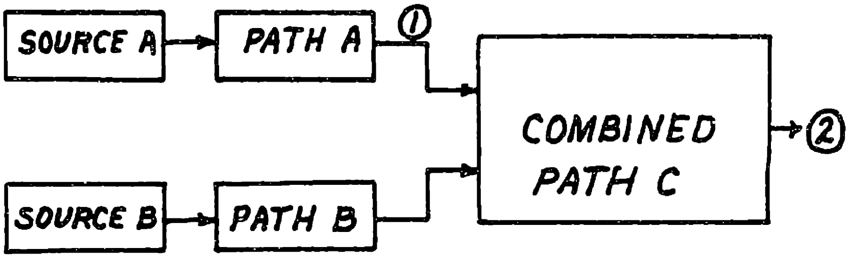

Fig. 2.7: Transmission Loss Experiment

Path A represents the longitudinal vibration of the connecting rod, path B represents the cylinder wall, and path C represents the block. Point 1 represents the big end of the connecting rod and point 2 represents the block surface. A random force with flat spectrum band limited from 200 to 5000 Hz was applied to the top of the piston (Source A). The ratio of velocity response spectrum at point 1 to velocity at point 2 was measured and is shown in Fig. 2.8.

The same velocity ratio measurement was made while driving the cylinder wall (Source B) with the same force. The results are also shown in Fig. 2.8. If the same velocity ratios are measured for response to piston slap excitation, the important of longitudinal vibration of the connecting rod may be evaluated. If this path can be shown to be unimportant, the more difficult problem of resolving the longitudinal force applied at the small end of the connecting rod may be avoided altogether.

To make the actual measurement, the piston was removed from the connecting rod, the rod was installed upside down with the crank at top dead center (see Fig. 2.3) and the shaker was attached to the small end of the rod. One accelerometer was mounted on the big end of the rod, and another was mounted on the block surface. The big end bearing was preloaded by using surgical rubber tubing to apply a constant force to the small end simulating cylinder pressure. Five different points on the block surface were actually used, but typical data is shown for only one. The acceleration data was recorded using the same procedure as for mobility data, and the data reduction algorithm is described in Appendix C.

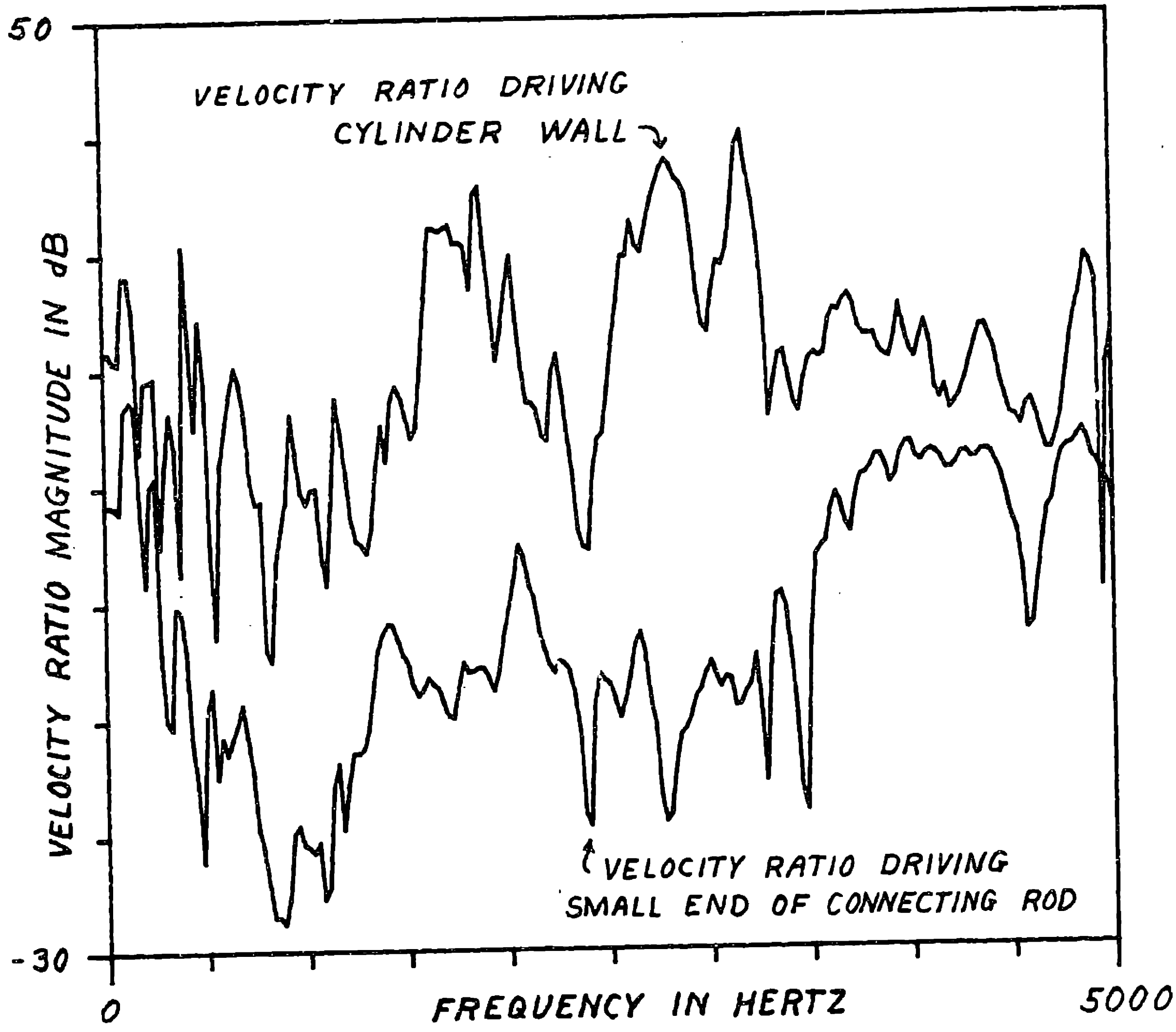

Figure 2.8 Velocity Ratios: Block Surface vs. Connecting Rod While Driving with Shaker

CHAPTER THREE: MEASUREMENTS ON A MOTORED ENGINE

Measurements on running engines are difficult to interpret because of the number of possible sources and uncertainty as to which is dominant. Simulation of piston slap using back-to-back connecting rods and a shaker as shown in Fig. 3.1 [26] alters the mass distribution of the connecting rod. This may introduce significant impacts at the crank bearings as well as change the piston-cylinder wall interaction dynamics. Therefore, it was decided to use a motored engine with modest peak cylinder pressure to simulate piston slap in a running engine. The level of excitation is thereby reduced; but insofar as the assumption of linear behavior is valid, piston slap in the motored engine should accurately represent piston slap in a running engine. The engine used was a four cylinder 2.369 litre Isuzu Model C240 diesel. Specifications for this engine are given in the Table of Specifications with Fig. 3.2.

3.1 Modifications to the Engine

For the purposes of this research, piston slap induced vibration is the signal of interest, and all vibration due to other sources is noise. The major source of noise would be combustion, and this has been eliminated. Gear and valve noise was eliminated by removing the timing idler gear. Since this gear is the only gear meshing with

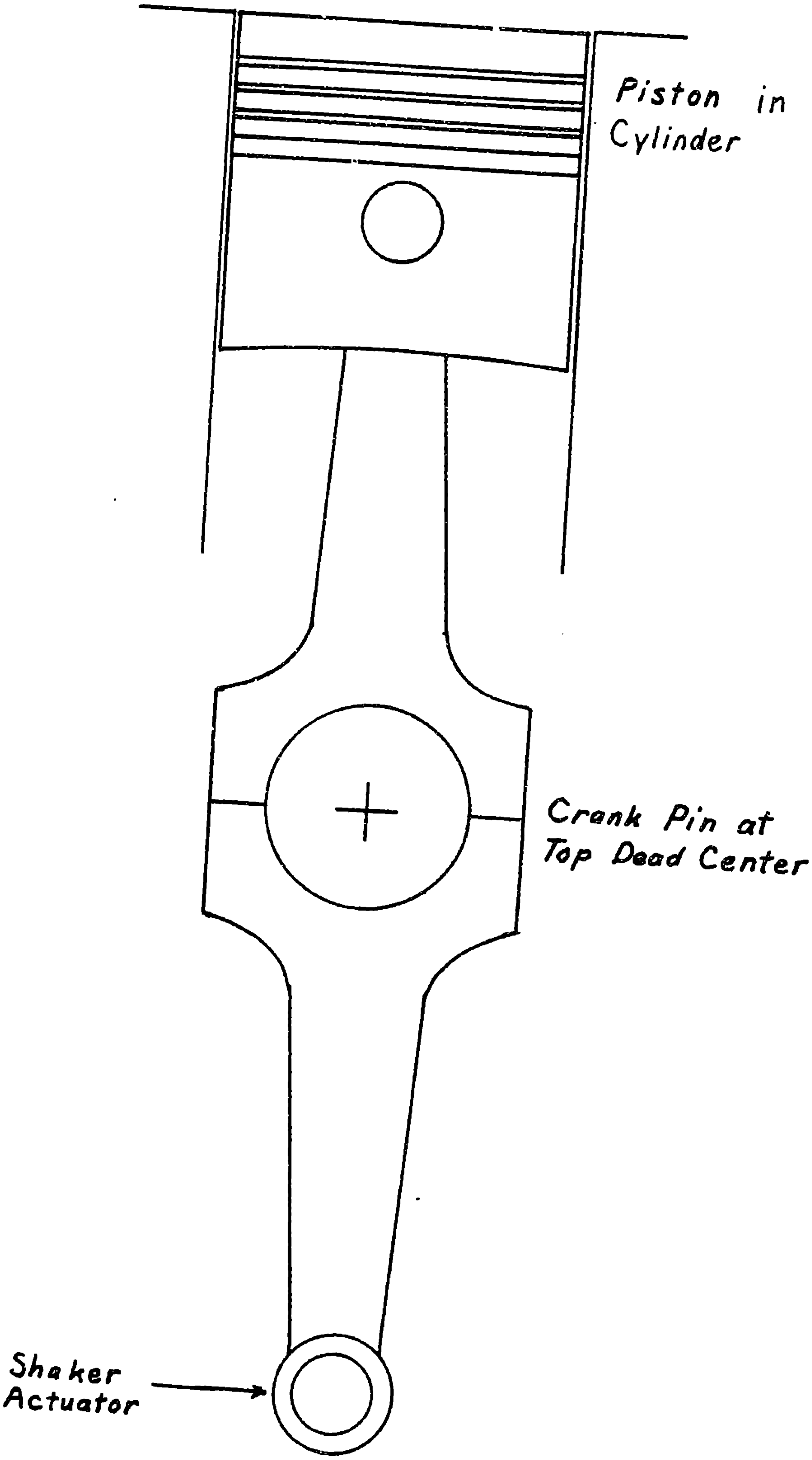

Figure 3.1 Back to Back Connecting Rods for Simulating Piston Slap with a Shaker [26]

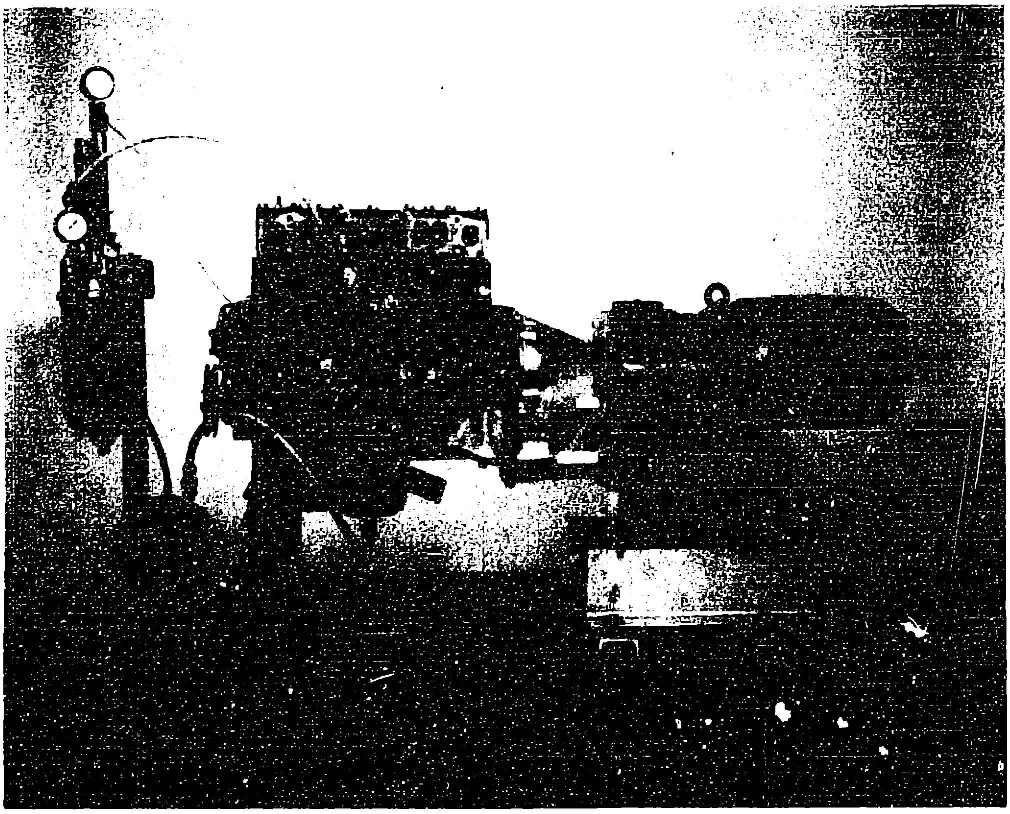

Figure 3.2: Photograph of Isuzu Engine and Electric Motor Drive

Table of Specifications, Isuzu Model C240

Type	Four stroke, four-cylinder in line
Bore	86 mm
Stroke	102 mm
Displacement	2.369 litre
Compression Ratio	20:1
Rated Power	74 horsepower at 3800 rpm
Rated Torque	116 ft-lbf. at 2000 rpm

Water Cooled, Dry Cylinder Liners

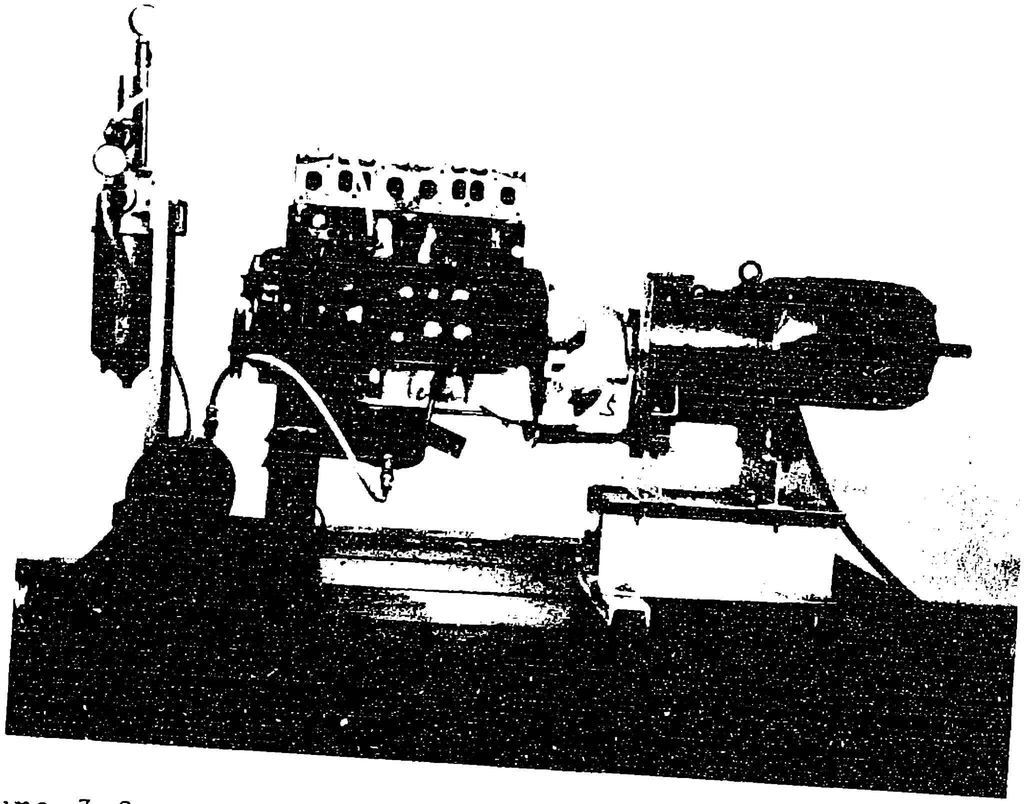

Figure 3.2: Photograph of Isuzu Engine and Electric Motor Drive

Table of Specifications, Isuzu Model C240

Type	Four stroke, four-cylinder in line
Bore	86 mm
Stroke	102 mm
Displacement	2.369 litre
Compression Ratio	20:1
Rated Power	74 horsepower at 3800 rpm
Rated Torque	116 ft-lbf. at 2000 rpm

Water Cooled, Dry Cylinder Liners

INTENTIONAL DUPLICATE EXPOSURE

the timing gear on the crankshaft, its removal stopped the camshaft and valve operation, oil pump, and injection pump. Three of the pistons were removed, leaving only the slap of the number 1 piston (in most cases) as a significant source of noise . The valves were sealed closed.

Lubrication was provided by an external electric powered oil pump. The oil was pumped from the sumpthrough a filter fitted with a relief valve and delivered to the oil gallery at 50 psi. A 5W non-detergent oil was used since it was readily obtainable and had, at room temperature, a viscosity approximately the same as 10W-40 engine oil at 100°C [27].

The crankshaft was driven by a three horsepower A.C. electric motor through a variable speed cone drive. The speed range was 600 rpm to 3600 rpm. A special front cover was made for the variable speed drive which mounted on the engine bell housing in place of the transmission. The clutch was replaced by a flexible coupling which took up any misalignment. The final misalignment between the crankshaft and the variable speed drive was estimated to be less than .003" parallel and .001"/1" angular. The engine was motored without pistons to demonstrate that the vibration level due to sources other than piston slap was low enough that good data could be taken. A photograph of the experimental set-up shown in Fig. 3.2.

As has been described, the major piston slap takes place as the crankpin moves through top dead center between the compression and power strokes. In order to get significant pressure at top dead center, it was necessary to seal the combustion chamber during the compression stroke.

The Isuzu is designed to have a 20:1 compression ratio with a Ricardo type pre-combustion chamber in the cylinder head. The bottom of this spherical chamber is formed by a hot plug which is pressed into the head. Since neither the cone drive nor the AC electric motor have good starting torque characteristics, the hot plug was removed in order to reduce the compression ratio. Even with the reduced compression ratio, it was necessary to start the engine from top dead center. In order to provide sufficient peak pressure to assure a pronounced piston slap impact, compressed air was supplied through a small orifice to the cylinder.

3.1.1 Instrumentation

The orifice and compressed air reservoir acted as a low pass filter so that an ordinary bordon tube pressure gauge was used to measure the mean cylinder pressure. The AC component of cylinder pressure was measured by a Kaig piezoelectric cylinder pressure gauge which was mounted in place of the injector. These details are shown in Fig. 3.3. The peak cylinder pressure was determined by adding the mean and time varying components.

An MTI Model KD38 Fotonic Sensor was used to detect a white timing mark painted on a black background on the pulley on the front end of the crank. The timing mark was used to determine the time of impact. A Bruel & Kjaer type 4344 accelerometer mounted in the water jacket on the impacted side of the cylinder through a freeze plug hole as discussed in Chapter 2 was used to measure cylinder wall vibration. The representative points on the block surface already chosen for the mobility measurements were used to locate accelerometers for simultaneous cylinder wall and block surface acceleration measurements.

For the measurements of longitudinal vibration of the connecting rod, an accelerometer was mounted on the big end of the rod. Special handling was required to lead the accelerometer cable from the moving rod to the crankcase. A two-beam linkage was built and connected by a pin joint to the connecting rod at one end and to the oil pan at the other end as shown in Fig. 3.4. In order to provide room in the crankcase for the linkage, the oil pan was turned so that the sump was at the front of the engine. The splash

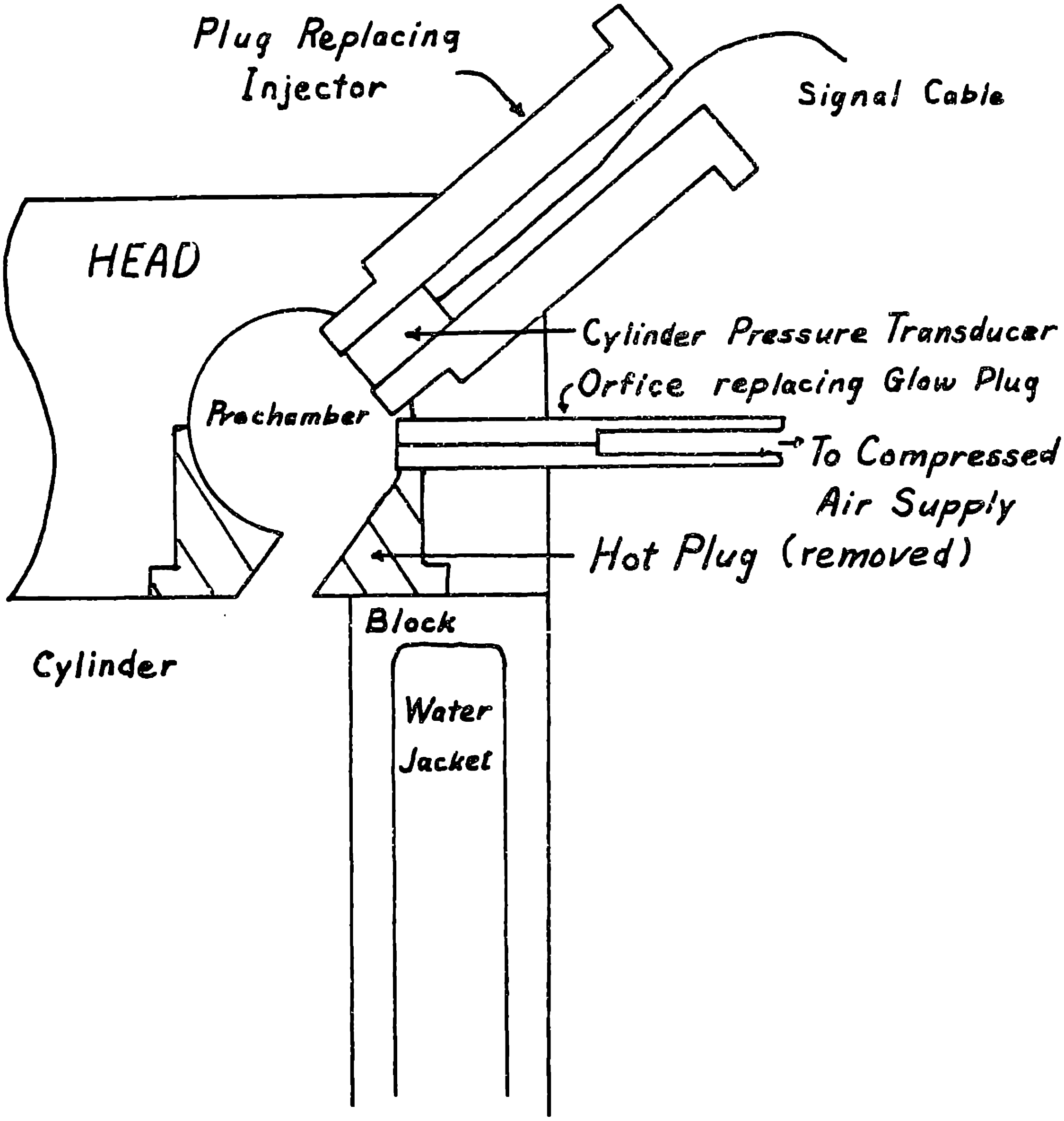

Figure 3.3: Cross Section of Combustion Chamber

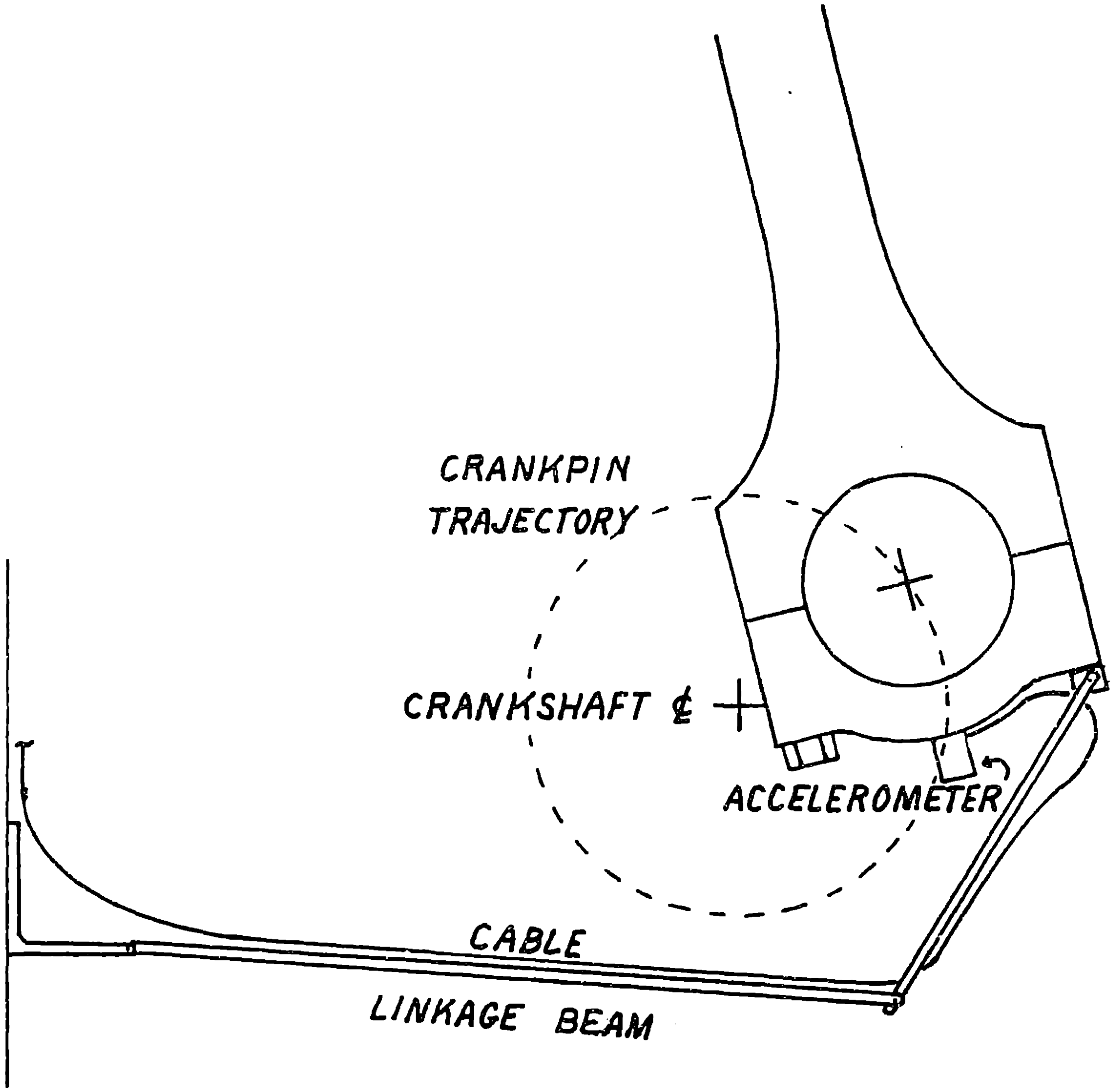

Figure 3.4: Two Beam Linkage to Carry Accelerometer Cable from Connecting Rod to Crank Case

baffle was also removed from the oil pan. The clearance between the bottom of the oil pan and the cable carrying linkage was minimal, so that it was necessary to prevent the accumulation of oil in the oil pan. A second oil pump was used to strip oil from the engine to an external sump where any entrained air would separate from the oil. The oil was then pumped into the engine as before.

3.2 Cylinder Wall and Block Surface Velocity

The engine was motored at 1000 rpm with a four bar mean cylinder pressure. The peak pressure indicated by the cylinder pressure transducer was 15 bar for a total of 19 bar. The piston operating clearance is approximately 0.004" (0.1 mm) which gives a piston slap impact at 8° after T.D.C. Simultaneous cylinder wall and block surface acceleration data was recorded on a Nagra SJ-IV tape recorder using the following procedure:

1. A 1.0 volt rms pure tone at ∿ 1 kHz was recorded simultaneously on each of the two channels for level calibration.
2. For each block surface point, cylinder wall acceleration data was recorded on Channel I and block surface acceleration data on Channel II.

Signal conditioning was identical to that described in Chapter 2 for the mobility data. This data was used to compute velocity energy spectra and velocity ratios using the algorithm described in Appendix C. The velocity energy spectra are averages of data from ten more impacts and are presented in dB re 1 $\frac{(\mathrm{m/sec})^2}{\mathrm{Hz}}$ or more explicitly, for the average impact:

$$\int_{-\infty}^{\infty} v^2(t)\,dt = \int_{0}^{\infty} V(f)V^*(f)\,df$$

where $v(t)$ is the time history of the average response to a piston slap impact (and therefore a signal with finite energy), and $V(f)V^*(f)$ is the velocity energy spectrum. Typical velocity spectra are shown in Figs. 3.5 and 3.6 for the cylinder wall and block surface, respectively. Background noise levels are included on the same plots. Background noise was measured by motoring the engine without pistons. Interpretation of the data is discussed in Chapter 4.

3.3 Connecting Rod Vibration

Simultaneous connecting rod big end and block surface acceleration data was recorded using the same procedure as described in Section 3.2. The connecting rod and block surface acceleration time history is shown in Fig. 3.7. It

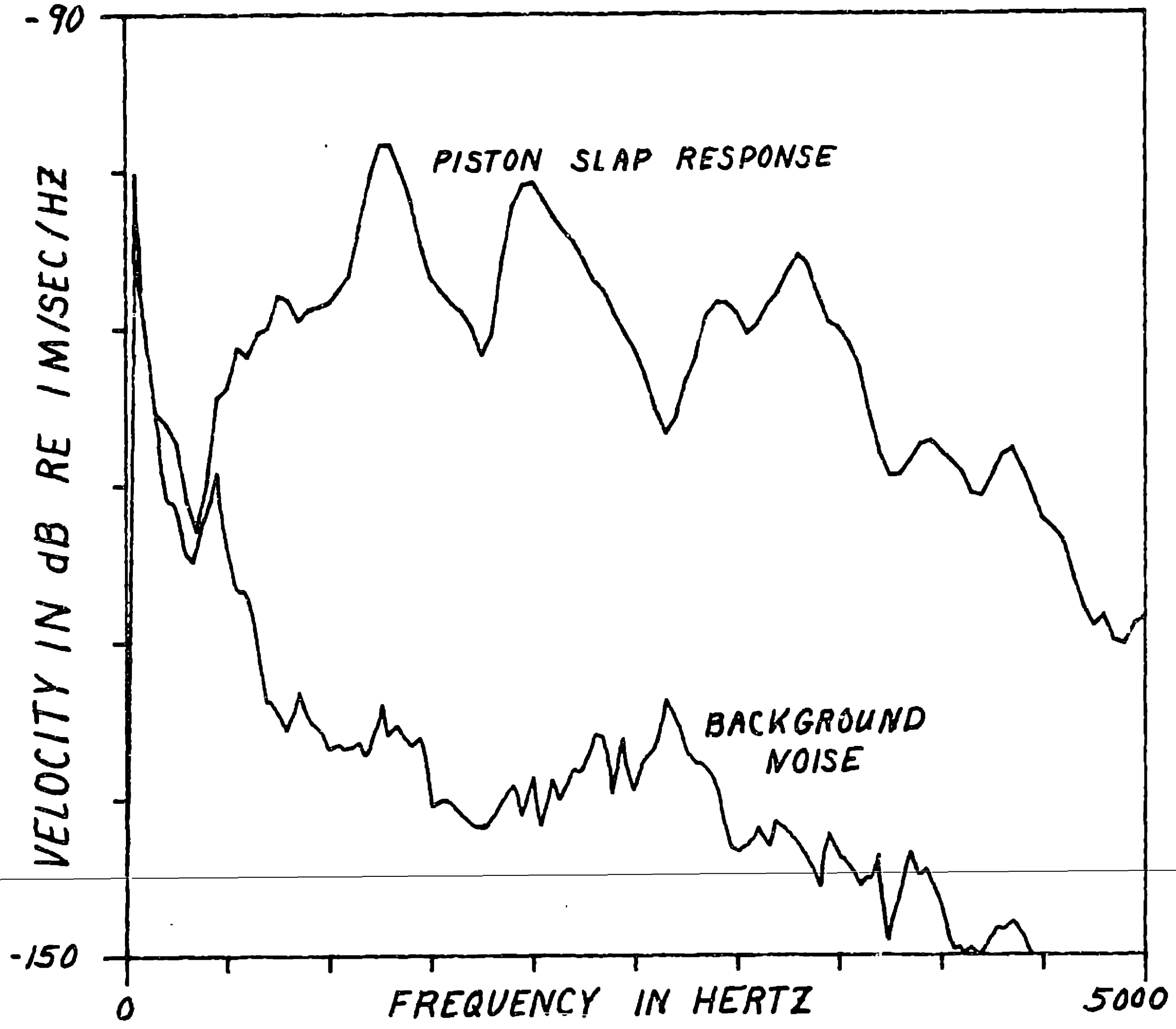

Figure 3.5: Background Noise Level, Cylinder Wall

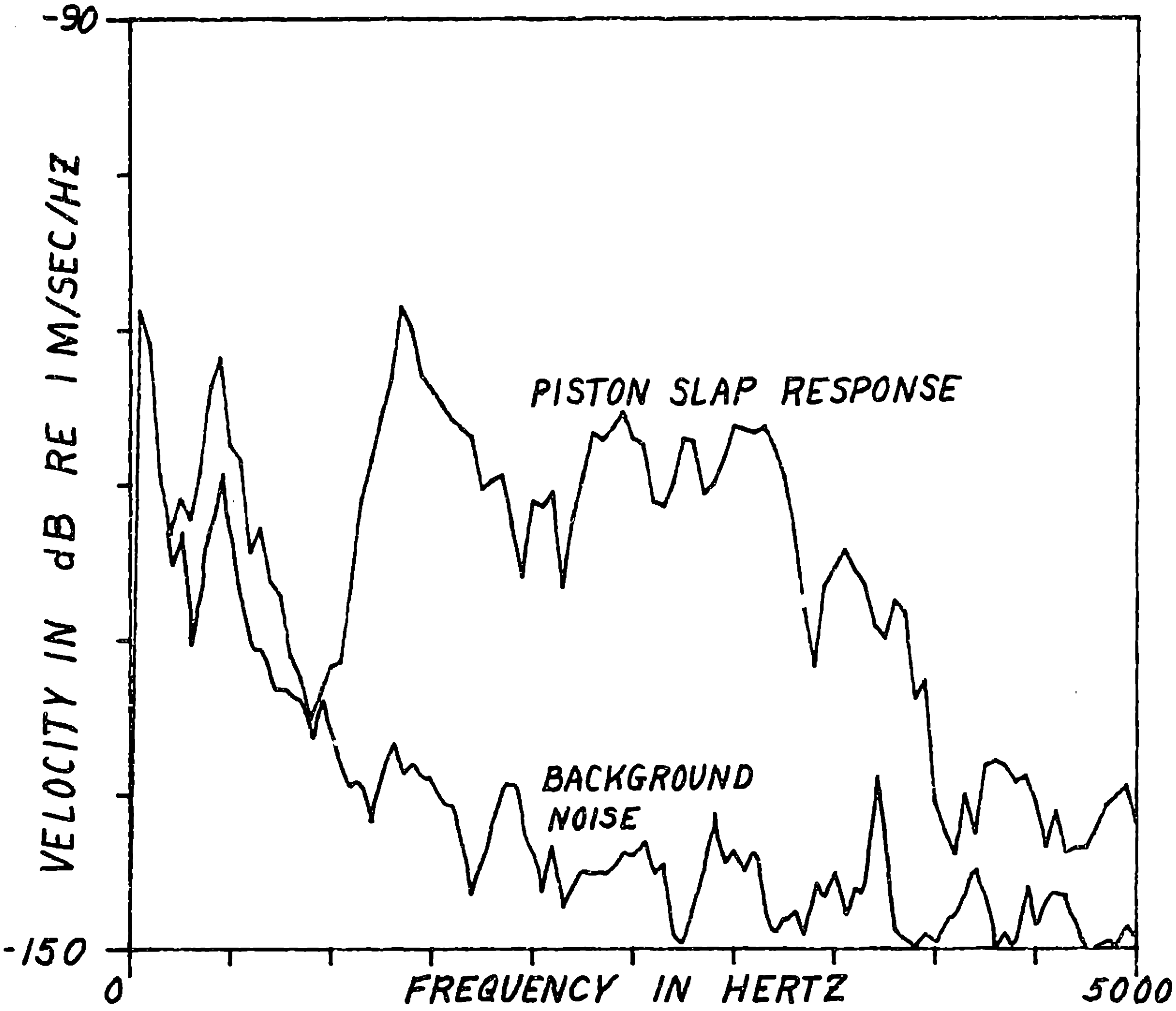

Figure 3.6: Background Noise Level, Block Surface

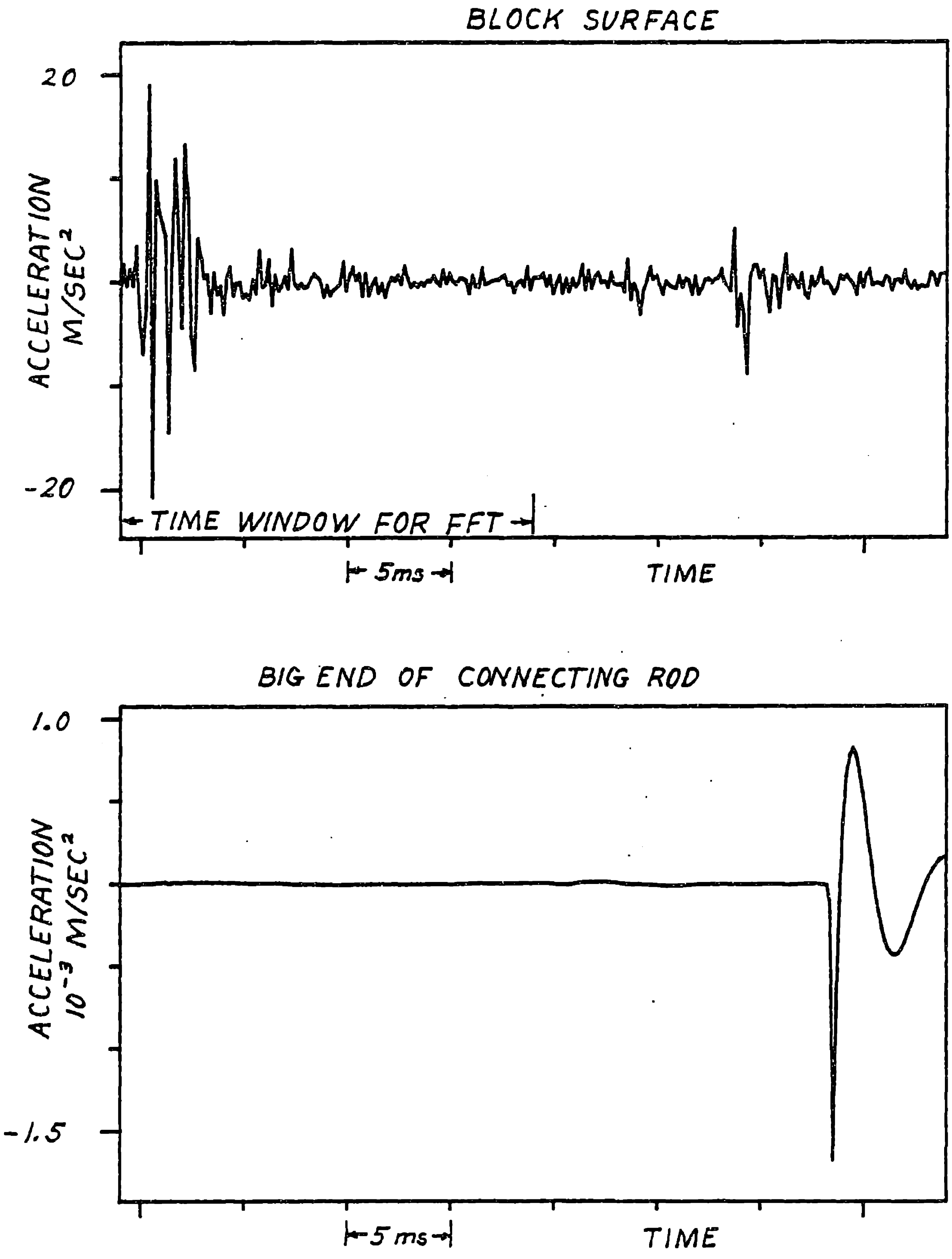

Figure 3.7: Block Surface/Connecting Rod Big End Acceleration; Motored Engine Data

is readily seen that the piston slap impact does not cause significant longitudinal vibration of the connecting rod. Relatively minor impacts are discernable at bottom dead center (note scale). These impacts are due to a change in direction of the axial load on the connecting rod. The block surface acceleration time record shows no corresponding impacts, so these impacts are apparently not important sources of noise.

CHAPTER FOUR: MODEL FOR PISTON SLAP

4.1 Lumped Parameter Models for Piston and Cylinder Wall

Simple lumped parameter models were constructed which would predict the measured drive point mobilities of the piston and cylinder wall in the frequency range of interest. For piston slap, this frequency range is approximately 500 Hz to 3000 Hz. Below 500 Hz combustion noise is dominant, assuming adequate intake and exhaust silencing [28]. Above 3000 Hz, A-weighting reduces the contribution to overall sound power.

The cylinder wall can be adequately modeled as a linear spring. Figure 4.1 shows the magnitude and phase of a $1.58*10^8$ nt/m spring compared with the measured drive point mobility of the cylinder wall. Agreement is excellent between 500 and 2500 Hz. The behavior of the cylinder wall in this frequency is locally determined since it shows no influence of modal resonances of the block. The zero at 300 Hz is due to the mass of the engine block ($\sim$90 Kg), and resonances below that frequency are rigid body modes of the engine on its stand.

The drive point mobility of the piston (Fig. 2.3) is substantially more complex. This behavior is modeled by a rational polynomial transfer function with four poles and

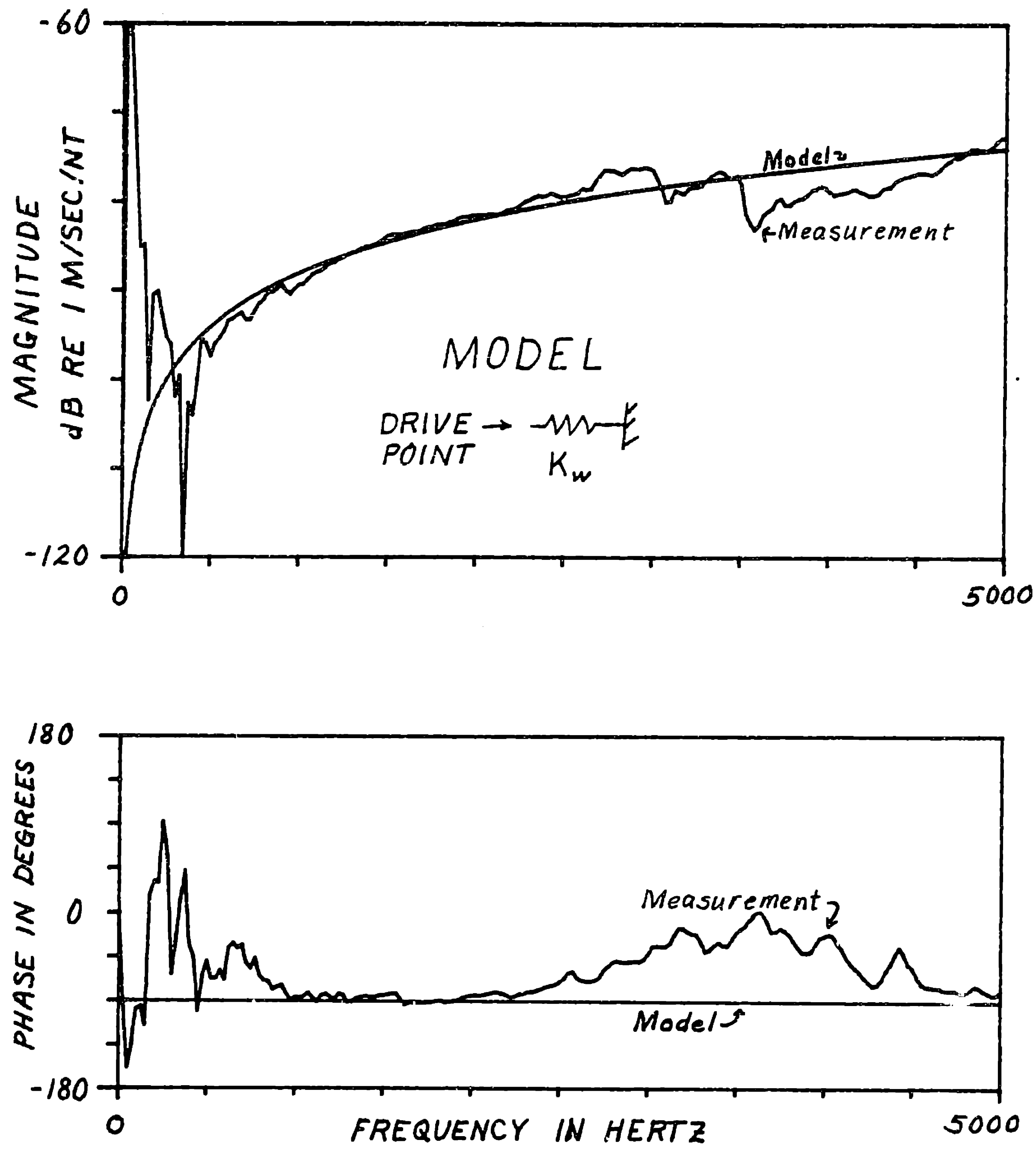

Figure 4.1: Drive Point Mobility of Cylinder Wall Comparison of Measurement and Model

four zeroes as listed in Table 4.1. A lumped parameter model using two masses and two springs is synthesized which has the desired drive point mobility. This model is shown in Fig. 4.2. The drive point mobility of the model is shown in Fig. 4.3. The measured drive point mobility is included for comparison. Although no dashpots are shown explicitly in the model, the zeroes and poles at finite frequency have nonzero real parts to give a small amount of damping. As is common practice when dealing with physical systems with small damping, the actual damping mechanism is not regarded as important. Damping is added in a mathematically tractable way, which in this case involves choosing the finite poles and zeroes to be in the right half of the s-plane in complex conjugate pairs. In this way, the system response is guaranteed to be finite and causal. The masses and springs in the model have important physical significance which will be discussed.

The first important feature in the measured drive point mobility is the complex conjugate pair of poles at 1600 Hz. Such a pair in a drive point mobility represents a free resonance of the system. By measuring acceleration at different points on the piston and connecting rod, it was determined that this resonance is a bending mode of the connecting rod. This bending mode will later be seen to play an important role in the transmission of piston slap induced

TABLE 4.1

POLES AND ZEROES OF PISTON-CONNECTING ROD DRIVE POINT MOBILITY

$$Y(f) = Y_0 \frac{(s-z_1)(s-z_1^*)(s-z_2)(s-z_2^*)}{(s-p_1)(s-p_2)(s-p_2^*)}$$

$$s = i2\pi f$$

$$p_1 = 0$$

$$p_2 = 2\pi(-100 + i\ 1600)$$

$$z_1 = 2\pi(-65 + i\ 1500)$$

$$z_2 = 2\pi(-200 + i\ 2900)$$

$$Y_0 = 2.8 \times 10^{-9}$$

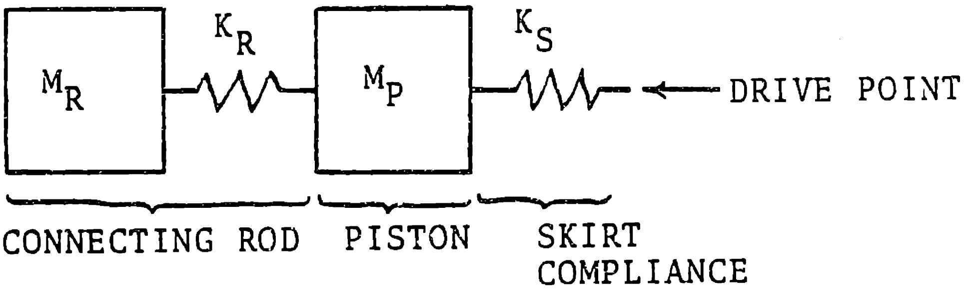

Figure 4.2: Lumped Parameter Model of Piston

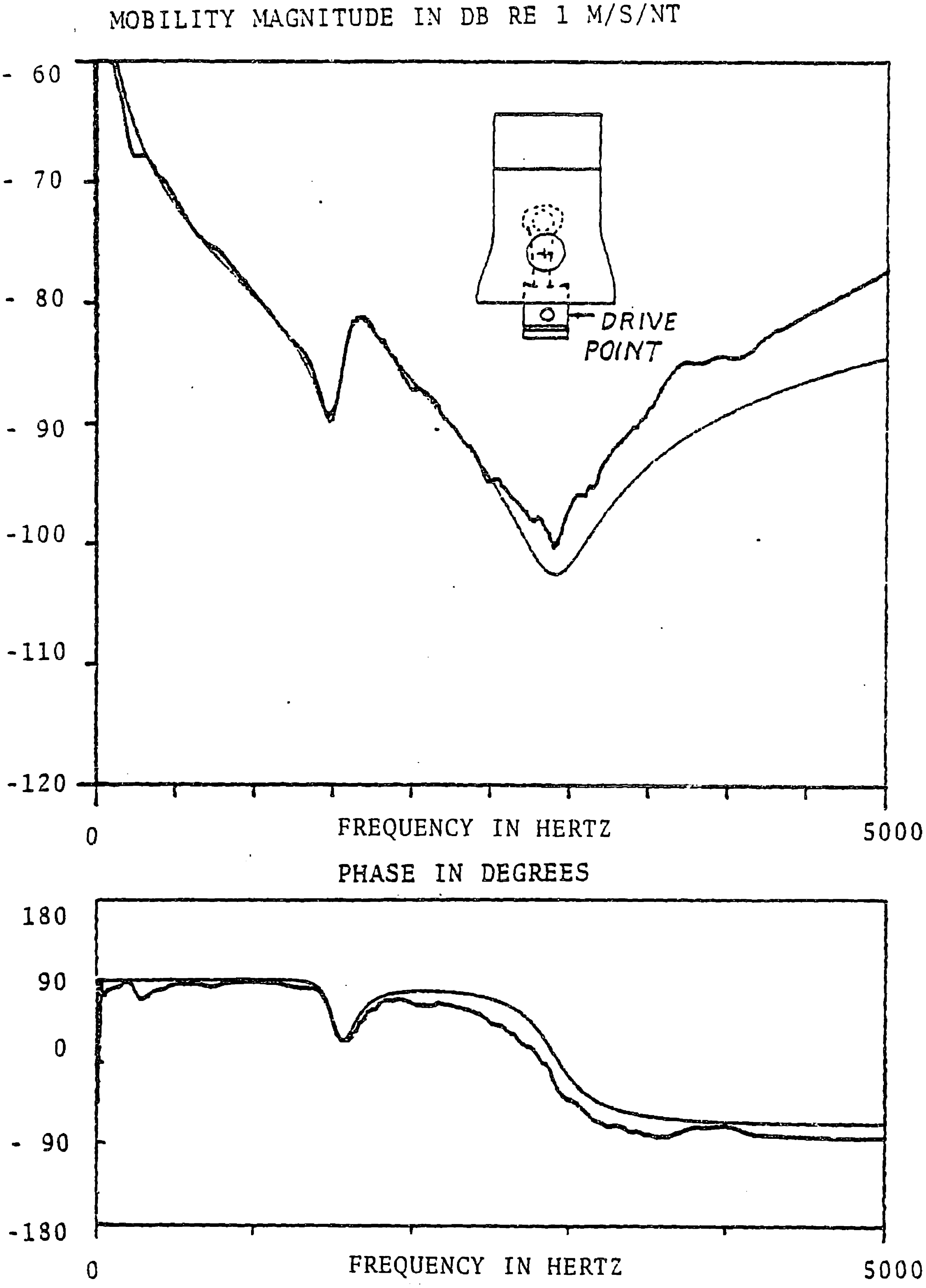

Figure 4.3: Comparison of Model with Measurement

vibration to the block surface. It also explains the zero at the same frequency in the spectrum of piston slap excited cylinder wall velocity.

The pole at zero indicates that the system is not tied to ground through a spring. Obviously, the displacement of the piston is constrained by the connecting rod being connected to the crankshaft, but this constraint does not appear in the linearized equations for small motions of the piston. Detailed calculations for the rigid body (low frequency) small displacement motion of the piston are shown in Appendix D. The inertia of the piston and small end of the connecting rod is represented by the total mass (M_p+M_r).

The pole as $f \to \infty$ indicates the structure is driven through a spring. The spring K_s in the model represents the local stiffness of the piston skirt. The model departs from the measurement at high frequency because there is a resonance above 5000 Hz which is not modeled. This resonance is the first resonant frequency of the piston. This was determined by isolating the piston and observing that the same resonance still appeared.

The mass M_R and spring K_R do not individually have physically significance. Together they represent the resonance of the connecting rod with the piston fixed.

The two pairs of zeroes at 1500 Hz and 2900 Hz are the two resonant frequencies of the model with the drive point fixed. In Appendix D it is shown that the total mass of the model equals the measured mass of the piston and small end of the connecting rod. Also, the free bending resonance of the connecting rod is computed using the Rayleigh-Ritz method which gives reasonable agreement with measurement.

4.2 Model of Piston-Cylinder Wall Iteration and Comparison with Measured Data

The interaction between the piston and cylinder wall has been observed in running engines using capacitive displacement gauges as well as accelerometers on the cylinder walls [13,29]. There is general agreement among researchers that once the piston makes contact, it remains in contact. There is no evidence of multiple impacts due to bouncing. Figure 4.4 shows a time record of cylinder wall vibration. It may be readily seen that there is an abrupt onset of vibration which decays to background vibration level.

For comparison, Fig. 4.5 shows the cylinder wall acceleration response (in time) to two force pulses one millisecond apart. The force was applied by striking the cylinder wall near the accelerometer with a PCB force gauge with a steel tip. The two sharp peaks are the impacts against the cylinder wall. The force gauge was not mounted

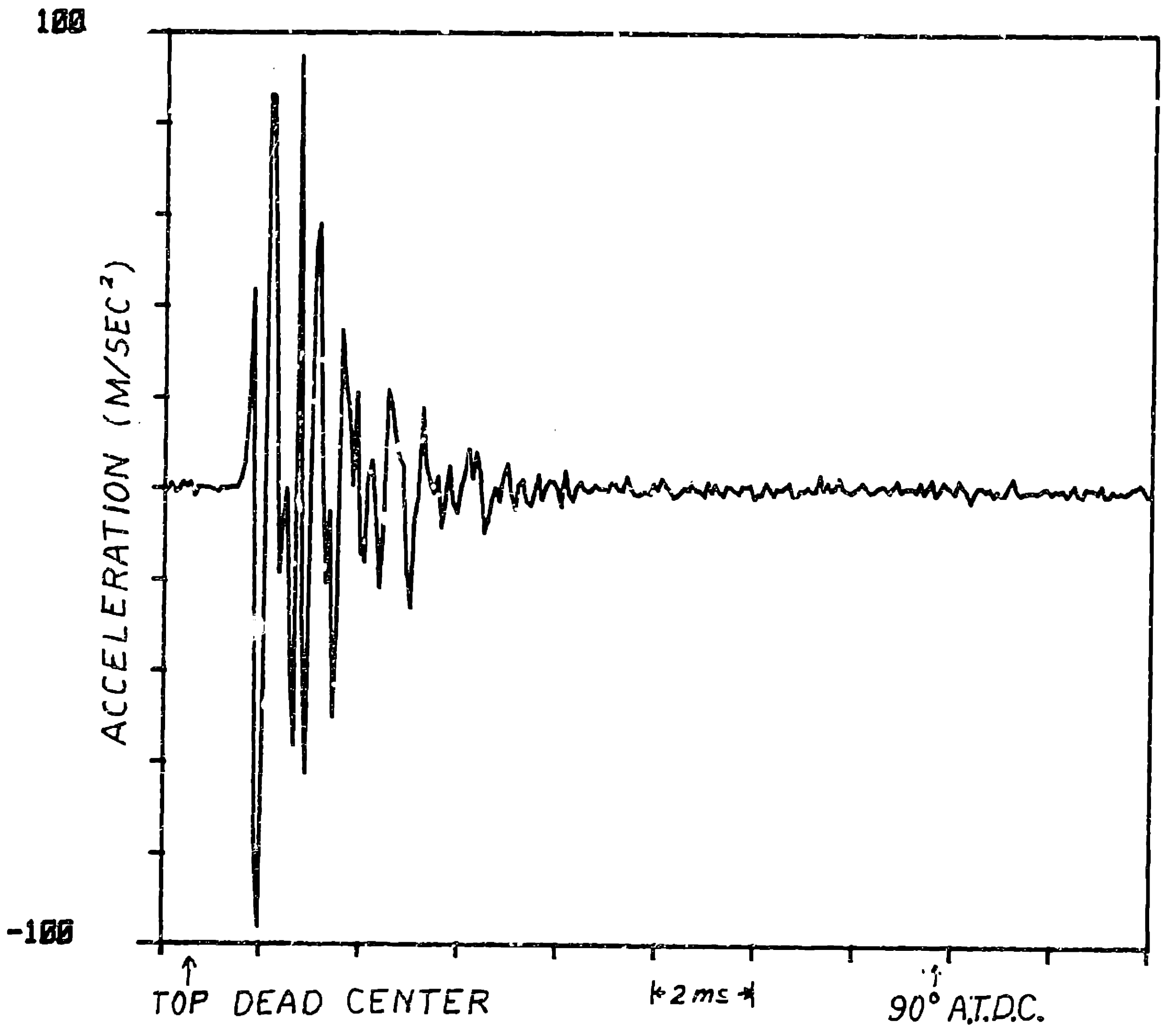

Figure 4.4: Cylinder Wall Acceleration

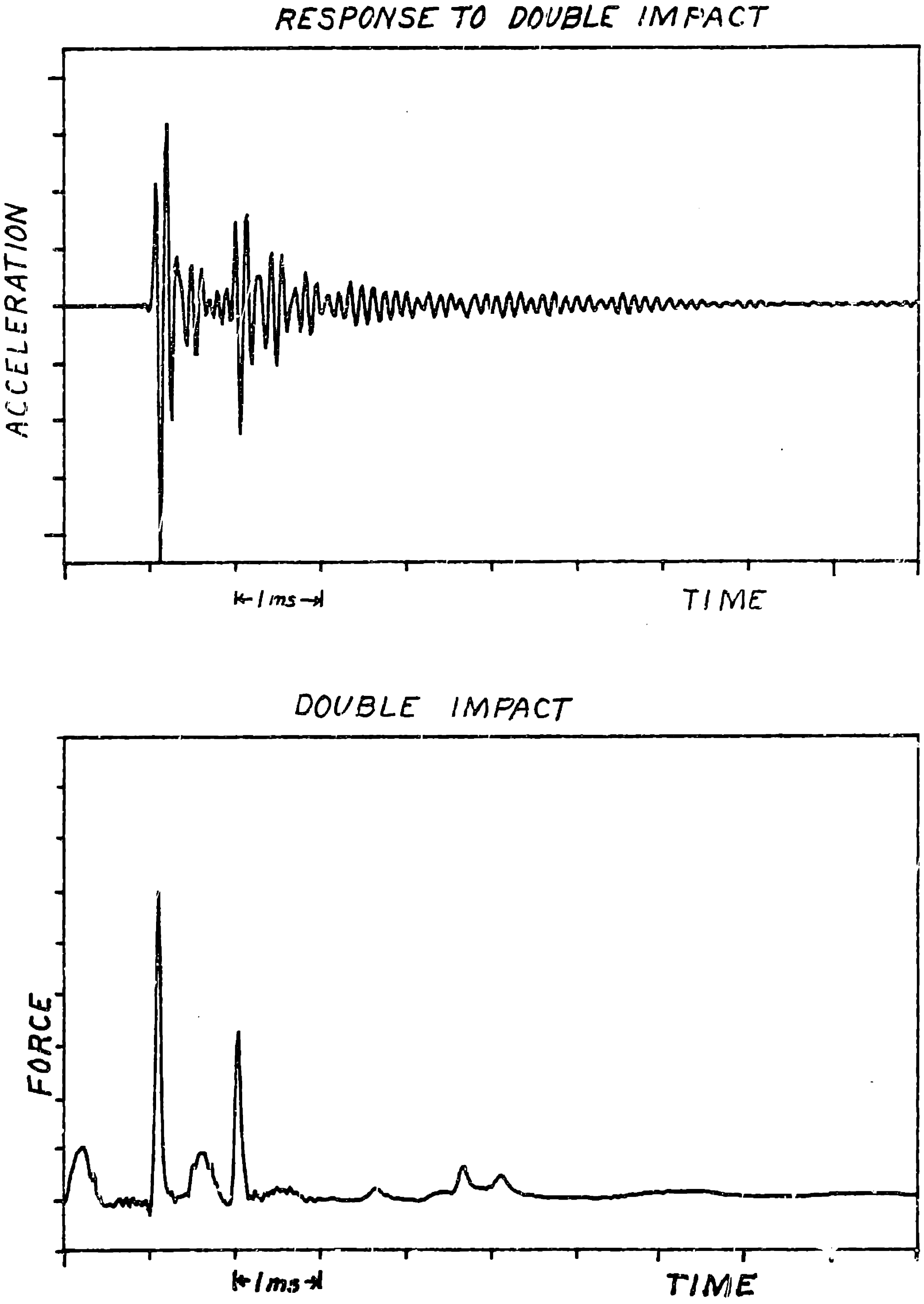

Figure 4.5: Double Impact and Acceleration Response of Cylinder Wall

on a hammer for this measurement; but instead it was held near the cylinder wall and struck with a separate hammer. This unconventional technique was used to generate multiple impacts. The broad peaks are spurious impacts on the back of the force gauge, and do not represent force applied to the cylinder wall. One may readily see both the effect of the two impacts and that the cylinder wall rings at about 8 kHz. Comparing Fig. 4.5 with Fig. 4.4 one may readily see that the response to piston slap is distinctly different. Apparently, the presence of the piston has an important effect on the cylinder wall vibration.

The piston-cylinder wall interaction is therefore modeled as shown in Fig. 4.6. The mass-spring model of the piston is attached to the spring model of the cylinder wall. Mass M_P is given an initial velocity V_0 equal to the translational velocity of the piston at time of impact. This velocity is calculated in Appendix E. The impulse response of the model is calculated for an impulse applied to M_P. The details of this calculation are found in Appendix D. Initial conditions of velocity V_0 and zero displacement at time t_0 are equivalent to applying an impulsive force of magnitude M_PV_0. This may be readily shown by conservation of momentum. Therefore, the properly scaled impulse response of the model represents the cylinder wall velocity.

Initial Conditions: $V_R = V_p = V_0$ at time of impact

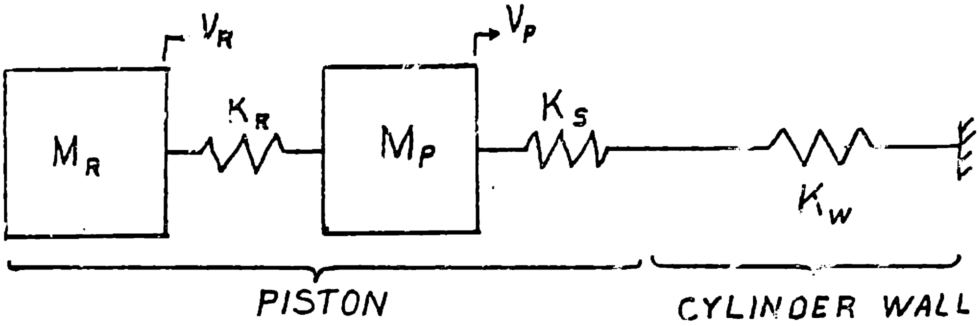

Figure 4.6: Model of Piston-Cylinder Wall Interaction

As mentioned in Section 2.2, access to the cylinder wall through the water jacket was not obtained at the exact location where the piston slap force is assumed to be applied. Fig. 4.7 shows the drive point mobility of the cylinder wall compared to the transfer mobility from the assumed impact point to the actual location of the cylinder wall accelerometer. These two curves are approximately the same shape and about 10 dB different in magnitude. This is modeled by a two spring velocity divider network shown in Fig. 4.8. This velocity divider has the same overall stiffness as cylinder wall.

This velocity divider is introduced into the model for the piston-cylinder wall interaction as shown in Fig. 4.9. The predicted and measured velocity spectra at the measurement point are shown together for comparison in Fig. 4.10. The agreement is good to 2500 Hz. Only two peaks are predicted, since there are only two degrees of freedom in the model.

4.3 Transmission of Vibrational Energy to Block Surface

As discussed in the introduction, most authors tacitly assume that path for piston slap induced vibration is the block structure. This is intuitive, since the cylinder wall is either an integral part of the block casting, or else it is a tightly fitting replacable liner.

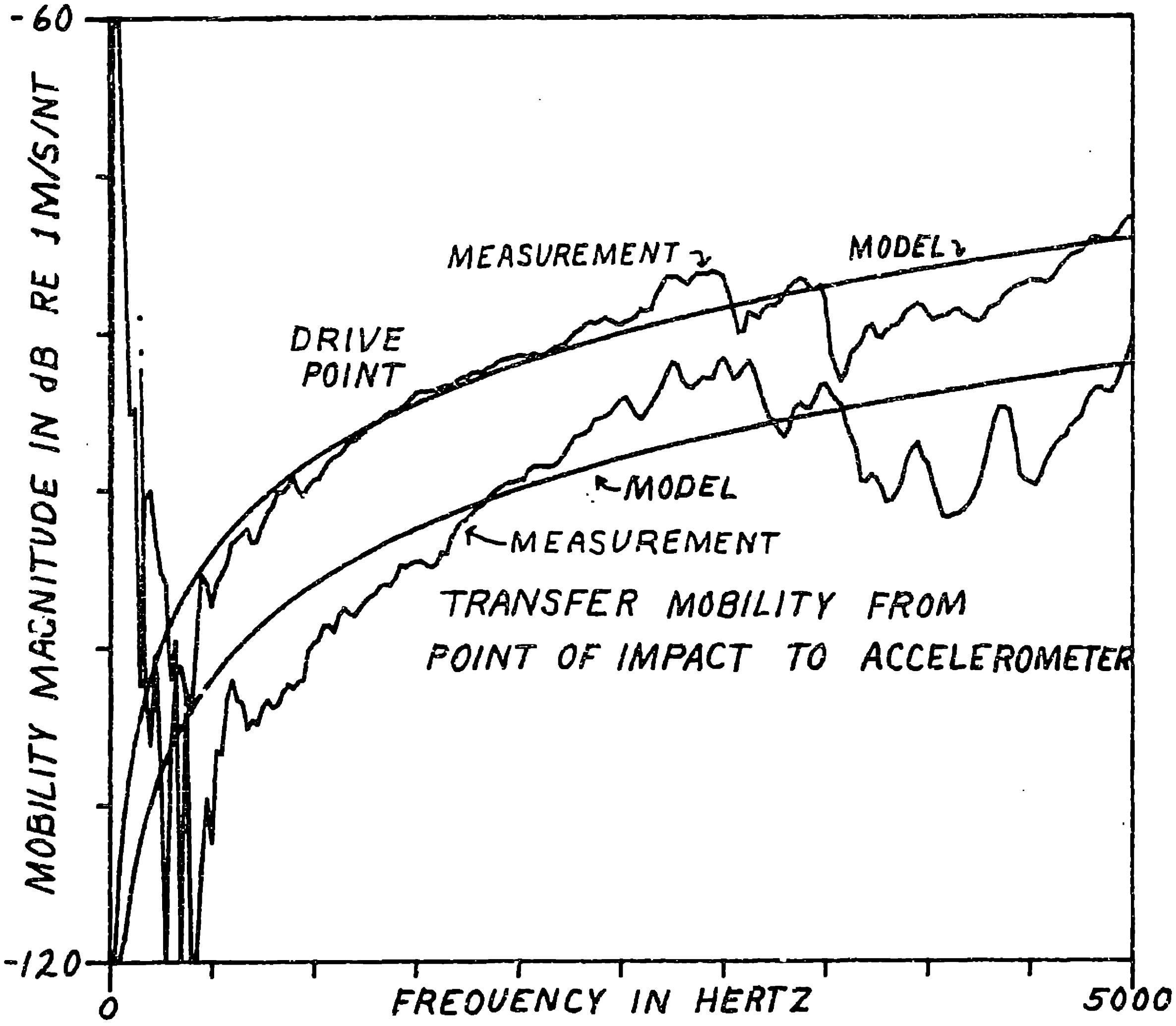

Figure 4.7: Cylinder Wall Mobilities, Comparison of Models with Measurements

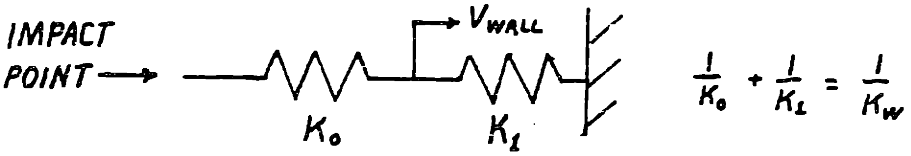

Figure 4.8: Model of Cylinder Wall

Initial Conditions: $V_R = V_p = V_0$ at time of impact

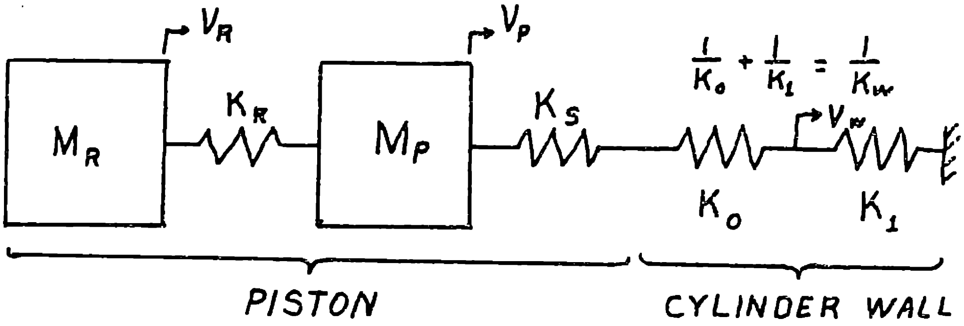

Figure 4.9: Model for Predicting Measured Cylinder Wall Vibration

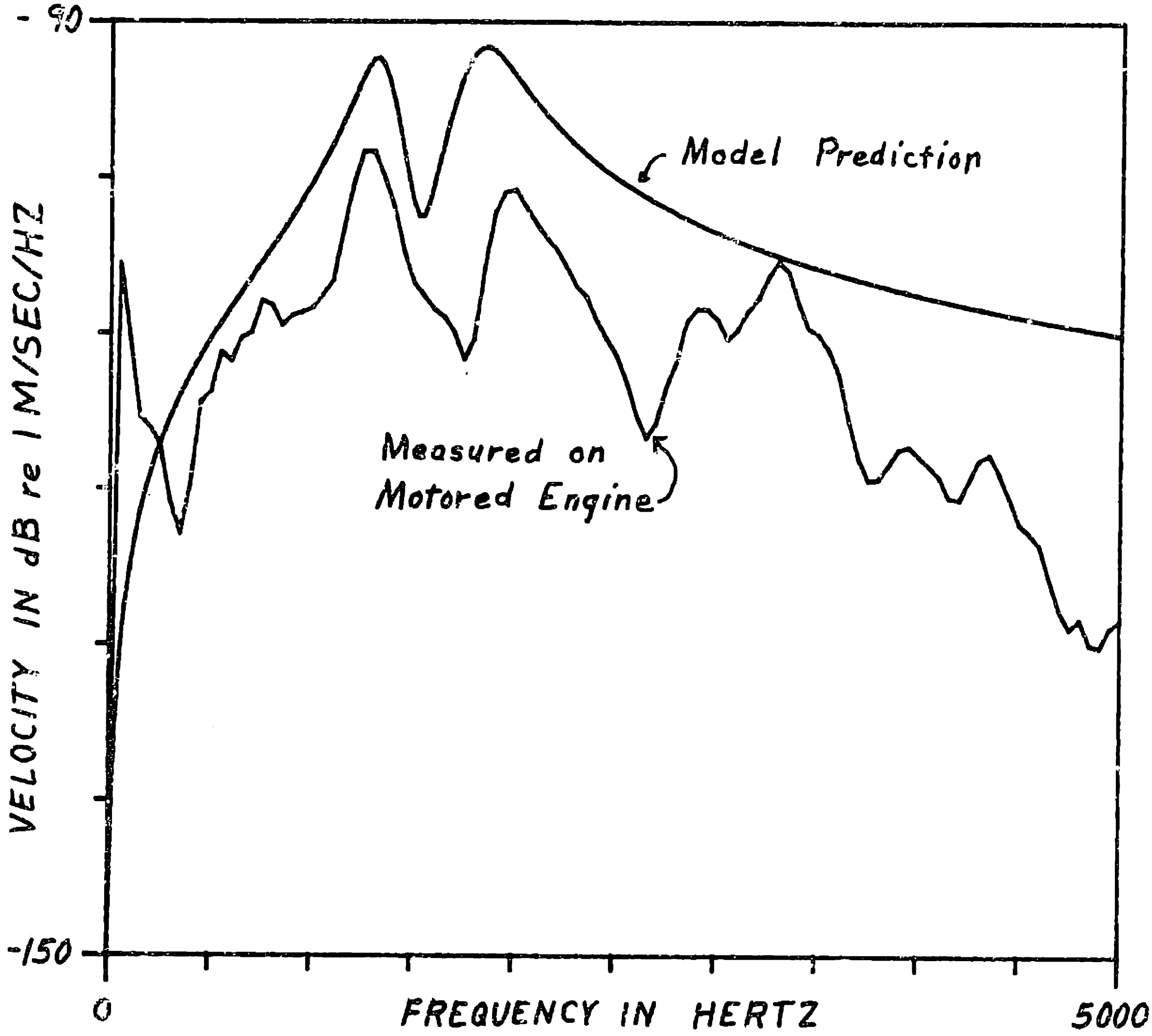

Figure 4.10: Comparison of Predicted and Measured Cylinder Wall Velocity Spectra

Nevertheless, transfer mobility measurements in Sections 2.3 and 2.4 indicate that the connecting rod plays an important role in vibration transmission. This section will examine both bending and axial vibration of the connecting rod, in the transmission of piston slap induced vibration. The comparison of velocity ratios as discussed in Appendix C will be used.

4.3.1 Axial Vibration of the Connecting Rod

Figure 4.11 shows the simultaneous acceleration records for the big end of the connecting rod and a representative point on the block surface. It is readily seen that any vibration at the big end of the connecting rod due to piston slap is insignificant compared to the background noise level. The burst of vibrational energy at 120° after TDC is due to an impact in the big end bearing as the axial force on the connecting rod changes direction. This impact can in turn be seen to cause no significant vibration at the block surface. Piston slap vibration data for a 20 millisecond time window (as indicated in Fig. 4.11) is taken for both connecting rod big end and block surface, and a ratio of velocity spectra is computed. The coherence for this transfer function for a ten record ensemble average is shown in Fig. 4.12. The low coherence indicates the signals are not related.

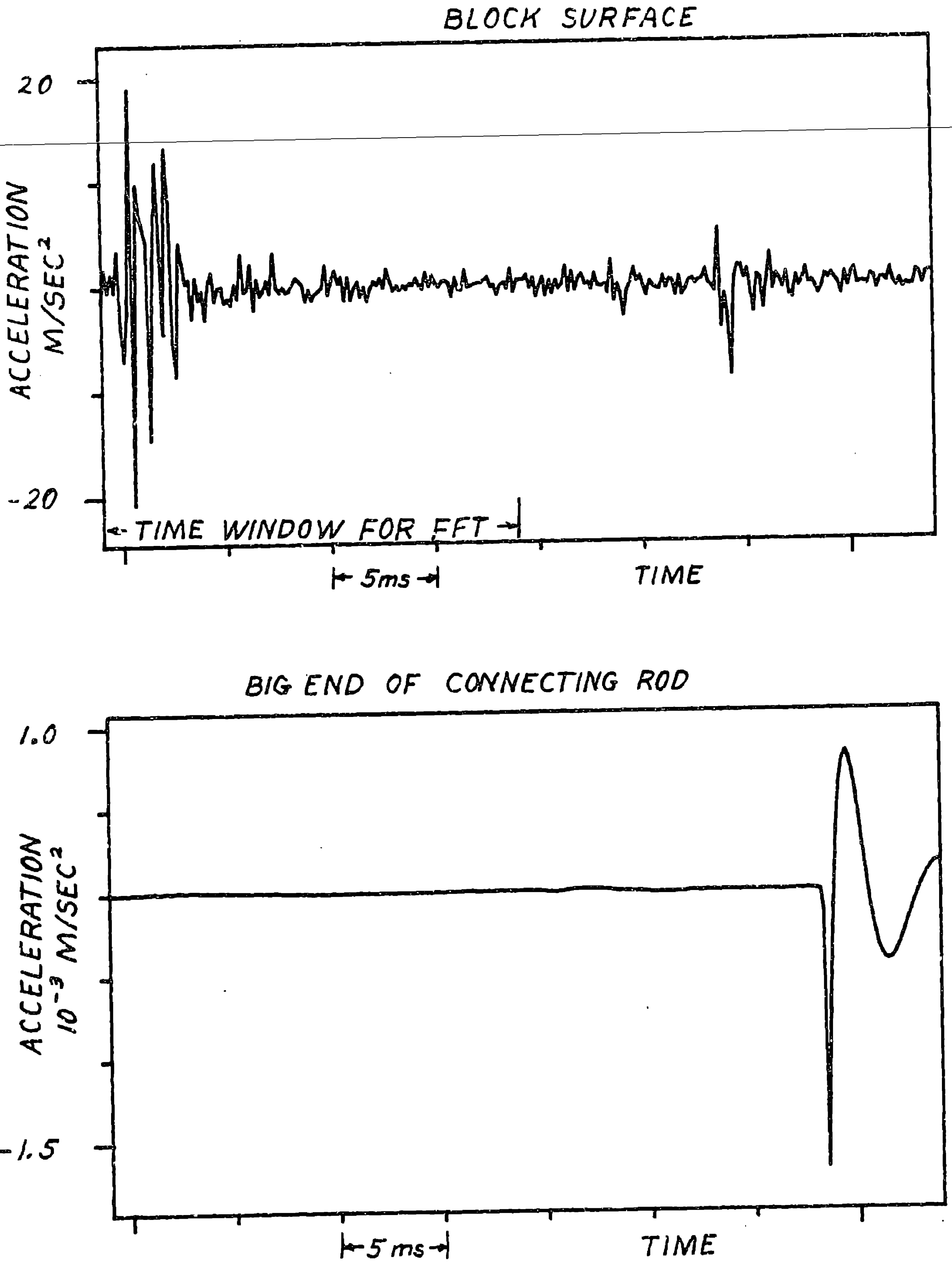

Figure 4.11: Block Surface/Connecting Rod Big End Acceleration; Motored Engine Data

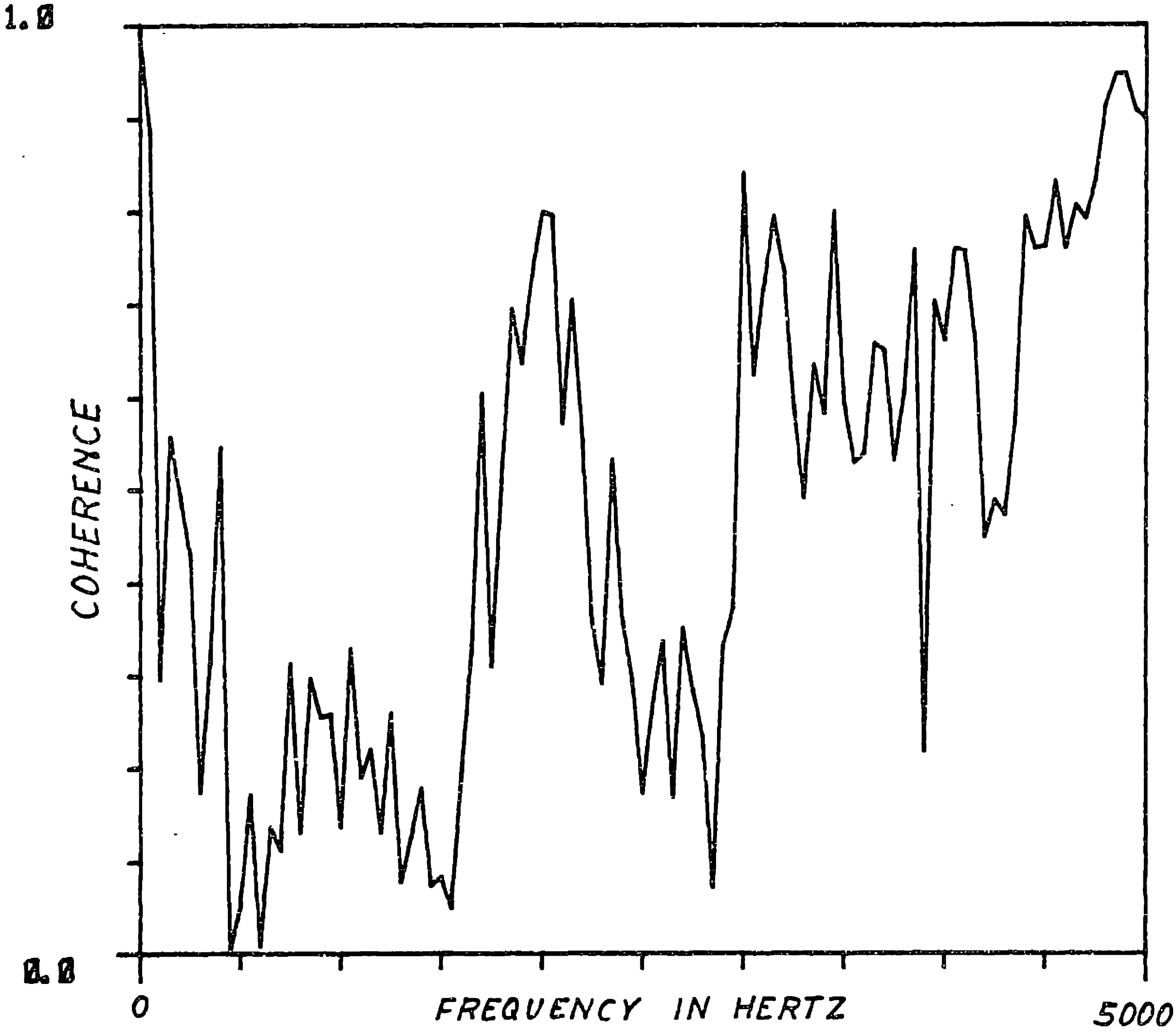

Figure 4.12: Coherence of Block Surface/Connecting Rod Velocity Ratio Data from Motored Engine

The velocity ratio is shown in Fig. 4.13 along with the two velocity ratios of Fig. 2.8. One may conclude from this data that axial vibration of the connecting rod contributes nothing of significance to the transmission path for piston slap induced vibration.

4.3.2 Bending Vibration of the Connecting Rod

Figs. 4.14 and 4.15 show the velocity ratio of block surface vibration versus cylinder wall vibration for two different points on the block surface. For comparison, the ratios of the measured transfer mobilities are shown on the same figures. In each figure, the upper plot shows the motored engine data compared to the combined block plus connecting rod path measured mobilities; while the lower plot shows the motored engine data compared with block path mobility alone. It is readily seen that in the 1000 to 2000 Hz frequency band, the combined path transfer mobility data gives an excellent prediction of the amount of vibrational energy actually transmitted to the block surface. The discrepancy between the motored engine data and the block path mobility data is almost entirely accounted for by the connecting rod path. The discrepancy at 2500 Hz is unaccounted for.

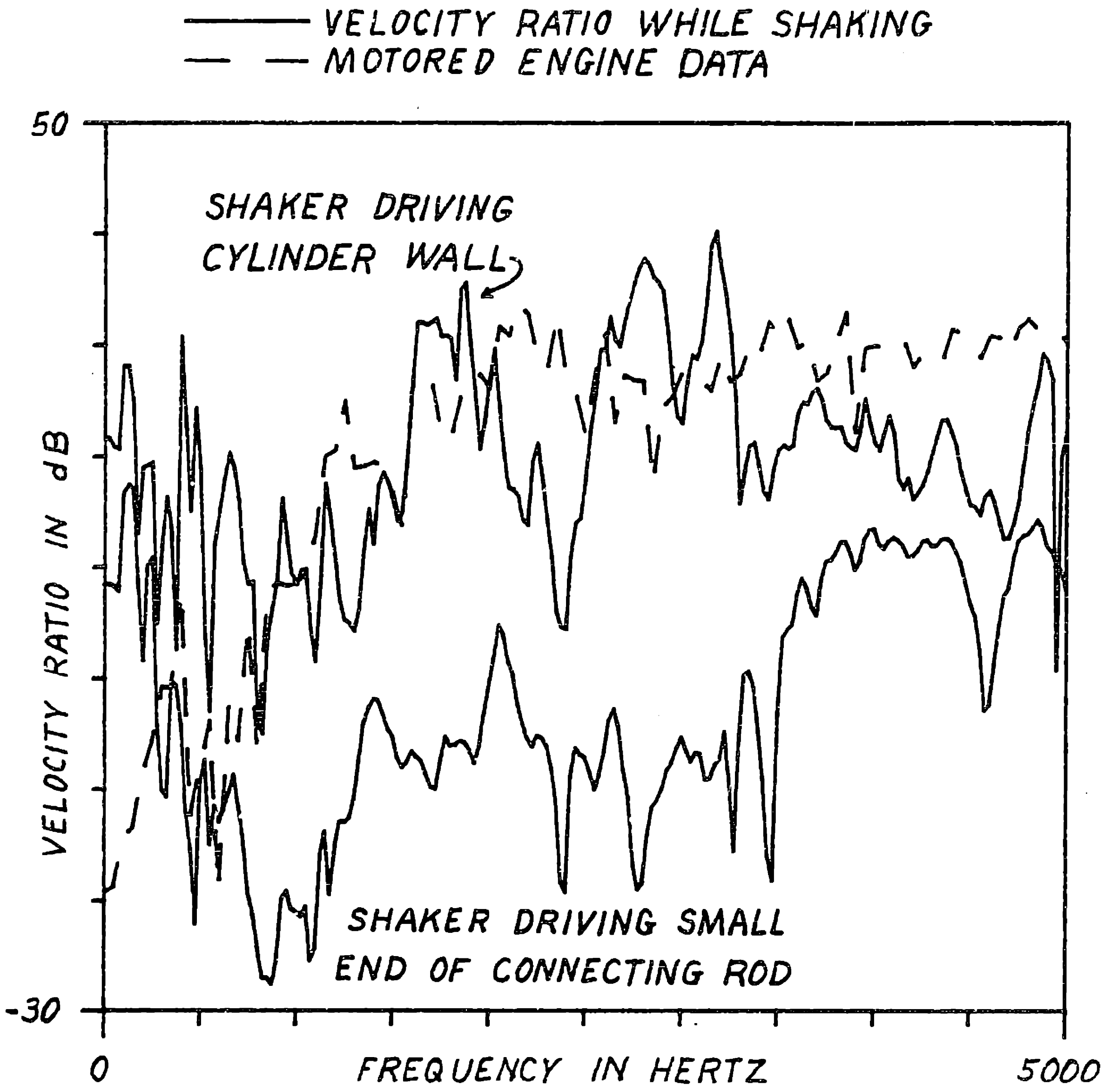

Figure 4.13: Velocity Ratios: Comparison of Motored Engine Data (Figure 2.8) with Velocity Ratio while Shaking

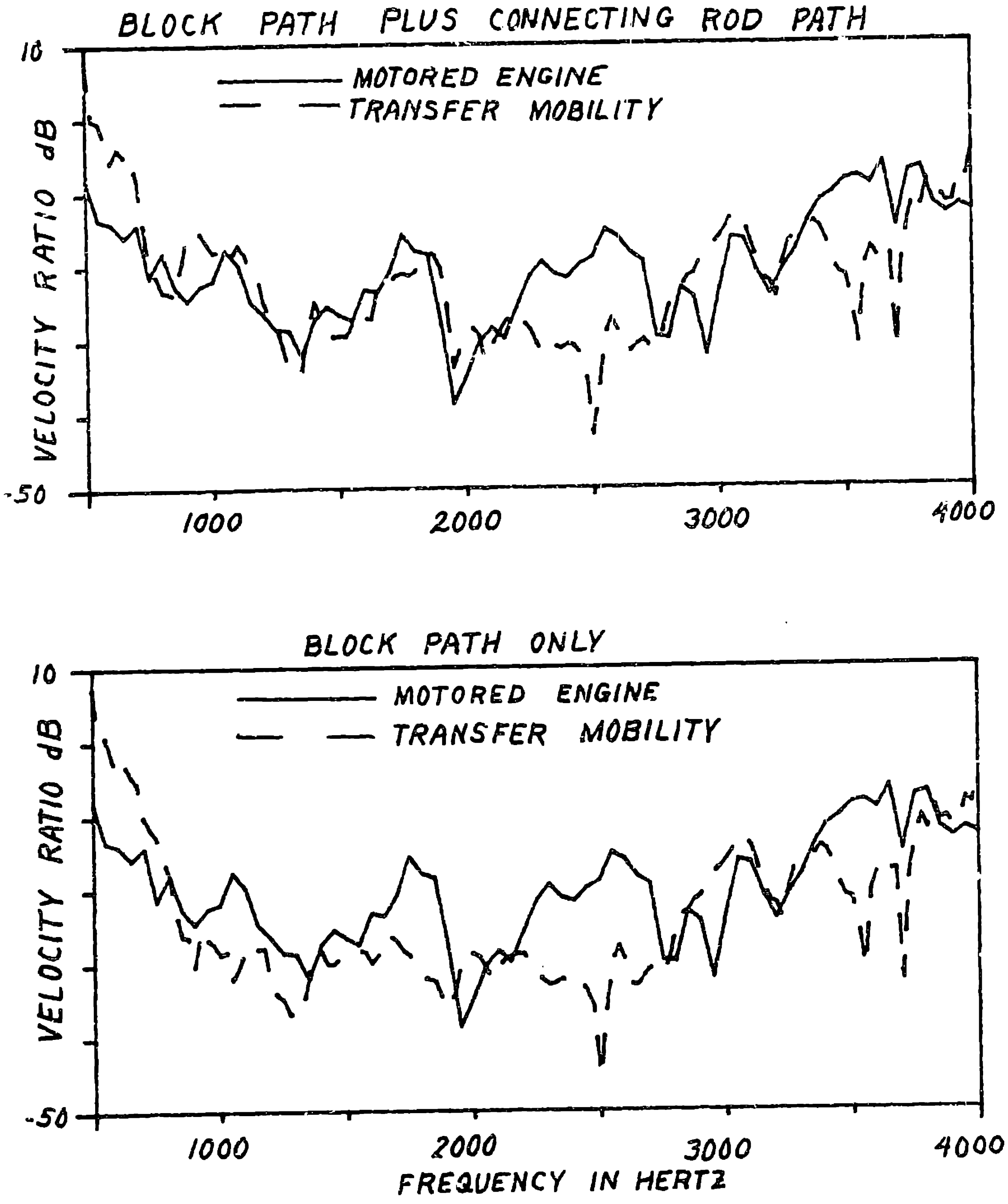

Figure 4.14: Comparison of Transfer Mobility Data with Motored Engine Data, Block Right Side

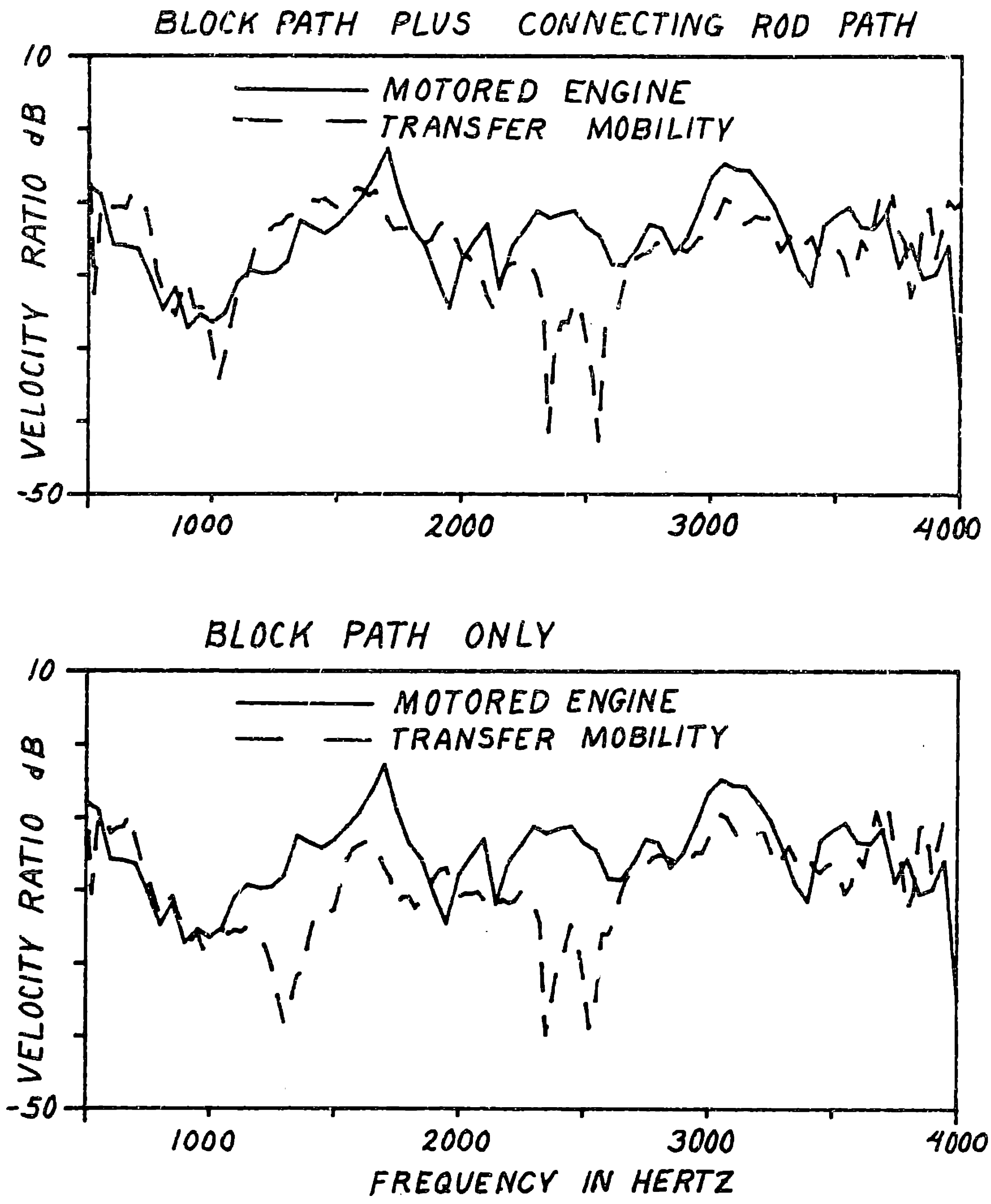

Figure 4.15: Comparison of Transfer Mobility Data with Motored Engine Data, Block Left Side

CHAPTER FIVE: CONCLUSIONS AND RECOMMENDATIONS

This research has resulted in new insights into the nature of piston slap. First, a simple two degree of freedom, pure translational model has been shown to give good qualitative predictions of piston slap induced cylinder wall vibration. Insofar as the model was generated from models of the piston and cylinder wall which individually account for the respective drive point mobilities, the role of each in piston slap may be said to be understood. It has been shown that the piston cannot be adequately modeled as a lumped mass.

Second, the connecting rod is shown to be an important path for piston slap induced vibration. This discovery would account for the observation reported by Zinchenko [1] that a probe of vibration levels on the block shows a peak near the top of the cylinder and another on the crankshaft casing. This path may not be important in vee-form engines with their more rigid block structure, but that should certainly be checked.

Finally, all mobility measurements made on the non-running engine have been compared to data taken on the motored engine. The mobility measurements provided important insight into the origins of piston slap, while the motored engine data provides important confirmation. This confirmation is of general value, since in the absence of data on a running engine or if there are multiple sources of equal importance, future researchers may use information from mobility measurements with confidence.

5.1 Conclusions on the Significance of Measured Mobilities

Much valuable information has been obtained from the mechanical mobility measurements made during this research program. A number of major simplifying assumptions were made in order to be able to draw conclusions from the measured mobility data. These assumptions were:

1. The engine structure is linear, time invariant, passive, and bilateral.
2. The measured discrete point applied forces and discrete point velocities adequately described an inherently continuous system.
3. Mobility measurements on a nonrunning engine adequately describe vibration transmission on a motored (or running) engine.
4. The piston-cylinder wall interaction can be adequately described by point contact.

The first assumption was addressed by making careful reciprocal pairs of transfer mobility measurements.

The excellent agreement achieved indicates that this assumption is valid. The second assumption may be considered a matter of degree. Obviously, if enough points are used and enough data is taken, the system can be described with arbitrary accuracy. The small number of points chosen for block surface velocity measurements were not intended to describe the entire engine, since such a result would be specific to the Isuzu C240. Rather, the intent was to see if measured transfer mobility data could be used to predict the transmission of piston slap vibration. The results in Chapter 4 are clearly positive. This is fortunate, since force is relatively easy to measure while no good experimental technique exists yet for measuring moments. The accuracy achieved is adequate for ranking of transmission paths which are different by 10 to 15 dB.

The third assumption is of upmost interest to anyone concerned with machinery noise. The extent to which non-running experimental data may be used to infer vibration transmission on a running machine will determine the extent to which relatively easy and safe measurements on non-running machines may be substituted for relatively difficult or perhaps impossible measurements on running machines. Here, the frequencies of interest (> 1000 Hz) are high compared to the rate of change of the engine configuration

(1000 RPM) so that one is assuming substantially quasi-static behavior. The time records of vibration acceleration show that most of the energy of a single piston slap event is contained in a time window of about 30° of crank angle. A much more difficult problem occurs when the frequencies of interest are not large compared to the running speed of the machine. This is an area of current research in machine dynamics, but not a significant problem in this study of piston slap.

The fourth assumption is clearly the weakest. The piston rotates as it crosses the cylinder due to the separation between its center of gravity and the center of the piston pin. This rocking has been predicted analytically and observed in running engines. As seen in Section 4.2, however, a pure translational model gives a reasonably good qualitative prediction of the cylinder wall velocity spectrum.

5.2 Recommendations for Reducing Piston Slap Noise

The discovery of the connecting rod path for piston slap induced vibration points to a possible new approach to reducing piston slap noise. As was pointed out in Section 1.3.1, proposals to date are aimed at reducing the intensity of the impact. Isolation of the cylinder liner for an engine of wet liner construction (which is typical of heavy duty engines) would only be effective at high frequencies. One expects that the connecting rod bending resonance would be lower in frequency for larger engines, so the actual upper frequency limit of the connecting rod path must be determined for each engine design. It may prove to be easier to achieve isolation in a limited frequency range rather than throughout a broader range.

At low frequencies, one would treat the connecting rod path. The resilient main bearings proposed by DeJong [23] for isolation of combustion induced vibration would be an obvious first step. Unfortunately, in the five years since they were proposed, no results have yet appeared in the open literature. Since it is connecting rod bending which is important for piston slap, the possibility of using a connecting rod design with radically different bending stiffness should be investigated.

5.3 Further Research

As mentioned in Section 5.1, the assumption of pure translation of the piston is inherently weak. It is well known that rotation is a significant component of the piston motion through the operating clearance at top dead center. This rocking is due to the separation between the piston center of gravity and the piston pin center. It has been described analytically as well as observed in running engines [12,5]. If rocking of the piston were taken into account, a three degree of freedom model would result which would predict three peaks in the cylinder wall vibration spectrum. It would be necessary to estimate the effective rotary stiffness of the piston in contact with the cylinder wall. It would also be necessary to evaluate the effect of the induced moment on the cylinder wall. Since it does not appear that this research would yield important improvements in piston slap noise, the author feels that future research towards reducing piston slap noise should first be aimed at treating the two transmission paths.

REFERENCES

1. Zinchenko, V.I., *Noise of Marine Diesel Engines*, Sudpromgiz, 1957. (an abstract of this book in English was prepared at BBN supported in part by contracts with MIT).

2. Evans, A.F., Contribution to discussion of paper by Bradbury, C.H., "The Measurement and Interpretation of Machinery Noise with Special Reference to Oil Engines", *Proc. Inst. Mech. Eng.*, 1952, Vol. 1B, No. 1 pp 1-18.

3. Mercy, K. R., "Analysis of the Basic Noise Sources in the Diesel Engine", ASME Paper No. 55-OGP-4 , 4 March 1955.

4. Bradbury, C. H., "Some Practical Aspects of Engine Noise", Congres International des Moteurs a Combustion Interne (CIMAC) Paper B-4, The Hague, 1955.

5. Meier, A., "Zur Kinematik der Kolbengerausche" (The Kinematics of Piston Noises) Automobiltechnische Zietschrift, Vol. 54, No. 6, June 1952, pp 123-128.

6. Austen, A.E.W. and Priede, T., "Origins of Diesel Engine Noise", *Proceedings of the Inst. of Mech. Eng. Symposium on Noise and Noise Suppression*, London, 1958.

7. Ross, D. and Ungar, E. E., "On Piston Slap as a Source of Engine Noise", ASME Paper 65-OGP-10, April 4-8, 1965.

8. Haddad, S. D., Pullen, H. L. and Priede, T., "Relation Between Combustion and Mechanically Induced Noise in Automotive Diesel Engines", 15th FISITA Congress, Paris, 1974.

9. Russel, M.F., "Recent CAV Research into Noise Emissions, and Fuel Economy of Diesel Engines," SAE Paper No. 770257, Feb-March 1977.

10. Ungar, E. E. and Ross, D. "Vibrations and Noise Due to Piston-Slap in Reciprocating Machinery", *J. Sound Vib.* (1965), *2* (2), 132-146.

11. Alvaraz, F. F., "Noise and Vibration Problems of Reciprocating Machinery," MSc Thesis, Dept. of Naval Architecture and Marine Engineering, MIT, May 1964.

12. Laws, A.M., Parker, D.A. and Turner, B., "Piston Movement as a Source of Engine Noise", Paper 1-29, *14th FISITA*, London, 1972.

13. Haddad, S.D. and Fortescue, P.W., "Simulating Piston Slap by an Analogue Computer", *J. Sound Vib.* (1977) *52*(1), 79-93.

14. Hempel, W., "Ein Beitrag zur Kenntnis der Seitenbervegung des Tauchkolbens," *Motortechnische Zeitschrift, V. 27*, No. 1, Jan. 1966, pp. 5-10.

15. Griffiths, W.J. and Skorecki, J., "Some Aspects of Vibration of a Single Cylinder Diesel Engine", *J. Sound Vib.* (1964) I (4), 345-364.

16. Ungar, E. E., Ross, D. and Alvarez, F. F. "Piston-Slap Noise in Reciprocating Machinery," Bolt Beranek and Newman, Inc., Report No. 1106, January 1964, Rev. 15, April 1964.

17. Steidle, W. and Wacker, E., "Kolbengerausche." *Automobiletechnische Zietschrfit, V. 77*, N. 10, Oct. 1975, pp. 293-298.

18. Haddad, S.D. and Howard, D.A., "Analysis of Piston Slap-Induced Noise and Assessment of Some Methods of Control in Diesel Engines," SAE Paper 800517, February 1980.

19. Pflaum, W., and Hempel, W., "The Distribution of Noise in Diesel Engines with Special Consideration of High-Pressure Turbocharging," Congres International des Moteurs a Combustion Interne (CIMAC) paper B-3, London, 1965.

20. Sander, W., Steidle, W., and Wacker, E., "Piston Movement and its Influence on Noise of Automotive Engines," *Diesel Engine Noise Conference, Proceedings P-80*, Society of Automotive Engineers, Detroit, February 26-March 2, 1979.

21. DeJong, R. G., and Manning, J.E., "Modeling of Vibration Transmission in Engines to Achieve Noise Reduction," (790360) *Diesel Engine Noise Conference, Proceedings P-80*, Society of Automotive Engineers, Detroit, February 26-March 2, 1979.

22. Oguchi, T., "Piston Slap Noise -- Its Transfer Through an Internal Combustion Engine," SM Thesis, Dept. of Mech. Eng., MIT, January 1979.

23. DeJong, R.G., "Vibrational Energy Transfer in a Diesel Engine," ScD Thesis, Dept. of Mech. Eng., MIT, August, 1976.

24. Okamura, H., "Experiments on the Transmission Paths and Dynamic Behavior of Engine Structure Vibrations. Parts I and II," *J. Acoust. Soc. Am., V. 67,* No. 2, Feb., 1980.

25. Ordubadi, A., "Component and Fault Identification in a Machine Structure Using an Acoustic Signal," ScD Thesis, Dept. of Mech. Eng., MIT, May 1980.

26. Haddad, S.D., and Pullen, H.L., "Piston Slap as a Source of Noise and Vibration in Diesel Engines", *Journal of Sound and Vibration* (1974) *34* (2) 249-260.

27. Baumesiter, T. (Editor-in-Chief) *Marks Standard Handbook for Mechanical Engineers,* Seventh Edition, McGraw-Hill, New York 1967.

28. Priede, T., "Some Studies into Origins of Automotive Diesel Engine Noise and its Control", *11th FISITA,* Munich, 1966.

29. Bendat, J.S. and Piersol, A.G., *Engineering Applications of Correlation and Spectral Analysis,* John Wiley & Sons, New York, 1980.

30. Den Hartog, J.P., *Mechanical Vibrations,* McGraw-Hill, New York 1956.

APPENDIX A: CALIBRATION OF THE IMPEDANCE HEAD

A Wilcoxon Model Z-602 impedance head was used as the force transducer for all the mobility measurements. The calibration procedure was primarily a useful way to gain familiarity with instrumentation and measurement techniques, since accurate values are given by the manufacturer. Nevertheless, the familiarity gained through this exercise is invaluable, and it provided an opportunity to make measurements that could be readily verified.

An impedance head is a device which is mounted between a shaker or other source of mechanical excitation and a structure which is to be vibrated. The impedance head contains two piezoelectric transducers, one which measures force and another which measures acceleration (see Fig. A1).

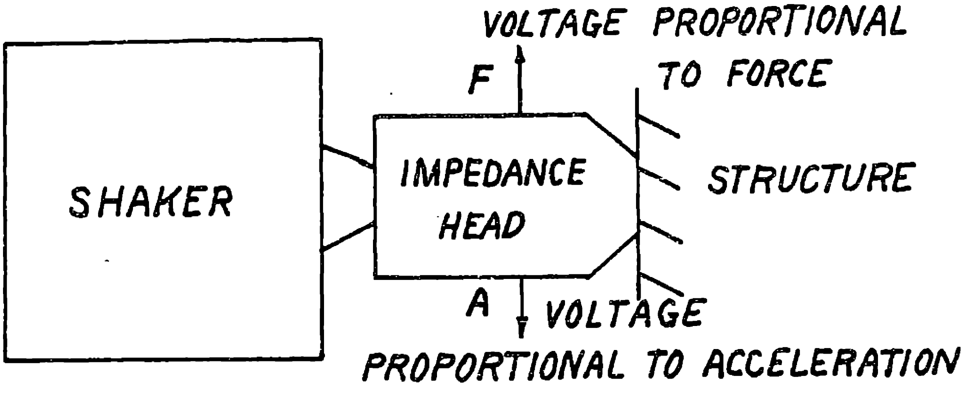

Figure A.1: Model of Ideal Impedance Head

Ideally these two quantities would be measured at the point where the impedance head contacts the test structure, but the sensitive elements must be packaged in a robust housing. The housing has finite mass and compliance, some of which lies between the sensitive elements and the structure being measured. This can be modeled, in the frequency range of interest, as an ideal impedance head driving the test structure through a mass and spring in series as shown in Fig. A2.

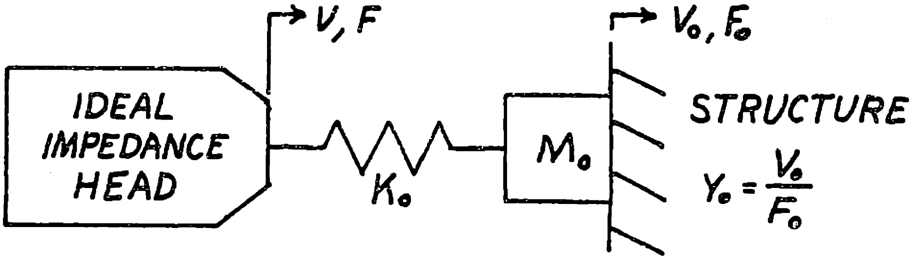

Figure A.2: Model of Behavior of Real Impedance Head

In Fig. A2, the indicated drive point mobility is $Y = \frac{V}{F}$, while Y_0 is the actual drive point mobility of the structure. If V_0 is the actual drive point velocity spectrum, and F_0 is the actual drive point force spectrum,

$$F_0 = F + i\omega\, M_0 V_0 \qquad \text{(A1)}$$

$$V_0 = V + \frac{i\omega}{K_0}\, F \qquad \text{(A2)}$$

or

$$\frac{F}{F_0} = 1 - i\omega\, M_0 \frac{V_0}{F_0} = 1 + \frac{Y_0}{Y_M} \tag{A3}$$

$$\frac{V_0}{V} = 1 + \frac{i\omega}{K_0}\, \frac{F}{V} = 1 - \frac{Y_K}{Y} \tag{A4}$$

where

$$Y_0 \equiv \frac{V_0}{F_0} \sim \frac{V}{F}, \quad Y_M = \frac{1}{-i\omega M}, \quad Y_K = -\frac{i\omega}{K}.$$

Equations A1 and A2 indicate how the drive point force and velocity are related to the output of the impedance head. Unless the mobility of M_0, the mass below the force gauge, is large with respect to the drive point mobility of the structure being measured, a correction term approximately equal to the output of the force gauge must be subtracted leaving results which may be dominated by noise. A similar analysis shows that the mobility of K_0, the stiffness below the accelerometer must be small compared to the mobility being measured. This is shown graphically in Fig. A3.

For typical engine structures, the drive point mobilities are small compared to the impedance head stiffness mobility so that the accelerometer will not give accurate measurements. For this reason, only the force gage was used, and a separate accelerometer was used to measure structural (load) acceleration.

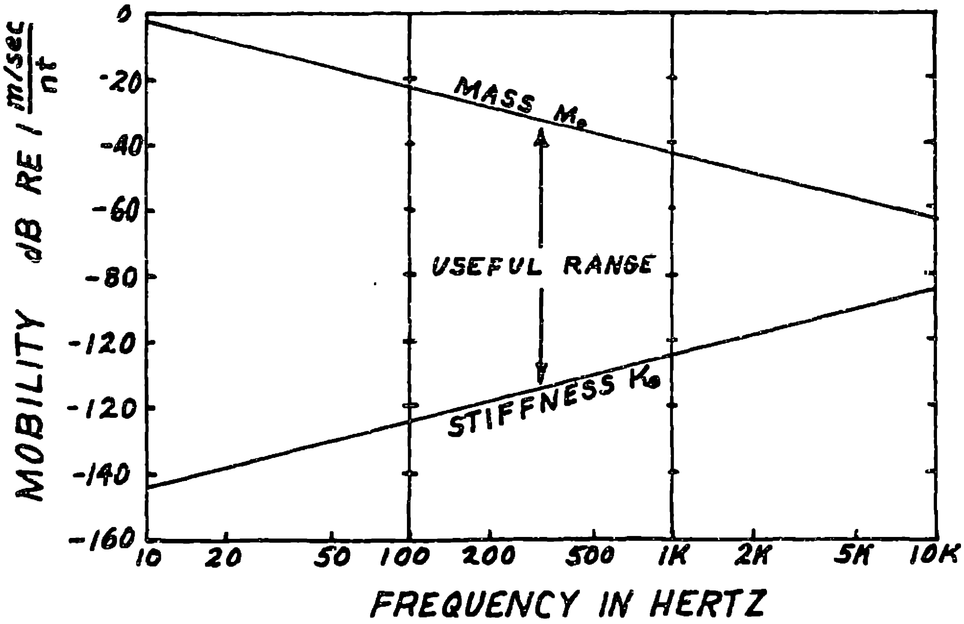

Fig. A3: Useful Range of Impedance Head

The complete calibration procedure involves the measurement of force sensitivity, acceleration sensitivity, mass below the force gauge, and stiffness below the accelerometer.

The acceleration sensitivity is easy, involving only a back-to-back comparison with an accelerometer of known sensitivity. A small reference accelerometer is used and the correction for a finite stiffness, Eq. (A4), is assumed negligible. This assumption is checked later and shown to be valid.

The force sensitivity and mass below the force gauge are determined by mounting a known calibration mass on the impedance head and measuring both force and acceleration while shaking. If S_F denotes the voltage sensitivity of the force gage and V_F denotes the output voltage spectrum, then:

$$V_F = S_F \cdot F. \tag{A5}$$

Since the total load on the force gauge is now M_0 plus the calibration mass M_1, it is seen from Fig. A2 and Eq. (A5) that:

$$F = \frac{V_F}{S_F} = (M_0+M_1)\cdot A. \tag{A6}$$

If the measurement is repeated with another calibration mass M_2, one obtains two equations in two unknowns (S_F and M_0). These equations are solved for force sensitivity and mass below the force gauge. A third calibration mass should then be used to check the results.

The impedance head stiffness may be measured by a technique similar to that used to measure the mass below the force gauge, however, the stiffness measured will include any compliance in the joint between the impedance head and the applied load plus any local compliance of the calibration load.

The lowest axial modes of an aluminum rod were found to be a suitable calibration load. The local behavior of the rod near the drive point is taken into account in the theoretical analysis, so the only potential uncertainty is the compliance of the joint. If the rod is mounted to the impedance head using the same procedure that will be used when making measurements, then any additional compliance measured in the calibration phase will also be present during measurements.

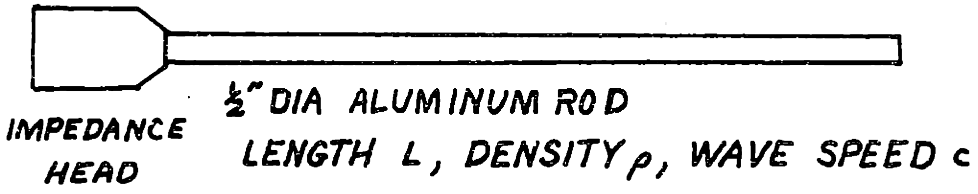

Figure A.4: Set-Up to Measure Drive Point Mobility of Rods

Fig. A.4 shows the impedance head mounted to measure the drive point mobility of a rod in axial vibration. The vibration of the rod is governed by the wave equation. It can be shown that the drive point mobility of this system is:

$$Y(\omega) = \frac{i}{\rho c} \cot \frac{\omega L}{c} \tag{A7}$$

where L is the length of the rod and ρ is the density per unit length and c is the bar wave speed in the rod. At low frequencies, the rod looks like a mass of $\rho \cdot L$. As the frequency is increased, the phase of the mobility stays the same and the magnitude decreases until at $\frac{\omega L}{c} = \frac{\pi}{2}$, the mobility goes to zero and the rod looks like an infinite mass. At a frequency slightly less than the 1/4 wave frequency, the apparent "mass" load on the impedance head will be in resonance against the impedance head stiffness, and the indicated mobility will be zero. By computing the mobility of the rod using equation (A8) one may infer the impedance head stiffness from the equation for resonant frequency $\omega_0^2 = \frac{K}{M}$. It is necessary to know the parameter $\frac{L}{c}$ with considerable accuracy, but since $\frac{c}{2L}$ is the cyclic frequency of the first axial force-free mode of the bar, one may simply suspend the bar at its center, tap on one end, and measure the resonant frequency with a counter using a microphone for a pick-up.

The impedance head stiffness and the mass below the force gauge were measured using these techniques and confirmed within 10% to be the same as the values given by the manufacturer.

The reduction of mobility data required correcting the output of the force gauge to compensate for the mass below the force gauge, M_0. For drive point mobilities, knowing $-i\omega V_0$ from a separate accelerometer, one finds from Eq. (A1):

$$\frac{F_0}{-i\omega V_0} = \frac{F}{-i\omega V_0} - M_0 \ . \qquad \text{(A8)}$$

To compute the actual drive point mobility, one subtracts the mass M_0 from the indicated inertance.

From Eq. (A1) again:

$$F = F_0 \ [\ 1 - \frac{i\omega \ M_0 V_0}{F_0}]$$

$$F_0 = F[1 + \frac{Y_0}{Y_M}]^{-1} \qquad \text{(A9)}$$

where as before $Y_0 = \frac{F_0}{V_0}$ and $Y_M = \frac{1}{-i\omega M}$. Therefore, to correct the indicated force to the actual force when computing transfer mobilities, it is necessary to know the drive point mobility. Appendix B, which describes the reduction of the mobility data, refers to Eqs. (A8) and (A9) when making this correction.

APPENDIX B: ALGORITHM FOR THE REDUCTION OF MOBILITY DATA

The mobility data consists of an input force signal and an output acceleration signal. As mentioned in Section 2.1, these signals, properly conditioned, were recorded simultaneously on a Nagra IV-SJ two channel direct tape recorder. The recorded data was played back through an antialiasing filter and a 12-bit A-D converter to a Data General Nova Computer and reduced by an FFT based signal processing algorithm.

As noted in Section 2.1 the input driving force was a band limited white noise stationary random process and an important result from the theory of random processes is that the output of a linear system with such an input must also be a stationary random process. The input or force channel of the mobility data is assumed to be free of noise, since the force gauge is used near the upper end of its range. Any noise in the measurement is assumed to be in the output or acceleration channel. The transfer function of acceleration data versus force data along with the associated coherence is calculated using the following algorithm.

1. The two channels were sequentially sampled at 12,500 Hz with a 10 μ-sec, delay between

channels.

2. Twenty data records of 512 points per channel were taken and stored on disk in scaled integer format.
3. The first and last 51 points were tapered to zero using a raised cosine window.
4. With one channel as the real part and one channel as the imaginary part, the data was transformed using a standard FFT algorithm.
5. The two autospectra were separated by using the symmetric and antisymmetric properties of transforms of real and imaginary time series.
6. The cross spectrum was computed by multiplying the force spectrum by the complex conjugate of the acceleration spectrum.
7. The ensemble total of the cross spectrum and both force and acceleration power spectra were computed.
8. The estimated transfer function was computed by dividing the total cross spectrum by the total force power spectrum.
9. The coherence was computed by dividing the magnitude squared of the total cross spectrum by both power spectra.

10. The transfer function, coherence, and force power spectrum were stored on disk.

Given the assumption of no input noise, this is an unbiased estimate of the transfer function [29]. The nyquest frequency is 6.25 kHz and data above 5 kHz is not used.

The transfer function results from the first program were used by a second program to compute mobility using the following algorithm.

1. The transfer function of calibration data was read from disk and the magnitude and phase were separately curve fit to straight lines (Fig. B1).
2. The transfer function of mobility data was read from disk in log magnitude-phase form and the fitted calibration curves were subtracted to account for transducer sensitivities, tape recorder misalignment, and sampling delay. The result is an indicated accerance $(\frac{A(\omega)}{F(\omega)})$ relative to a known calibration mass, except for the difference in amplifier gains.

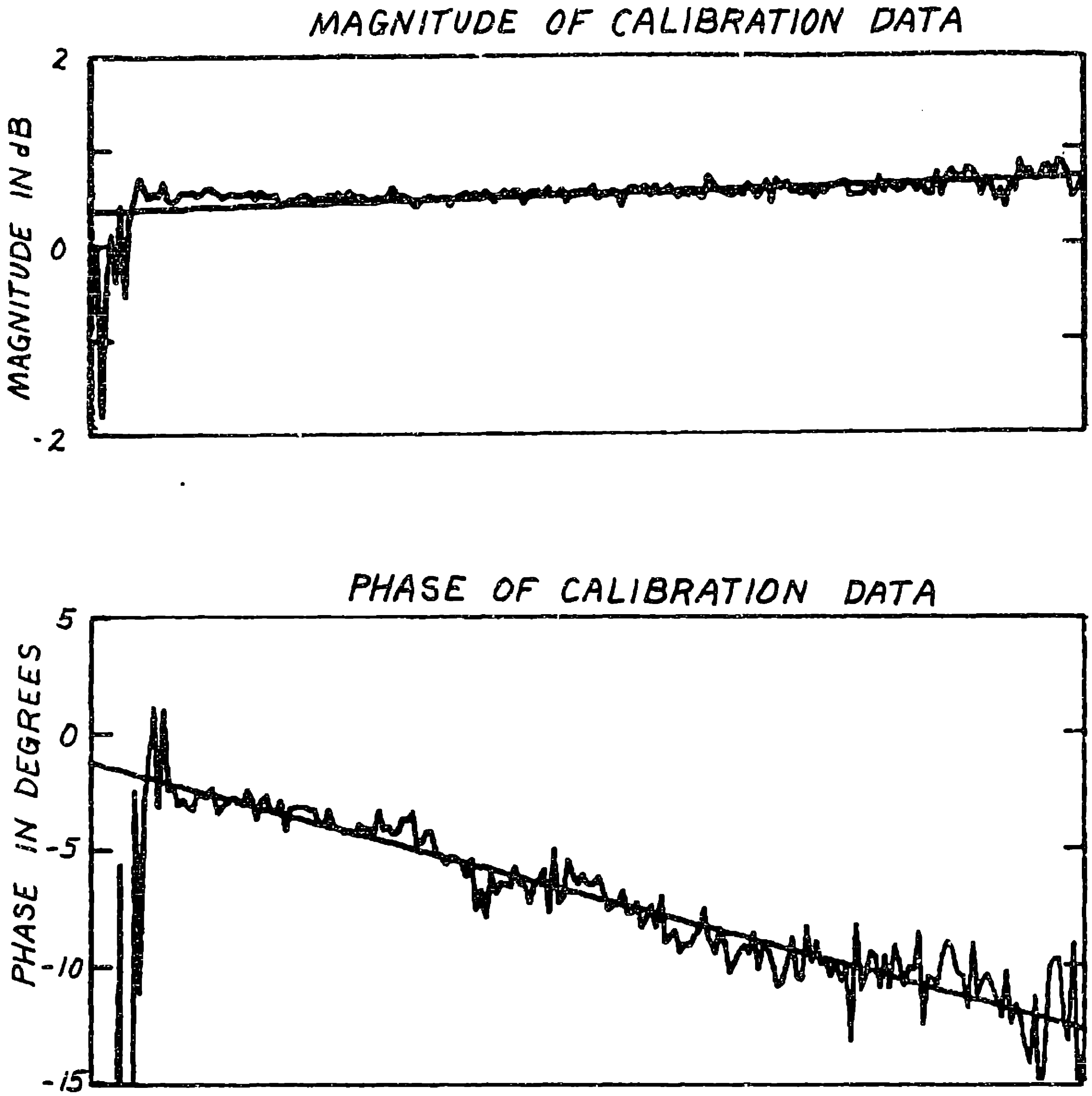

MAGNITUDE OF CALIBRATION DATA

PHASE OF CALIBRATION DATA

Figure B.1: Straightline Curve Fit to Magnitude and Phase of Calibration Data

3. The calibration mass and amplifier gains used while recording calibration data and mobility data were input and used to correct the indicated accelerance to absolute level re 1 kg^{-1}.
4. The effect of the mass below the force gauge which was examined in Appendix A was subtracted out by using Equation A8 or A9 depending on whether a drive point or transfer mobility was to be computed.
5. The corrected accelerance was divided by $-i\omega$ to give mobility and the result was stored on disk.

Program listings are not included since special machine dependent subroutines were employed to increase computing speed.

APPENDIX C: VELOCITY RATIOS

It is postulated that piston slap may be modeled as a transient force applied at some point on the cylinder wall. If an accelerometer is mounted on the water jacket side of the cylinder wall at this point, then the measured velocity response spectrum during piston slap may be divided by the drive point mobility to infer a driving force. The inferred force spectrum may then be multiplied by the appropriate transfer mobility to predict the block surface velocity response spectrum, i.e., if:

V_{cw} = velocity spectrum of cylinder wall
Y_{DP} = drive point mobility of cylinder wall
V_{BS} = velocity spectrum of block surface
Y_{CB} = transfer mobility from cylinder wall to block surface
F = force spectrum applied to cylinder wall

then

$$F = V_{cw}/Y_{DP} \tag{C.1}$$

$$V_{BS} = F \cdot Y_{CB}. \tag{C.2}$$

Therefore

$$\frac{V_{BS}}{V_{cw}} = \frac{Y_{CB}}{Y_{DP}}. \tag{C.3}$$

The actual comparison that will be made is the ratio of piston slap velocity responses to the corresponding ratio of measured mobilities as indicated in Eq. (C.3).

Vibration data taken from the motored engine was presented as the ratio of two velocity spectra. The engine was modified so that piston slap was the dominant source of vibration, and the time records were windowed to capture the transient response to the piston slap (see Fig. 3.7). Since the time window represented only one third of a crank revolution, as much of the background vibration as possible was eliminated. Nevertheless, it may be assumed that the desired signals were contaminated by noise.

The fundamental problem in system identification is shown schematically in Fig. C.1 where each variable is shown in transform pairs.

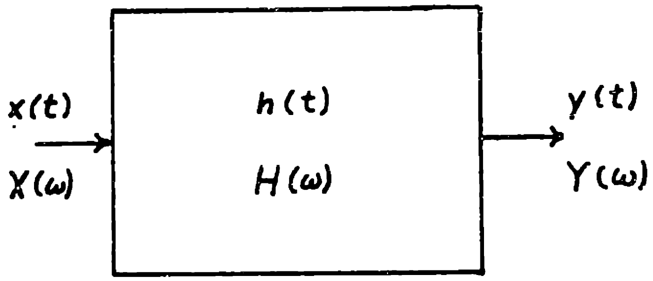

$$y(t) = \int_{-\infty}^{\infty} x(\tau)\, h(t-\tau)\, d\tau$$

Fig. C.1: Basic Linear System

If $x(t)$ is not necessarily an input, then $h(t)$ does not have to be causal even for a physically realizable passive system. It is only assumed that $x(t)$ and $y(t)$ are linearly related.

It can be shown [29] that if one signal is free of noise while the other signal is contaminated by noise, then for stationary random processes, an unbiased estimate of $H(\omega)$ is possible. Let $x(t)$ be measured free of noise. Let $\hat{y}(t)$ be the result of attempting to measure $y(t)$ where:

$$\hat{y}(t) = y(t) + n(t) \tag{C.4}$$

where $n(t)$ is the uncorrelated noise.

If one takes N finite time records of $x(t)$ and $\hat{y}(t)$ and therefore makes N estimates of $X(\omega)$ and $Y(\omega)$

$$\begin{aligned} X_i(\omega) &= \frac{1}{T}\int_{-T/2}^{T/2} x(t)e^{i\omega t}\,dt \\ \hat{Y}_i(\omega) &= \frac{1}{T}\int_{-T/2}^{T/2} \hat{y}(t)e^{i\omega t}\,dt \end{aligned} \qquad i = 1,N \tag{C.5}$$

then the unbiased estimate of $H(\omega)$ is

$$\hat{H}(\omega) = \frac{\langle \hat{Y}_i(\omega)\hat{X}_i^*(\omega)\rangle_N}{\langle \hat{X}_i(\omega)\hat{X}_i^*(\omega)\rangle_N} \tag{C.6}$$

where $< \ >_N$ denotes ensemble average. This is the classic method of averaging cross spectra and power spectra. If there is noise on both channels, the estimate of the power spectrum $X(\omega)X^*(\omega)$ is now biased. This is shown as follows:

$$\hat{x}(t) = x(t) + n_x(t) \qquad \text{C.4}$$

where:

$\hat{x}(t)$ is the measurement

$x(t)$ is the signal of interest

$n_x(t)$ is the noise associated with the measurement

Then:

$$E[\hat{X}(\omega)\hat{X}^*(\omega)] = E[X(\omega)X^*(\omega)] + E[X(\omega)\ N_x^*(\omega)] + E[X^*(\omega)N_x(\omega)] + E[N_x(\omega)N_x^*(\omega)]$$

$$E[\hat{X}(\omega)\hat{X}^*(\omega)] = E[X(\omega)X^*(\omega)] + E[N(\omega)N_x^*(\omega)] \qquad (C.7)$$

Therefore:

$$E[\hat{H}(\omega)] = \frac{E(H(\omega)]}{(1+E[N_x(\omega)N_x^*(\omega)]/E[X(\omega)X^*(\omega)]} \qquad (C.8)$$

For the motored engine data where noise was a concern, it was decided to re-examine the estimator for the transfer function $H(\omega) = \frac{V_2(\omega)}{V_1(\omega)}$ for the two velocity signals $v_1(t)$ and $v_2(t)$ which represent response to piston slap. Let the measurements be:

$$\hat{v}_1(t) = v_1(t) + n_1(t)$$
$$\hat{v}_2(t) = v_2(t) + n_2(t) \qquad (C.9)$$

where $n_i(t)$ is the zero mean uncorrelated random noise on each channel. Transforming to the frequency domain one finds:

$$\hat{V}_1(\omega) = V_1(\omega) + N_1(\omega) \qquad (C.10a)$$

$$\hat{V}_2(\omega) = V_2(\omega) + N_2(\omega) \qquad (C.10b)$$

Assuming that $N_1(\omega)$, the noise on channel 1 is small compared with the signal $V_1(\omega)$ for all values of ω (see Fig. 3.5), then:

$$\frac{1}{\hat{V}_1(\omega)} = \frac{1}{V_1(\omega)} [1 - \frac{N_1(\omega)}{V_1(\omega)}] \qquad (C.11)$$

Multiplying (C.5b) and (C.6) and taking the expected value one finds:

$$\begin{aligned} E[\frac{\hat{V}_2}{\hat{V}_1}] &= E[(V_2(\omega)+N_2(\omega)) \frac{1}{V_1(\omega)}(1 - \frac{N_1(\omega)}{V_1(\omega)})] \\ &= E[\frac{V_2(\omega)}{V_1(\omega)}] + E[\frac{N_2(\omega)}{V_1(\omega)}] - E[\frac{V_2(\omega)N_2(\omega)}{V_1(\omega)V_1(\omega)}] \\ &\qquad - E[\frac{N_2(\omega)N_1(\omega)}{V_1(\omega)V_1(\omega)}] \end{aligned}$$

$$E[\frac{\hat{V}_2}{\hat{V}_1}] = E[\frac{V_2(\omega)}{V_1(\omega)}] \qquad (C.12)$$

The expectation terms containing $N(\omega)$ go to zero since the noise is zero mean and uncorrelated with other signals. Therefore, an improved estimator for the velocity transfer function is the ensemble average of single record estimates of the transfer function. That is, an ensemble of N records of length T for both velocity channels, one estimates:

$$\hat{H}(\omega) = \left\langle \frac{[\hat{V}_2(\omega)]_i}{[\hat{V}_1(\omega)]_i} \right\rangle_N \tag{C.13}$$

The motored engine vibration data was reduced using both estimators and the results are compared in Fig. C.2. At some frequencies, averaging transfer functions gives a greater magnitude for the velocity ratio than averaging cross spectra, but for most frequencies there is no discernable difference. Therefore, the motored engine velocity ratio data was reduced by averaging cross spectra.

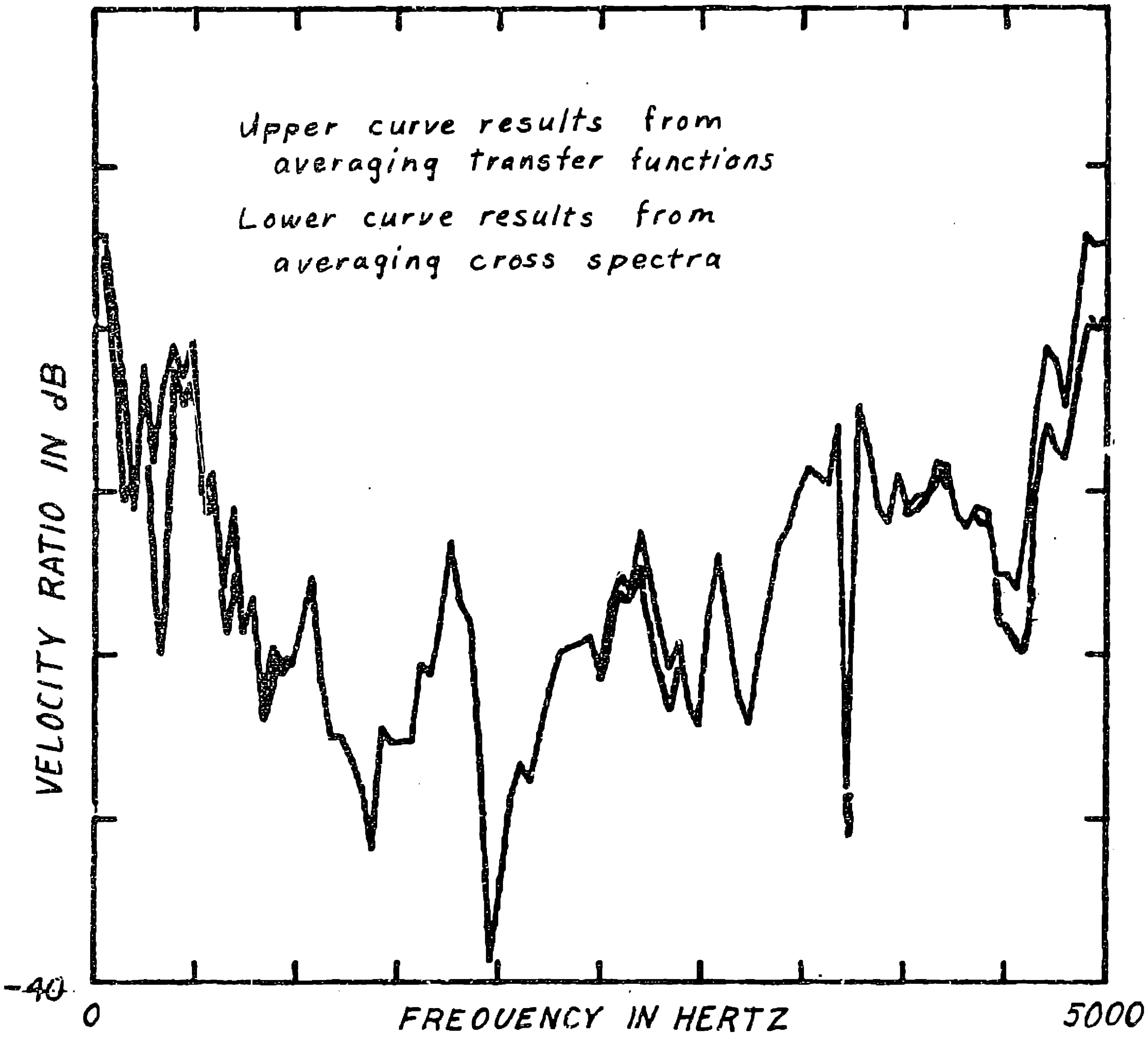

Figure C.2: Velocity Ratio Results, Comparison of Two Estimation Algorithms Using Same Data

APPENDIX D: MODELING THE PISTON AND CONNECTING ROD

D.1 The Connecting Rod

The approximate dimensions of the connecting rod are as shown in Fig. D.1. This is a drawing of an idealized connecting rod used to calculate mass, center of gravity, and moment of inertia using $\rho_s = 7.85$ g/cc as the density of steel.

Calculated mass, small end: $\rho_s \pi (r_o^2 - r_i^2)\, h = 200$ g

big end: $\rho_s \pi (R_o^2 - R_i^2) H^2 = 604$ g

beam: $\rho_s L_B (h \cdot H - \pi a^2) = \underline{288}$ g

Total: 1092 grams

Actual weight of connecting rod with small end bearing and big end bearing cap: 1090 grams.

In addition, the bolts holding the bearing cap and the big bearing inserts total 144 grams.

Calculated center of gravity considering first moment about center of small and bearing:

small end: $200 \text{ g} \cdot 0 = 0$

beam: $302\text{g}\ (r_o + \frac{L_B}{2}) = 2174.4$

big end $(604 \text{ g} + 144 \text{ g}) \cdot \ell = \underline{12566.4}$

14741 g - cm

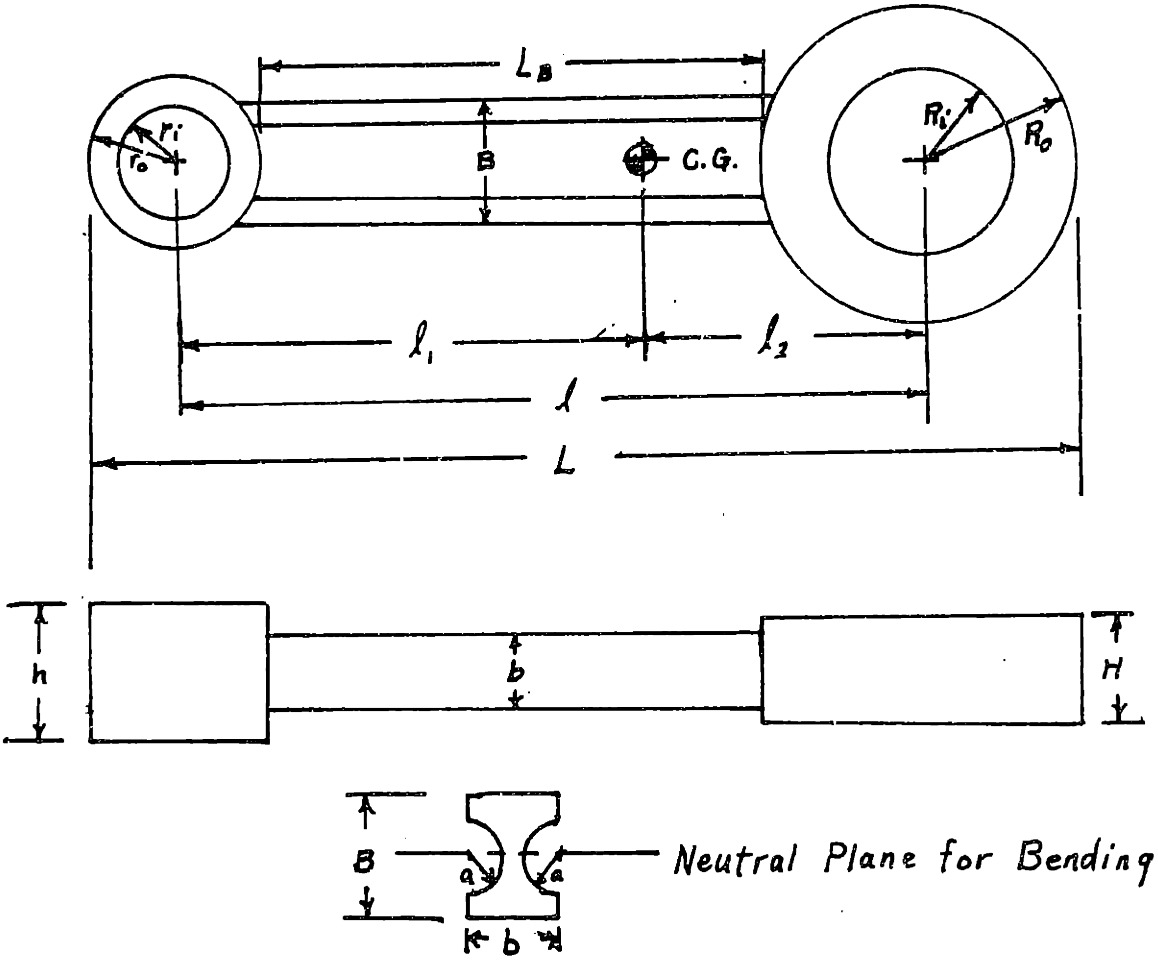

r_o = 2.05 cm

r_i = 1.35 cm

h = 3.4 cm

l = 16.8 cm

l_1 = 11.9 cm

l_2 = 4.9 cm

R_o = 3.93

R_i = 2.8

H = 3.0 cm

b = 1.95 cm

B = 2.5 cm

a = 0.7 cm

L_B = 11 cm

L = 23 cm

Figure D.1: Idealized Connecting Rod

Calculated $\ell_1 = \frac{14741}{1236} = 11.9$ cm.

The center of gravity determined by balancing the connecting rod on a knife edge is at $\ell_1 = 11.8$ cm.

Calculated moment of inertia:

Small end: $I_1 = \rho h \frac{\pi}{2}[r_o^4 - r_i^4] = 601$ g - cm^4

Big end: $I_2 = \rho H \frac{\pi}{2}[R_o^4 - R_i^4] = 6550$ g - cm^4

Bearing cap bolts: $I_{bolts} \sim m R_o^2 = 1513$ g - cm^4

beam:

Moment of inertia of cross section:

$$\frac{bB^3}{12} - \frac{\pi}{4} a^4 = 2.54 \text{ cm}^4$$

Cross section area:

$$A_{cs} = bB - \pi a^2 = 3.34 \text{ cm}^2$$

Moment of inertia of beam:

$$I_{Beam} = \rho A_{cs} L_B \left[I_{cs} + \frac{L_B^2}{12}\right] = 3638 \text{ g - cm}^2$$

Total moment of inertia about CG of connecting rod:

$$I_{total} = \sum_i I_i + r_i M_i$$

I_i is moment of inertia of i<u>th</u> element about its own CG

r_i is distance of i<u>th</u> element from CG of structure

M_i is mass of i<u>th</u> element

$$I_{total} = 601 + 200 \cdot 11.9^2 + 8063 + (604+144) \cdot 4.9^2 + 3638 + 288\left(11.9 - \frac{11}{2} - 2.05\right)^2$$

$$I_{total} = 64000 \text{ g-cm}^2 \quad \text{(calculated)}$$

The moment of inertia of the connecting rod was measured using a torsional pendulum and found to be 66.7 kg-cm^2. Fig. D.2 shows the set-up for this experiment. The period of a torsional pendulum with unknown stiffness and known moment of inertia was measured by timing three sets of 40 cycles each. The connecting rod was attached to the pendulum with the CG of the connecting rod aligned with the torsional spring. The period of the loaded pendulum was measured by timing three sets of 30 cycles each. The period of the torsional pendulum of stiffness K and moment of inertia I_o is given by the equation

$$T_o = \frac{2\pi}{\omega} = 2\pi\sqrt{\frac{I_o}{K}} \tag{D.1}$$

The period of the pendulum loaded by inertia I is

$$T_1 = 2\pi\sqrt{\frac{I_o + I}{K}}$$

therefore:

$$\frac{I_1 + I_o}{I_o} = \left[\frac{T_1}{T_o}\right]^2$$

Using the data shown in Fig. D2, the moment of inertia

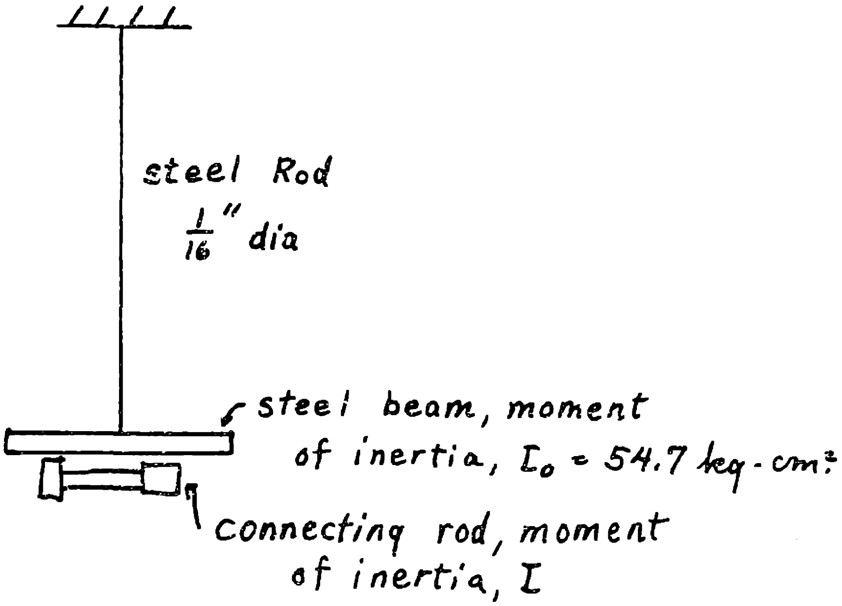

Time for 40 cycles without connecting rod, 3 trials:	Time for 30 cycles with connecting rod, 3 trials:
78.1 sec.	87.1 sec.
78.1 sec.	87.3 sec.
77.9 sec.	87.2 sec.

Figure D.2: Torsional Pendulum to Measure Moment of Inertia of Connecting Rod of the connecting rod is found to be $I = 66.7$ kg - cm^2.

D.2 Rigid Body Motion of the Connecting Rod for Small Displacements:

Fig. D.3 defines forces and velocities for infinitesimal rotation of the connecting. For translation of the center of gravity (CG):

$$F_1 + F_2 = M\,[\frac{\ell_2}{\ell}\,\ddot{x}_1 + \frac{\ell_1}{\ell}\,\ddot{x}_2] \qquad (D.2)$$

For rotation about the center of gravity:

$$\ell_1 F_1 - \ell_2 F_2 = I\ddot{\alpha} = I\,(\frac{\ddot{x}_1 - \ddot{x}_2}{\ell}) \qquad (D.3)$$

One question of interest is whether piston slap results in significant impacts in the big end bearing of the connecting rod. This possibility is examined by setting $\ddot{x}_2 = 0$ in equations (D.2) and (D.3) and solving for $\frac{F_2}{F_1}$.

$$\frac{\ell}{\ell_2}\,\frac{F_1}{M} + \frac{\ell}{\ell_2}\,\frac{F_2}{M} = \frac{\ell\ell_1}{I}\,F_1 + \frac{\ell\ell_2}{I}\,F_2$$

$$F_2 = F_1\,\frac{[M\ell_1\ell_2 - I]}{[M\ell_2^2 + I]} \qquad (D.4)$$

Using the measured values for M, ℓ_1, ℓ_2. and I:

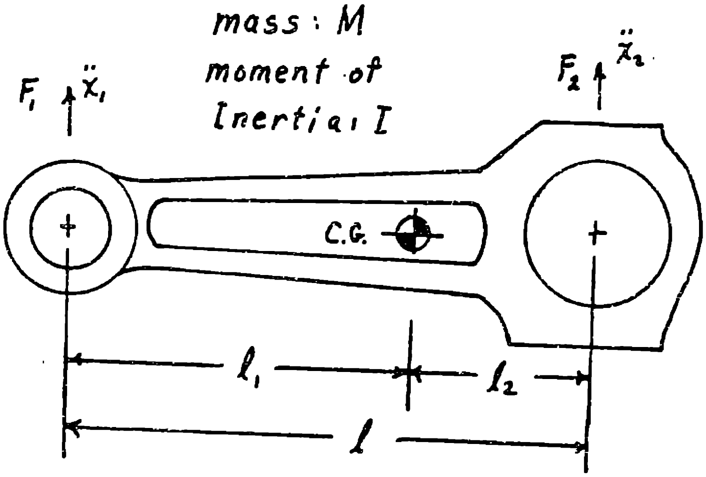

Figure D.3: Forces and Velocities for Infinitesimal Rotations of Connecting Rod

$$F_2 = \frac{1.23 \cdot 5 \cdot 11.8 - 66.7}{1.23 \cdot 5^2 + 66.7} F_1 = 0.06 F_1$$

For this connecting rod design, therefore, one does not expect piston slap to cause significant impacts in the big end bearing.

D.3 Equivalent Mass of the Small End of the Connecting Rod

If the big end of the connecting rod is pinned (i.e., $\ddot{x}_2 = 0$, but rotation is allowed) then the equivalent mass of the small end is defined as $\left.\frac{F_1}{\ddot{x}_1}\right|_{\ddot{x}_2=0}$. Substituting equation (D.4) for F_2 in equation D.2 one finds:

$$F_1 + F_1 \frac{M\ell_1\ell_2 - I}{M\ell_2^2 + I} = M \frac{\ell_2}{\ell} \ddot{x}_1$$

$$F = \left[\frac{M\ell_2^2 + I}{\ell^2}\right] \ddot{x}. \qquad \text{(D.5)}$$

Using measured values of M_1, ℓ_2, I, and ℓ, one finds the equivalent mass is 0.34 kg. The mass of the piston and piston pin is 0.9 kg for a total of 1.24 kg.

D.4 Free Bending Resonance of the Connecting Rod

An approximate value for the natural frequency of the connecting rod in bending was computed using the Rayleigh-

Ritz method [30]. The connecting rod is modeled as shown in D.4 and bending is in the plane of the figure. The two ends are modeled as rigid cylinders with both mass and moment of inertia, and the center of the connecting rod is modeled as an elastic beam of length 2ℓ, density per unit length of ρA, and bending stiffness EI. The displacement of the beam u(x) is approximated by the first four Legendre Polynomials with coefficients u_i as follows:

$$u(x) = P_o(x) + u_1P_1(x) + u_2P_2(x) + u_3P_3(x) \tag{D.6}$$

Useful properties of the Legendre Polynomials are given in Table D.1.

Both translational momentum and angular momentum must be zero for the free-free resonance:

Momentum (non-dimensional)

$$\begin{aligned} 0 = {} & \hat{M}_1(1-u_1+u_2-u_3) + \hat{M}_2(1+u_1+u_2+u_3) + \int_{-1}^{1} P_0(x)dx \\ & -r_1M_1(u_1-3u_2+6u_3) + \hat{r}_2\hat{M}_2(u_1+3u_2+6u_3) \end{aligned} \tag{D.7}$$

Angular Momentum (non-dimensional; about origin x = 0)

$$\begin{aligned} 0 = {} & -\hat{M}_1(1+\hat{r}_1)[(1-u_1+u_2-u_3) - \hat{r}_1(u_1-3u_2+6u_3)] \\ & + \hat{M}_2(1+\hat{r}_2)[(1+u_1+u_2+u_3) + \hat{r}_2(u_1+3u_2+6u_3)] \\ & + \int_{-1}^{1} u_1P_1(x) + \hat{I}_1(u_1-3u_2+6u_3) + \hat{I}_2(u_1+3u_2+6u_3) \end{aligned} \tag{D.8}$$

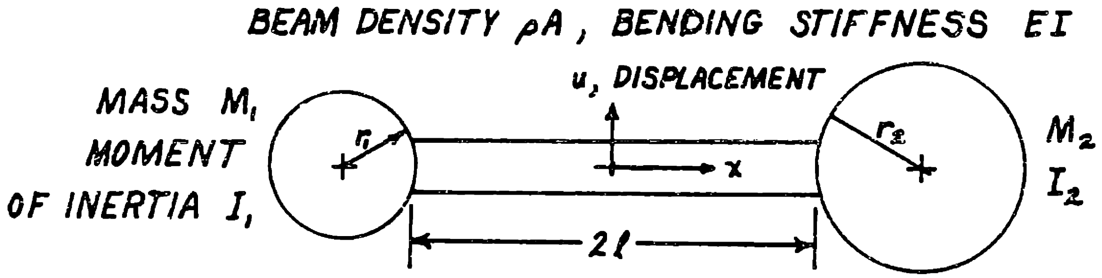

MODEL OF CONNECTING ROD

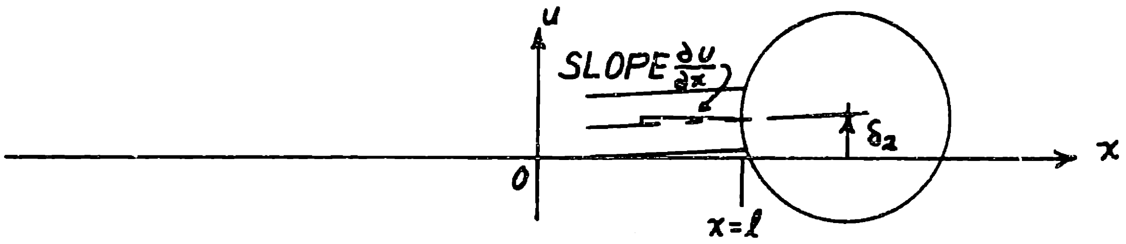

ROTATION OF I_2: $\frac{\partial u}{\partial x}\Big|_{x=\ell}$

DISPLACEMENT OF M_2: $\delta_2 = u(\ell) + r_2 \frac{\partial u}{\partial x}\Big|_{x=\ell}$

DISPLACEMENT OF M_1: $\delta_1 = u(-\ell) - r_1 \frac{\partial u}{\partial x}\Big|_{x=-\ell}$

Figure D.4: Model of Connecting Rod for Rayleigh-Ritz Method

TABLE D.1

PROPERTIES OF LEGENDRE POLYNOMIALS $P_n(x)$

$P_n(x)$, $-1 \leq x \leq 1$, $P_n(1) = 1$, $P_n(-1) = (-1)^n$

orthogonality: $\int_{-1}^{1} P_i(x)P_j(x) = 0$ for $i \neq j$

n	$P_n(x)$	$P'_n(x)$	$P''_n(x)$	$\int_{-1}^{1} P_n^2(x)dx$	$P'_n(-1)$	$P'_n(1)$
0	1	0	0	2	0	0
1	x	1	0	2/3	1	1
2	$\frac{3x^2}{2} - \frac{1}{2}$	3x	1	2/5	-3	3
3	$\frac{5x^3}{2} - \frac{3x}{2}$	$\frac{15x^2}{2} - \frac{3}{2}$	15x	2/7	6	6

These two equations are solved for u_1 and u_2 as functions of u_3.

Using the orthogonality properties of the Legendre polynomials to compute the kinetic energy of the beam:

$$\int_{-1}^{1} [P_o(x) + u_1P_1(x) + u_2P_2(x) + u_3P_3(x)]^2\, dx$$

$$= 2 + \frac{2}{3} u_1^2 + \frac{2}{5} u_2^2 + \frac{2}{7} u_3^2$$

For the lumped masses at the ends, the kinetic energy is due to both translation and rotation. Therefore, the total kinetic energy of the model is;

$$\begin{aligned} \text{K.E.} = \frac{1}{2} \rho A\ell\, \omega_n^2\{&\hat{M}_1[(1-u_1+u_2-u_3) - \hat{r}_1(u_1-3u_2+6u_3)]^2 \\ &+ \hat{M}_2[(1+u_1+u_2+u_3) + \hat{r}_2(u_1+3u_2+6u_3)]^2 \\ &+ [2 + \frac{2}{3} u_1^2 + \frac{2}{5} u_2^2 + \frac{2}{7} u_3^2] \\ &+ \hat{I}_1(u_1-3u_2+6u_3)^2 + \hat{I}_2(u_1+3u_2+6u_3)^2\} \end{aligned}$$

Potential energy is due entirely to bending.

$$\text{P.E.} = \frac{EI}{2\ell^3} \int_{-1}^{1} [P_o''(\hat{x})+u_1P_1''(\hat{x})+u_2P_2''(\hat{x})+u_3P_3''(\hat{x})]^2 d\hat{x}$$

$$= \frac{EI}{2\ell^3} [6u_2^2+150u_3^2] \, . \qquad \text{(D.10)}$$

The natural frequency is found by equating the kinetic energy and potential energy and solving for ω_n. Since assumed mode methods always give an upper bound on the exact natural frequency (assuming the original model is correct), one finds the minimum value of ω with respect to the free parameter u_3. The numbers assumed for this model give a value of $\frac{\omega_n}{2\pi} = 1340$ Hz. The measured natural frequency of this mode is 1850 Hz, which is reasonable agreement given the approximate nature of the model.

D.5 Lumped Parameter Model of Piston-Connecting Rod

The measured drive point mobility of the piston and connecting rod when mounted on the crankshaft can be accurately approximated over the frequency range of 0 to 2500 Hz by a function which is a ratio of two polynomials in frequency. Fig. 4.3 shows this comparison. The poles and zeroes (Table 4.1) were chosen in order to fit the model with the measurement. The chosen form of the drive point mobility can be modeled by a two degree of freedom lumped parameter system as shown in Fig. D.5 along with the "equivalent circuit" using the voltage-velocity analogy. The mobilities of each element are shown along with the corresponding symbol. The drive point mobility of the model is written by inspection from the circuit diagram using rules for series and parallel combinations.

$$Y(\omega) = \frac{i\omega}{K_s} + \cfrac{1}{-\, i\omega M_p + \cfrac{1}{\cfrac{-i\omega}{K_r} + \cfrac{1}{-i\omega M_r}}}$$

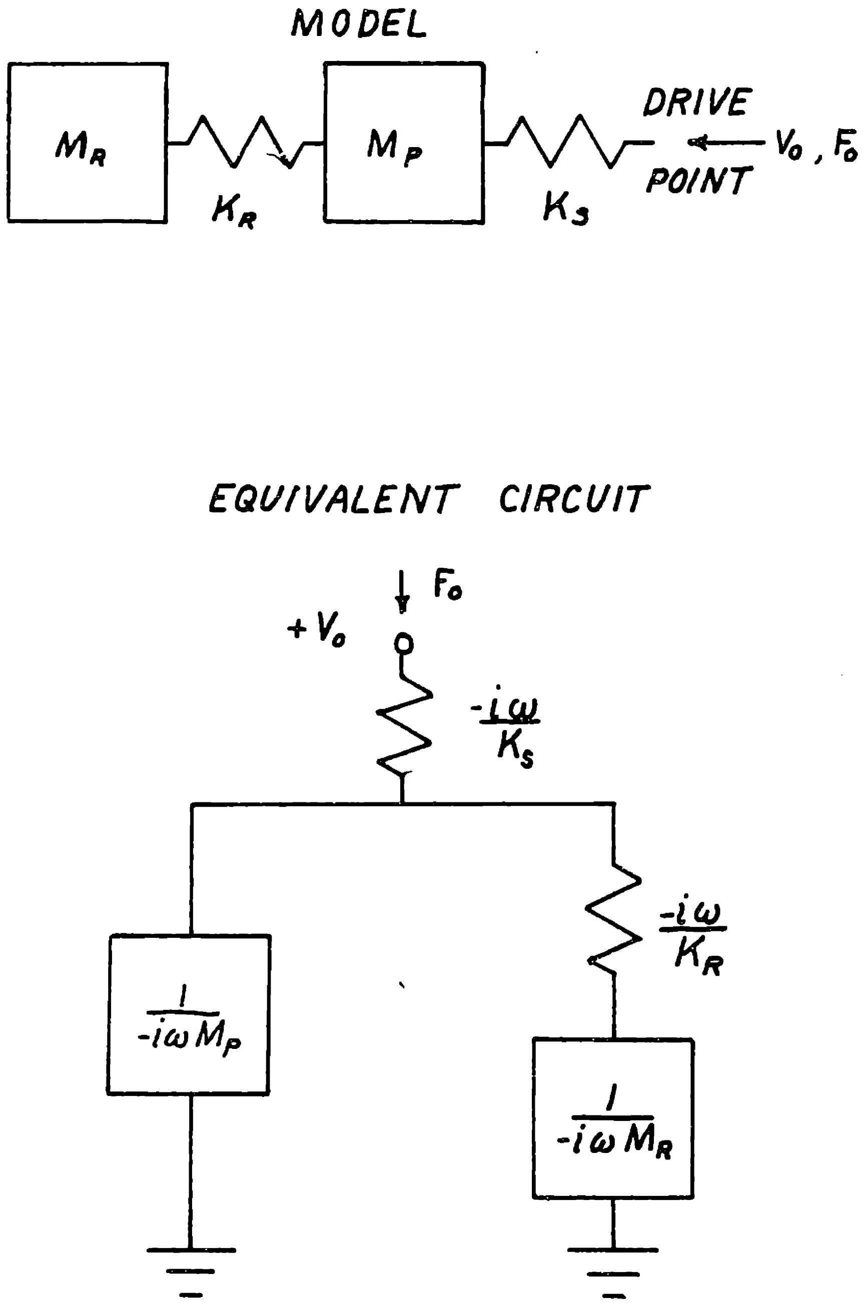

Figure D.5: Lumped Parameter Model of Piston with Equivalent Circuit

Substituting:

$$\omega_R^2 = \frac{K_R}{M_R} \quad \text{and} \quad \omega_s^2 = \frac{K_s}{M_p}$$

one may show that:

$$Y(\omega) = \frac{1}{-i\omega M_p}\left[\frac{-\omega^2}{\omega_s^2} + \frac{1 - \omega^2/\omega_R^2}{1+M_R/M_p - \omega^2/\omega_R^2}\right] \tag{D.11}$$

Finding the limits as $\omega \rightarrow 0$ and $\omega \rightarrow \infty$

$$\lim_{\omega\to 0} Y(\omega) = \frac{1}{-i\omega M_p(1+M_R/M_p)} = \frac{1}{-i\omega(M_p+M_R)} \tag{D.12}$$

$$\lim_{\omega\to\infty} Y(\omega) = \frac{1}{-i\omega M_p} \left(\frac{-\omega^2}{\omega_s^2}\right) = \frac{-i\omega}{K_s} \tag{D.13}$$

From the curve fit to the measured data neglecting damping which is small:

$$Y(\omega) = \frac{Y_o}{-i\omega} \frac{(\omega_1^2-\omega^2)(\omega_2^2-\omega^2)}{(\omega_o^2-\omega^2)} \tag{D.14}$$

where

$\omega_1/2\pi = \text{Im}[Z_1] = 1500$

$\omega_2/2\pi = \text{Im}[Z_2] = 2900$

$\omega_3/2\pi = \text{Im}[p_2] = 1600$

$Y_o = 2.8 \times 10^{-9}$

Substituting into Eqs. (D.12) and (D.13) for the limiting behavior one finds

$$\lim_{\omega\to} Y(\omega) = \frac{1}{-i\omega(M_p+M_R)} = \frac{Y_o}{-i\omega}\left[\frac{\omega_1^2\omega_2^2}{\omega_o^2}\right]$$

$$M_p+M_R = 1.21 \text{ kg}$$

$$\lim_{\omega\to\infty} Y(\omega) = \frac{-i\omega}{K_s} = \frac{Y_o}{-i\omega} \frac{(-\omega^2)(-\omega^2)}{(-\omega^2)}$$

$$K_s = \frac{1}{Y_o} = 3.54 \times 10^8 \text{ nt/m}$$

From equations D.10 and D.14 one also finds

$$Y(\omega) = \frac{1}{-i\omega K_s}\left[\frac{\omega_R^2\omega_s^2-\omega^2(\omega_R^2+K_R/M_p+\omega_s^2)}{K_R(1/M_R+1/M_p)-\omega^2}\right]$$

$$= \frac{Y_o}{-i\omega}\left[\frac{\omega_1^2\omega_2^2-(\omega_1^2+\omega_2^2)\omega^2-\omega^4}{\omega_o^2-\omega^2}\right] \qquad \text{(D.15)}$$

Equating corresponding terms:

$$\omega_o^2 = K_R(\frac{1}{M_R}+\frac{1}{M_p}) \qquad \text{(D.16)}$$

$$\omega_R^2 + \frac{K_R}{M_p} + \omega_s^2 = \omega_1^2 + \omega_2^2$$

$$\omega_s = \frac{K_s}{M_p} = \omega_1^2 + \omega_2^2 - \omega_o^2 \qquad \text{(D.17)}$$

Substituting in known values one may find:

$K_s = 3.54 \times 10^8$ nt/m

$M_p = 1.107$ kg

$M_R = 0.103$ kg

$K_R = 9.5 * 10^6$ nt/m

The total mass of the model; $M_p + M_R$, is 1.2. kg compared to the measured mass of 1.24 kg for the piston plus small end of the connecting rod.

D.6 Model for Piston-Cylinder Wall Interaction

The model for piston-cylinder wall interaction is discussed in Section 4.2. The models previously constructed for the piston and cylinder wall are connected together as shown in Fig. D.6. The two masses M_R and M_p are each given an initial velocity v_o at t_o, the time of impact, and the model predicts the response of the system for all time $t > t_o$. Since v_o is finite and there is damping in the model, the response has finite energy which will correspond to the energy of one piston slap event. The initial conditions may be included by using the Laplace transform of the equations or by driving the system with an impulse force equal to the initial momentum. The two methods are equivalent, however, the latter will be followed. A force spectrum $F_R(\omega) = M_R V_o$ will drive M_R and a force spectrum of

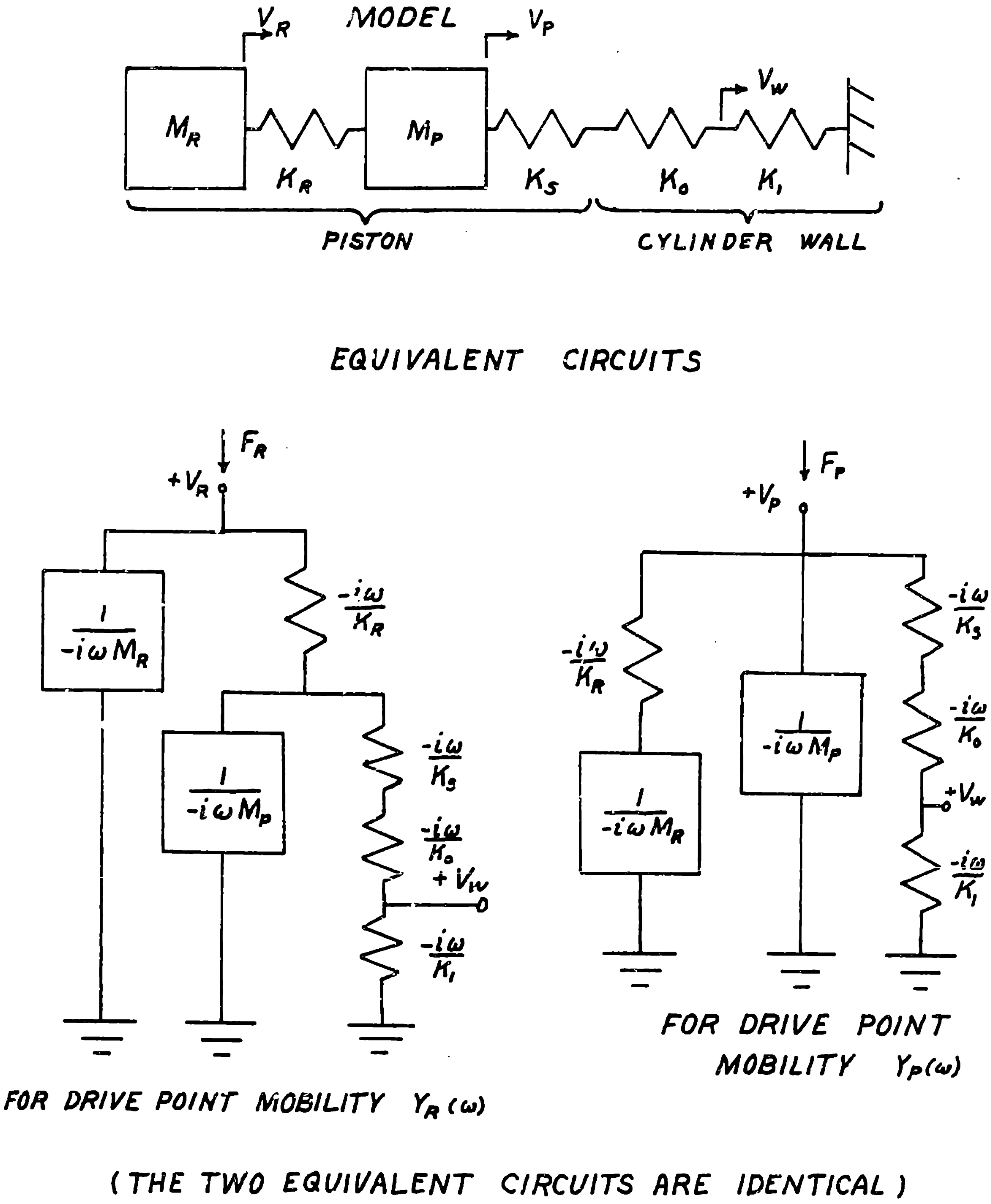

Figure D.6: Model for Piston-Cylinder Wall Interaction with Equivalent Circuit

$F_p(\omega) = M_pV_o$ will drive M_p. From the equivalent circuit diagram in Fig. D.6 we first write the drive point mobilities for the two masses. For mass M_p

$$Y_p(\omega) = \left[\frac{1}{\frac{1}{-i\omega M_R} - \frac{i\omega}{K_R}} - i\omega M_p - \frac{K_t}{i\omega}\right]^{-1}$$

where $\frac{1}{K_t} = \frac{1}{K_s} + \frac{1}{K_w} = \frac{1}{K_s} + \frac{1}{K_o} + \frac{1}{K_1}$

also let $\omega_R^2 = \frac{K_R}{M_p}$ and $\omega_t^2 = \frac{K_t}{M_p}$

$$Y_p(\omega) = \frac{-i\omega}{K_t}\left[\frac{1 - \omega^2/\omega_R^2}{\Delta}\right] \tag{D.18}$$

where

$$\Delta = 1 - \omega^2\left(\frac{1}{\omega_R^2} + \frac{M_R}{K_T} + \frac{1}{\omega_T^2}\right) + \frac{\omega^4}{\omega_t^2\omega_R^2} \tag{D.19}$$

For mass M_R:

$$Y_R(\omega) = \cfrac{1}{-i\omega M_R + \cfrac{1}{\cfrac{-i\omega}{K_R} + \cfrac{1}{-i\omega M \quad \frac{K_t}{-i\omega}}}}$$

$$Y_R(\omega) = \frac{-i\omega}{K_R}\;\frac{1 + \frac{K_R}{K_T} - \frac{\omega^2}{\omega_T^2}}{\Delta} \tag{D.20}$$

The drive point mobilities determine the drive point velocity in response to an applied force. The desired output velocity is V_w as indicated in Fig. D.6. The transfer mobilities are derived by multiplying by the relevant velocity divider expressions. First calculate the response at M_p due to the initial conditions imposed on M_R:

$$Y_{RP} = \frac{\dfrac{1}{-i\omega M_p + K_t/-i\omega}}{\dfrac{1}{-i\omega M_p + K_t/-i\omega} - \dfrac{i\omega}{K_t}} \cdot Y_R(\omega)$$

$$Y_{RP}(\omega) = \frac{K_R/K_T}{1 + \dfrac{K_R}{K_T} - \dfrac{\omega^2}{\omega_T^2}} - \frac{-i\omega}{K_R} \left[\frac{1 + \dfrac{K_R}{K_T} - \dfrac{\omega^2}{\omega_T^2}}{\Delta}\right]$$

$$Y_{RP}(\omega) = \frac{-i\omega}{K_T} \frac{1}{\Delta} \qquad \text{(D.21)}$$

Multiply the two input force spectra by their respective mobilities to find the velocity response of M_p:

$$V_p(\omega) = F_p Y_p + F_R Y_{RP} \qquad \text{(D.22)}$$

$$V_p(\omega) = \frac{-i\omega}{K_t} \left[\frac{M_p V_o (1 - \omega^2/\omega_o^2) + M_R V_o}{\Delta}\right]$$

$$V_p(\omega) = \frac{-i\omega}{K_t} M_p V_o \left[\frac{1 + M_R/M_p - \omega^2/\omega_o^2}{\Delta}\right] \qquad \text{(D.23)}$$

Using velocity divider relationship to determine the velocity at the cylinder wall:

$$V_w(\omega) = \frac{-i\omega/K_1}{-i\omega/K_T} V_p$$

One finds after multiplying numerator and denominator by $\omega_t^2\omega_R^2$:

$$V_w(\omega) = -i\omega V_o \frac{K_T}{K_I} \left[\frac{\omega_R^2 + K_R/M_p - \omega^2}{\omega_R^2\omega_1^2+\omega^2(\omega_R^2+K_R/M_p+\omega_t^2)-\omega^4}\right] \qquad (D.24)$$

The motored engine data is presented as an energy density spectrum for one piston slap event such that the total energy is

$$E_T = \int_{-\infty}^{\infty} v_w^2(t)\,dt = \int_0^{\infty} S_{V_w}(f)\,df \qquad (D.25)$$

From Parceval's theorem one finds

$$\int_{-\infty}^{\infty} v_w^2(t)\,dt = \frac{1}{2\pi} \int_{-\infty}^{\infty} V_w(\omega)V_w^*(\omega)\,d\omega$$

Therefore, the energy spectral density is defined by:

$$S_{V_w}(f) = 2V_w(2\pi f)V_w^*(2\pi f) \qquad (D.26)$$

or in pole-zero form:

$$S_{V_w}(f) = 2V_o^2\left(\frac{K_T}{K_1}\right)^2 \left| \frac{f(if-z_o)(if-z_o^*)}{2\pi(if-p_1)(if-p_1^*)(if-p_2)(if-p_2^*)} \right|^2 \tag{D.27}$$

where

$$z_o = \frac{-i\omega_o}{2\pi}(1+i\eta_o)$$

$$p_1 = \frac{-i\omega_1}{2\pi}(1+i\eta_1)$$

$$p_2 = \frac{-i\omega_2}{2\pi}(1+i\eta_2)$$

$\omega_o = \omega_R^2 + \frac{K_R}{M_p}$ is the root of the numerator of Eq. D.24

ω_1 and ω_2 are the roots of the denominator Δ

η_o, η_1, and η_2 are the loss factors associated with the poles and zero.

Using known values of K_s, M_p, K_R, and M_R from above and also:

$$K_w = 1.58 \times 10^8$$

$$K_1 = 3.96 \times 10^8$$

one may compute the following:

$$\frac{\omega_o}{2\pi} = 1670 \text{ Hz}$$

$$\frac{\omega_1}{2\pi} = 1336 \text{ Hz}$$

$$\frac{\omega_2}{2\pi} = 1805 \text{ Hz}$$

The following loss factors were assumed:

$$\eta_o = 0.052$$

$$\eta_1 = 0.082$$

$$\eta_2 = 0.097$$

The response of the model shown in Fig. 4.10 was computed using these values.

APPENDIX E: PISTON MOTION THROUGH THE CLEARANCE AT TOP DEAD CENTER

The following analysis is an approximation to the piston motion through the operating clearance at top dead center. Friction and rotation of the piston are neglected. The primary result of interest is the piston velocity at time of impact. Geometry and parameters of interest are defined in Fig. E.1.

The reaction force R which holds the piston against the cylinder wall during the compression stroke goes to zero as the crank pin passes under the piston pin. Then, the horizontal component of the axial load carried by the connecting rod accelerates the piston through the operating clearance δ to impact the major thrust side of the cylinder. Let L be the axial compression load carried by the connecting rod.

$$L \cos \theta = P \cdot A - M r \omega^2$$

$$L \sin \theta = R \qquad \text{before T.D.C.}$$

$$\ell \sin \theta = r \sin \omega t \qquad t = 0 \quad \text{at T.D.C.}$$

let x(t) denote the displacement of the piston through the clearance δ after T.D.C. For small angles θ near T.D.C.:

$$\theta \approx \frac{r}{\ell} \omega t \tag{E1}$$

$$L \approx P \cdot A - M r \omega^2 \tag{E2}$$

$$R \approx \frac{r}{\ell} \omega t \, [PA - M r \omega^2] \tag{E3}$$

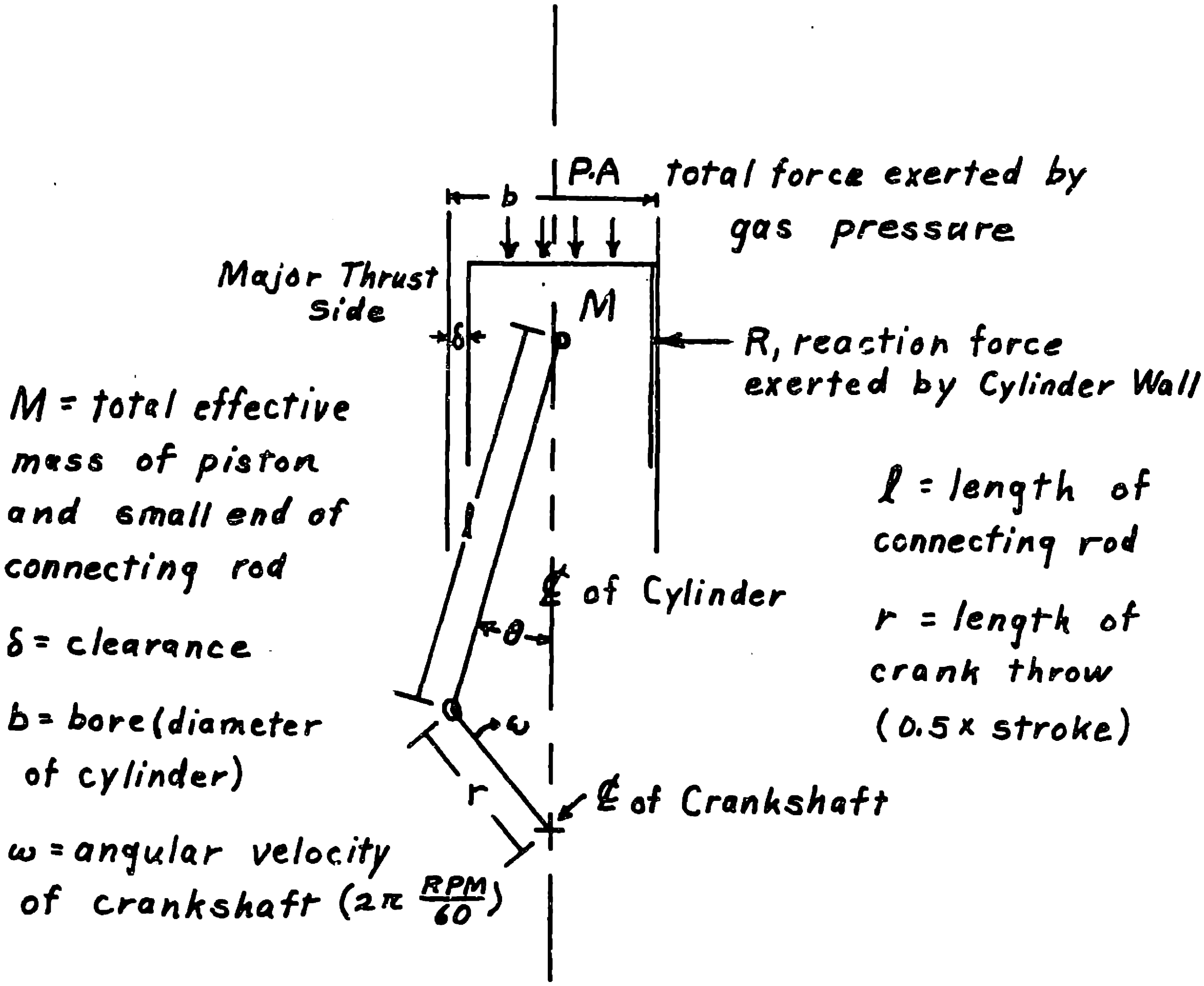

Figure E.1: The Piston at Top Dead Center

Immediately after T.D.C.:

acceleration: $$M\ddot{x} = \frac{r}{\ell}\,\omega t\,[P\ A - M\ r\ \omega^2] \tag{E4}$$

velocity: $$\dot{x} = [\frac{PA}{M} - r\omega^2]\ \frac{r}{\ell}\ \omega\ \frac{t^2}{2} \tag{E5}$$

displacement: $$x\ [\frac{PA}{M} - r\omega^2]\ \frac{r}{\ell}\ \omega\ \frac{t^3}{6} \tag{E6}$$

Solving for t_o, the time of impact:

$$x(t_o) = \delta = [\frac{PA}{M} - r\omega^2]\ \frac{r}{\ell}\ \omega\ \frac{t_o^3}{6} \tag{E7}$$

$$t_o = [\frac{6\delta}{\omega r/\ell}\ (\frac{PA}{M} - r\omega^2)^{-1}]^{1/3} \tag{E8}$$

The analysis by Griffiths and Skorecki [15] reduces to this result for the impact at top dead center before the power stroke. They reported a calculated time of impact of 13° after T.D.C. compared with 14° observed in their experimental engine. Given the following values for the engine used for this research:

bore = 86 mm
r = 51 mm
ℓ = 168 mm
P = 19 bar
δ = 0.004"
M = 1.21 kg
1000 = RPM

One may compute

$$r/\ell = 0.304$$

$$\omega = 105 \text{ rad/sec}$$

$$[\frac{PA}{M} - r\omega^2] = 8500 \text{ m/sec}^2$$

$$\delta = 10^{-4} \text{ m}$$

Substituting into equation E.8:

$$t_o = [\frac{6\cdot 10^{-4}}{105\cdot 304}] \cdot \frac{1}{8500}]^{1/3}$$

t_o = 1.3 ms. or 7.8° after T.D.C.

Substituting into Eq. E.5:

$$v_o = 8500 \cdot 0.304 \cdot 105 \cdot \frac{(.0013)^2}{2}$$

$$v_o = 0.23 \text{ m/sec}$$

The computed time of impact agrees very well with the observed time of 8° after T.D.C. Therefore, this simple analysis may be assumed to give a good estimate of v_o, the transverse velocity of the piston at time of impact.